
Electronic Thesis and Dissertation Repository

9-2-2015 12:00 AM

Mapping the Impact and Plasticity of Cortical-Cardiovascular Interactions in Vascular Disease Using Structural and Functional MRI

Udunna C. Anazodo
Western University

Supervisor

Keith S St Lawrence

The University of Western Ontario Joint Supervisor

J Kevin Shoemaker

The University of Western Ontario

Graduate Program in Medical Biophysics

A thesis submitted in partial fulfillment of the requirements for the degree in Doctor of Philosophy

© Udunna C. Anazodo 2015

Follow this and additional works at: <https://ir.lib.uwo.ca/etd>



Part of the [Medical Biophysics Commons](#)

Recommended Citation

Anazodo, Udunna C., "Mapping the Impact and Plasticity of Cortical-Cardiovascular Interactions in Vascular Disease Using Structural and Functional MRI" (2015). *Electronic Thesis and Dissertation Repository*. 3214.

<https://ir.lib.uwo.ca/etd/3214>

This Dissertation/Thesis is brought to you for free and open access by Scholarship@Western. It has been accepted for inclusion in Electronic Thesis and Dissertation Repository by an authorized administrator of Scholarship@Western. For more information, please contact wlsadmin@uwo.ca.

MAPPING THE IMPACT AND PLASTICITY OF CORTICAL-CARDIOVASCULAR
INTERACTIONS IN VASCULAR DISEASE USING STRUCTURAL AND
FUNCTIONAL MRI

(Thesis format: Integrated Article)

by

Udunna Chinyelu Ukaoma Anazodo

Graduate Program in Medical Biophysics

A thesis submitted in partial fulfillment
of the requirements for the degree of
Doctor of Philosophy

The School of Graduate and Postdoctoral Studies
The University of Western Ontario
London, Ontario, Canada

© Udunna C Anazodo 2015

Abstract

There is growing interest in the role of vascular disease in accelerating age-related decline in cerebrovascular structural and functional integrity. Since an increased number of older adults are surviving chronic diseases, of which cardiovascular disease (CVD) is prevalent, there is an urgent need to understand relationships between cardiovascular dysfunction and brain health. It is unclear if CVD puts the brains of older adults, already experiencing natural brain aging, at greater risk for degeneration. In this thesis, the role of CVD in accelerating brain aging is explored. Because physical activity is known to provide neuroprotective benefits to brains of older adults, the role of physical activity in mediating disease effects were also explored.

Using novel neuroimaging techniques, measures of gray matter volume and cerebrovascular hemodynamics were compared between groups of coronary artery disease patients and age-matched controls, to describe regional effects of CVD on the brain. In a sub-set of patients, imaging measures were repeated after completion of a 6-month exercise training, part of a cardiac rehabilitation program, to examine exercise effects. Differences in cerebrovascular hemodynamics were measured as changes in resting cerebral blood flow (CBF) and changes in cerebrovascular reactivity (CVR) to hypercapnia (6% CO₂) using a non-invasive perfusion magnetic resonance imaging technique, arterial spin labelling (ASL). We found decreased brain volume, CBF and CVR in several regions of the brains of coronary artery disease patients compared to age-matched healthy controls. The reductions in CBF and CVR

were independent of underlying brain atrophy, suggesting that changes in cerebrovascular function could precede changes in brain structure. In addition, increase in brain volume and CBF were observed in some regions of the brain after exercise training, indicating that cardiac rehabilitation programs may have neurorehabilitation effects as well.

Since, CBF measured with ASL is not the [gold] standard measure of functional brain activity, we examined the regional correlation of ASL-CBF to glucose consumption rates (CMRglc) measured with positron emission tomography (PET), a widely acceptable marker of brain functional activity. Simultaneous measurements of ASL-CBF and PET-CMRglc were performed in a separate study in a group of older adults with no neurological impairment. Across brain regions, ASL-CBF correlated well with PET-CMRglc, but variations in regional coupling were found and demonstrate the role of certain brain regions in maintaining higher level of functional organization compared to other regions.

In general, the results of the thesis demonstrate the impact of CVD on brain health, and the neurorehabilitation capacity of cardiac rehabilitation. The work presented also highlights the ability of novel non-invasive neuroimaging techniques in detecting and monitoring subtle but robust changes in the aging human brain.

Keywords

Cardiovascular disease, cardiac rehabilitation, aerobic exercise training, arterial spin labelling, cerebral blood flow, cerebrovascular reactivity, voxel-based morphometry, PET-MRI.

Co-Authorship Statement

The work presented in Chapter two was previously published in *NeuroImage: Clinical* 2013 Oct 6; 3:388-395, by: Udunna C Anazodo, J Kevin Shoemaker, Nevin Suskin, and Keith S St. Lawrence. JK Shoemaker and KS St. Lawrence contributed to the study design, provided supervision and reviewed the manuscript. N Suskin assisted in participant recruitment, provided supervision, and reviewed the manuscript. I contributed to study design, recruited study participants, performed all neuroimaging data collection and analysis, and was responsible for writing the manuscript.

Chapter three is from a manuscript submitted in June 2015 and under review at *Journal of Cerebral Blood Flow and Metabolism [Manuscript ID: JCBFM-0365-15-ORIG]*. The authors are Udunna C Anazodo, J Kevin Shoemaker, Nevin Suskin, Tracy Ssali, Danny JJ Wang, and Keith S St. Lawrence. JK Shoemaker and KS St Lawrence contributed to the study design, provided supervision and reviewed the manuscript. N Suskin assisted in participant recruitment and provided supervision. T Ssali assisted with data analysis. DJJ Wang developed the magnetic resonance imaging pulse sequence used for brain perfusion imaging and reviewed the manuscript. I contributed to study design, recruited study participants, performed all neuroimaging data collection and analysis, and was responsible for writing the manuscript.

Chapter four has been adapted from the paper entitled "Feasibility of simultaneous whole-brain imaging on an integrated PET-MRI system using an enhanced 2-point Dixon attenuation correction method", published in *Frontiers in Neuroscience* 2015 (8):434 by Udunna C Anazodo, Jonathan D Thiessen, Tracy Ssali, Jonathan Mandel, Matthias Günther, John Butler, William Pavlosky, Frank S Prato, R Terry Thompson, and Keith St Lawrence. KS St Lawrence contributed to study design, provided supervision and reviewed manuscript. JD Thiessen assisted with data analysis and reviewed the manuscript. M Günther developed the magnetic resonance imaging pulse sequence used for brain perfusion imaging and reviewed the manuscript. I designed the study, recruited study participants, performed the experiments and analyzed the data,

and was responsible for writing the manuscript. The remaining authors helped with data collection and reviewed the manuscript.

Acknowledgments

"It takes a village to raise a child" Igbo(Nigeria) Proverb

The author wishes to acknowledge the contribution of several people to the work described in this thesis. I would like to thank Professor Keith S St Lawrence for his supervision, guidance and support throughout the pursuit of my doctoral studies. Keith, thank you for providing an environment for me to pursue ideas, questions and methods that my restless inquisitive mind ventured into, including those that lead down a long fruitless road. Your patience and understanding is inspiring. I would also like to thank my co-supervisor, Professor J Kevin Shoemaker for his invaluable insights and mentorship. Kevin, you always made time to discuss my project. Your excitement was infectious even when I felt less optimistic of the outcomes.

I am grateful to the guidance and mentorship of the following; Dr Terry R Thompson, member of my advisory committee, Dr Frank S Prato, who always made time to answer any questions I had, and Dr Jonathan D Thiessen, who was invaluable in providing support for the PET-MRI study.

To Arlene Fleischhauer, Tim Hartley, Maria Francis and John Butler, I am grateful for the interest you have shown to this work and the assistance given during data collection. I simply will not have been able to complete this work without your support. To Jennifer Hadway, Laura Morrison and Lise Desjardins, the animal technicians at Professor St Lawrence's lab, even though we did not work together on this thesis,

whenever I needed equipments for my CO₂ apparatus, you all were there to help me. You girls were my moral and emotional rock. I can come and vent at any time. Thank you.

I would like to thank Fang Liu for taking time to introduce me to Matlab and for teaching me the basics. Harini Pandithasekera, Tracy Ssali and Kyle Veredecchia, you all are the best lab members one can ask for.

Finally to my mother and siblings, I would like to thank you all for your love and support. Your prayers kept me going. To my late Father, Professor Uche Godwin Nzoko Anazodo (PhD), I dedicate this thesis to you and your legacy. You were my first research mentor. You taught me the dedication to the pursuit of knowledge - perseverance, self-motivation and self-regulation. You inspired me to seek till I find. Rest in peace.

Table of Contents

Abstract	i
Co-Authorship Statement.....	iv
Acknowledgments (if any).....	vi
Table of Contents	viii
List of Tables	xiii
List of Figures	xiv
List of Appendices	xvi
List of Abbreviations	xvii
1 CHAPTER 1	1
1.1 Clinical Relevance	1
1.2 Coronary Artery Disease.....	2
1.2.1 Cardiovascular disease defined.....	2
1.2.2 Review of coronary circulation.....	4
1.2.3 CAD impairment to coronary perfusion	7
1.2.4 Pathogenesis of coronary artery disease	8
1.2.5 Risk factors for coronary artery disease.....	11
1.2.6 Current therapeutic interventions.....	12
1.3 Cerebral hemodynamics.....	16
1.4 Brain changes associated with normal aging	19
1.4.1 Evidence of age-related changes in the brain	21
1.4.2 Neurobiology of normal brain aging.....	25
1.4.3 Effect of age on brain function	26
1.5 Brain changes associated with CAD and increased risk for CAD.....	27
1.5.1 Changes in brain structure	28

1.5.2	Changes in brain function	29
1.6	The potential neuroplastic effects of aerobic exercise training	31
1.6.1	Defining physical fitness training	31
1.6.2	Effects of moderate intensity aerobic fitness training on brains of older adults.....	33
1.6.3	Plausible neurobiological mechanisms	36
1.7	Quantification of regional brain changes using MRI.....	38
1.7.1	VBM measurements of gray matter volume changes	39
1.7.2	Measuring cerebrovascular hemodynamics	41
1.8	Do local alterations in hemodynamics signify impairment in neuronal activity?.....	48
1.9	Thesis Outline	50
1.9.1	An investigation of changes in regional gray matter volume in cardiovascular disease patients, per and post cardiovascular rehabilitation (Chapter 2).....	50
1.9.2	Impaired cerebrovascular function in coronary artery disease patients, and recovery following cardiac rehabilitation (Chapter 3).....	51
1.9.3	Simultaneous whole-brain imaging of cerebral perfusion and glucose metabolism on a hybrid PET-MRI scanner (Chapter 4)	51
1.9.4	Conclusion and Future Work (Chapter 5).....	52
1.10	References.....	52
2	Chapter 2	82
2.1	Introduction.....	82
2.2	Methods.....	84
2.2.1	Participants.....	84
2.2.2	Clinical assessments of health	84
2.2.3	Clinical assessments of cardiac rehabilitation	85
2.2.4	MRI data acquisition.....	85

2.2.5	Voxel-based morphometry analysis	86
2.2.6	Statistical analysis	88
2.3	Results	89
2.3.1	Cardiovascular disease effects	89
2.3.2	Effects of cardiac rehabilitation	94
2.4	Discussion	97
2.4.1	Cardiovascular disease effects	97
2.4.2	CAD-related effects: Brain atrophy	98
2.4.3	Effect of rehabilitation: neuroplasticity	101
2.4.4	Study consideration.....	102
2.5	Conclusion	104
2.6	References	104
3	Chapter 3	110
3.1	Introduction:.....	110
3.2	Materials and Methods:.....	111
3.2.1	Participants.....	111
3.2.2	Experimental design.....	112
3.2.3	Clinical measurements	113
3.2.4	MRI data acquisition.....	114
3.2.5	Perfusion-weighted analysis	115
3.2.6	Assessment of structure-independent CBF effects	117
3.2.7	Statistical analysis	119
3.3	Results.....	120
3.3.1	Study demographics.....	120
3.3.2	Baseline clinical measures	121

3.3.3	Baseline brain imaging: Cardiac disease effects.....	123
3.3.4	Cardiac rehabilitation effects	126
3.4	Discussion.....	127
3.4.1	Study considerations	132
3.4.2	Conclusion	134
3.5	References.....	134
4	Chapter 4.....	139
4.1	Introduction.....	139
4.2	Materials and Methods.....	141
4.2.1	Participants.....	141
4.2.2	PET-MRI image acquisition	142
4.2.3	MR attenuation map (μ -map) generation and PET image reconstruction.....	144
4.2.4	Image Analysis.....	145
4.3	Results.....	147
4.3.1	Study Participants	147
4.3.2	Evaluation of MRAC methods.....	148
4.3.3	Correlations of perfusion to glucose uptake	151
4.4	Discussion.....	156
4.5	References.....	162
5	Chapter 5	167
5.1	Summary of Findings.....	167
5.1.1	Changes in Brain Structure Associated with Cardiovascular Disease....	167
5.1.2	Impact of Cardiovascular Disease on Brain Hemodynamics	168
5.1.3	Potential Neuroprotective Benefits of Cardiac Rehabilitation.....	168

5.1.4 Can CBF Measured with ASL Serve as a Suitable Marker of Brain Function	169
5.2 Relevance of Findings.....	170
5.3 Future work.....	171
5.3.1 Longitudinal and Epidemiology studies	171
5.3.2 Exercise.....	172
5.3.3 Characterizing white matter structure in coronary artery disease patients.	173
5.4 References.....	173
Appendices	176
Curriculum Vitae	184

List of Tables

Table 1.1: Major Risk Factors for Coronary Artery Disease.....	11
Table 1.2: Interventions employed in management of CAD	12
Table 1.3: Potential benefits of regular exercise for cardiovascular disease patients.....	16
Table 2.1: Study participant characteristics. The mean and standard deviation are presented for clinical variables measured at baseline in CAD patients and controls.	90
Table 2.2: Local maxima of clusters of significant change in GM volume in the pre-CR CAD patient group compared to controls.	93
Table 2.3: Local maxima of clusters of significant change in GM volume in the CAD post CR (Post >Pre).	96
Table 2.4: Cluster of GMV recovery after 6 months of CR (N=24). Small volume correction ($p < 0.05$, FWE).	97
Table 3.1: Study demographics.....	122
Table 3.2: Results of multimodal voxel-by-voxel multivariate analysis.	126
Table 4.1: Study Demographics.....	148
Table 4.2: Group mean and standard deviation (std) of absolute and relative PETdx and PETdxbone activity concentration (kBq/ml) in regions of interest across the brain.	151
Table 4.3: Results of voxel-by-voxel Pearson correlation within thirteen regions of interest.....	154
Table 4.4: Results of independent samples t-test in gray matter comparing rCBF to rPET.	155

List of Figures

Figure 1.1: Vascular disease modulation of vasodilation mechanisms of coronary arteries.	6
Figure 1.2: Vascular disease modulation of vasoconstriction mechanisms of coronary arteries.....	8
Figure 1.3: A concise description of the pathogenesis of atherosclerosis	10
Figure 1.4: Time courses of CBF and ETCO ₂ during hypercapnia.	18
Figure 1.5: Illustration of overt age-related brain changes seen on structural MR images.	21
Figure 1.6: Axial images of CBF and CVR in a single subject.	42
Figure 1.7: Continuous ASL label and control conditions.	43
Figure 2.1: Differences in GMV between CAD patients and age-matched controls measured at baseline.	92
Figure 2.2: GMV changes over time in CAD patient pre and post CR.	95
Figure 3.1: Illustration of the pipeline for multimodal voxel-wise multivariate analysis of variance performed to determine the singular effect of CAD on regional CBF.	119
Figure 3.2: Regions of interest analysis from voxelwise-comparisons.	125
Figure 3.3: Regions of differences in regional CVR compared between CAD patients and controls at baseline.....	125
Figure 3.4: Regions of differences in regional CBF compared in CAD patients before and after CR.	127
Figure 4.1: Illustration of a Dixon+bone μ -map generated in a representative subject..	149

Figure 4.2: Line profile	150
Figure 4.3: Regions of interest group means percent relative difference (% RD).....	150
Figure 4.4: Whole-brain group maps of relative perfusion and relative glucose uptake.	152
Figure 4.5: Whole brain voxel-by-voxel comparison between rCBF and rCMRglc	153

List of Appendices

Appendix A: An Overview of the Optimized VBM approach as implemented in SPM8.....	178
Appendix B: Copyright Agreement information	181
Appendix C: Ethics Approval	182

List of Abbreviations

- α - labelling efficiency
- λ - blood/tissue water partition coefficient
- τ - label duration
- ω - PLD = post labelling delay
- ΔM - Perfusion-weighted
- 2/3D - two/three-dimension
- ACE - angiotensin-converting enzyme
- AD - Alzheimer's disease
- ANCOVA - Analysis of covariance
- ASL - Arterial spin labelling
- BDNF - Brain-derived neurotrophic factor
- BMI - Body mass index
- BOLD - Blood -oxygen- level-dependent
- BPM - Biological parametric mapping
- BR - breathing rate
- CABG - coronary artery bypass graft
- CAD - coronary artery disease
- CASL - Continuous arterial spin labelling
- CBF - Cerebral blood flow
- CBV - Cerebral blood volume
- CIMT - Common carotid intima media thickness
- CMRglc - Glucose consumption

CMRO₂ - Cerebral metabolic rate of oxygen

CO₂ - Carbon dioxide

CR - Cardiac rehabilitation

CSF - Cerebrospinal fluid

CT - Computed tomography

CTAC - Computed tomography-based attenuation correction

CVD - Cardiovascular disease

CVR - Cardiovascular reactivity

DTI - Diffusion tensor imaging

DARTEL - diffeomorphic anatomical registration using exponentiated Lie

EF - Ejection fraction

EPI - Echo-planar imaging

ETCO₂ - end tidal carbon dioxide

F - Flow

FA - Fractional anisotropy

FDG - ¹⁸F-labeled fluorodeoxyglucose

FDR - False discovery rate

FOV - Field of view

FWE - Family-wise error

FWHM - Full-width-half-maximum

GRASE - Gradient-and-spin-echo imaging

GM - Gray matter

GMV - Gray matter volume

H₂¹⁵O - Radioactive water

HbA1c - glycated hemoglobin

HDL - High density lipoprotein

hs-CRP - high-sensitive C-reactive protein

ICBM - International consortium on brain mapping

LCA - Left coronary artery

LDL - Low density lipoprotein

M₀ - Net equilibrium magnetization

MoCA - Montreal Cognitive Assessment

MCI - Mild cognitive impairment

METs - Metabolic equivalent of tasks

MI - Myocardial infarction

MNI - Montreal Neurological Institute

MPRAGE - Magnetization Prepared Rapid Acquisition gradient-echo sequence

MRAC - MRI-derived attenuation correction

MRI - Magnetic resonance imaging

NO - Nitric oxide

P₁ - inflow pressure

P₂ - outflow pressure

P_aCO₂ - Partial pressure of carbon dioxide

pCASL - Pseudocontinuous arterial spin labelling

PASL - Pulsed arterial spin labelling

PET - Positron emission tomography

PET_{dx} - PET data attenuation corrected using Dixon sequence

PET_{dxbone} - PET data attenuation corrected using enhanced Dixon method

PCI - Percutaneous coronary intervention

RCA - Right coronary artery

RD - Relative density

RF - Radiofrequency

SNR - signal to noise ratio

SPM - Statistical Parametric Mapping

tSNR - Temporal signal-to-noise ratio

TA - total acquisition time

TE - Echo time

TR - Repetition time

TI - Inversion time

T1 - Longitudinal relaxation time constant

T1_b - T1 of blood

TCD - transcranial Doppler ultrasound

UTE - Ultra-short echo

VBM - voxel-based morphometry

VO₂max - maximal oxygen consumption

WM - White matter

WMH - White matter hyperintensities

1 CHAPTER 1

"A good head and a good heart are always a formidable combination" Nelson Mandela

1.1 Clinical Relevance

Cardiovascular disease is one of the most prevalent chronic diseases among older adults¹, accounting for the second highest healthcare cost in Canada². One in five Canadians over the age of 65 has a history of coronary artery disease (CAD), which is the most prevalent form of cardiovascular disease³. As the population of older adults continues to climb exponentially⁴ and the survival rate for CAD continue to increase, an overwhelming need to understand disease effects and improve quality of life in the elderly are imperative. At the societal level, age-related chronic diseases such as CAD pose an obvious financial and social burden, while at the individual level, the gradual loss of function from chronic diseases pose a threat to successful aging.

Rowe and Kahn defined successful aging as a combination of the ability to maintain a low risk for disease and disease-related disability, preserve a high mental and physical functional capacity and continue an active engagement in life⁵. Considerable efforts are being made to achieve successful aging in older adults with CAD, including primary and secondary interventions aimed at minimizing risks of recurrence and improving overall cardiovascular function³. However, recent evidence⁶ points to the possibility of comorbid neurological impairments that could threaten the mental capacity of CAD patients and curtail their active engagement in life.

It is well known that brain atrophy, cerebral hypoperfusion, white matter disease and impairments in cognitive function are associated with risk factors for CAD in asymptomatic older adults⁶. Longitudinal and epidemiological studies in individuals with

increased risk factors for CAD have concluded that risk factors such as hypertension, diabetes and high blood cholesterol advance age-related changes in the structure and function of the brain⁷⁻¹². Some researchers have gone as far as suggesting that dementia, including Alzheimer's disease, could be associated with vascular disease, since chronic vascular dysfunction can limit adequate blood supply to the brain and in doing so trigger a cascade of events that eventually lead to neurodegeneration^{13,14}. However, the *direct* impact of CAD on the structure and function of the aging brain has not yet been characterized. Identifying the impact of CAD on the brain could aid in devising strategies that facilitate successful aging in these individuals such as cognitive remediation and physical activity.

The interaction of CAD, age and cerebrovascular degeneration is complex. Non-invasive neuroimaging techniques are crucial not only in studying this complex interaction, but they are becoming clinically relevant for identifying, monitoring and assessing clinical outcomes of CAD effects on the brain. This introductory chapter will define CAD, discuss concepts of normal brain aging, review premature brain aging associated with CAD risk factors, and discuss the role of physical activity in mediating successful aging. A section is also dedicated to the discussion of the brain imaging techniques used in this thesis to characterize CAD effects on the brain.

1.2 Coronary Artery Disease

1.2.1 Cardiovascular disease defined

The World Health Organisation defines cardiovascular disease as a class of diseases that affect the heart and blood vessels within the heart, within the brain and

around the body (www.who.int, Fact sheet 317). In 2009 an estimated 1.6 million Canadians had heart disease or stroke and 1 in 3 adults over the age of 65 were diagnosed with heart disease². The cost of care for cardiovascular diseases in Canada was over \$22.2 billion in 2000² and is projected to rise as the number of older adults continue to increase¹⁵. Similar enormous economic burden for cardiovascular disease has been reported for other industrialized countries such as the United States^{15,16}, Europe^{15,16}, Australia¹⁵ and Japan¹⁶. Cardiovascular disease can be grouped into two types;

- I. Diseases due to atherosclerosis, namely, coronary artery diseases including myocardial infarction, cerebrovascular diseases such as stroke, and vessel diseases such as hypertension and peripheral vascular disease.
- II. Diseases due to damage to the heart or disorder of the heart, namely: cardiac arrhythmias, congestive heart failure, cardiomyopathy meaning abnormal heart muscle, congenital heart disease, which refers to malformation of the heart from birth defect, and rheumatic heart disease, which is due to damage to the heart muscle/valve from streptococcal bacteria⁴.

Atherosclerotic diseases are the most common form of cardiovascular disease, affecting mostly adults over the age of 65 and contributing to almost 80% of the entire cardiovascular disease burden⁴. Coronary artery disease, being the most prevalent form is an inflammatory response to atherosclerotic lesions in coronary arteries¹⁷. The rest of this section will focus on CAD and discuss the pathogenesis, risk factors, clinical presentation and current therapeutic interventions for CAD. First, a brief review of coronary circulation is presented, because abnormal circulation is a significant part of CAD pathophysiology.

1.2.2 Review of coronary circulation

This review is culled from Principles of Anatomy and Physiology textbook by Tortora and Derrickson¹⁸ and review articles by Ramanathan and Skinner¹⁹, Feliciano and Henning²⁰ and by Muller-Delp²¹.

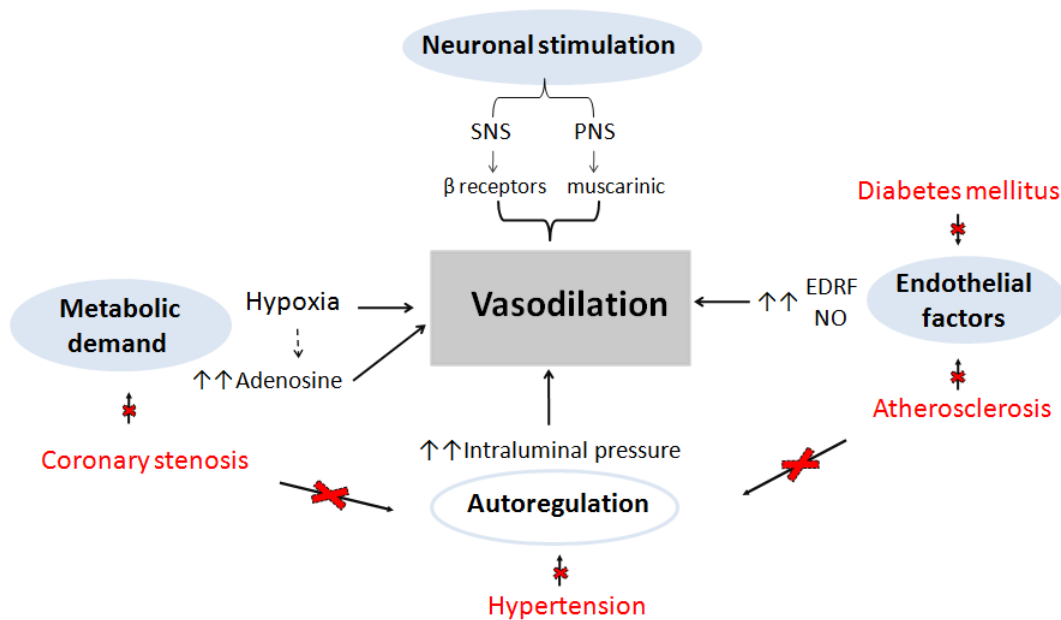
All circulation to the heart comes from the aortic root, which branches out to the right coronary artery (RCA) and left coronary artery (LCA). The RCA and LCA run on the surface of the myocardium and are referred to as the epicardial or conduit vessels, as they offer very little resistance (5%)²⁰ to coronary flow. The RCA and LCA branch out to more epicardial vessels that divide further into smaller branches as the vessels travel deeper to supply the transmural myocardium. These subendocardial vessels are the resistance vessels that dilate during increased myocardial oxygen demand to increase coronary blood flow. The RCA and branches from the RCA supply blood to the right atrium, right ventricle, posterior wall of left ventricle, and posterior portion of the interventricular septum. On the other hand, the LCA and branches from the LCA supply blood to the left atrium, lateral and anterior wall of left ventricle, and remainder of the interventricular septum. The junction at the aortic root where the coronary arteries arise are controlled by the aortic valve which opens during systole to allow blood flow to the systemic and central arteries, and closes during diastole to allow blood flow to the coronary arteries. Therefore unlike all arteries in the body, which are perfused during systole, the coronary arteries are mostly perfused during diastole. This is because, during systole the contraction of heart muscles compresses the cardiac tissue including the subendocardial coronary arteries, and only when the heart muscle is relaxed at diastole is the myocardium perfused by the coronary arteries. The increased left intraventricular

pressure during systole forces the aortic valve to open to the aorta while closing to the coronary arteries, and when the pressure in the left ventricle rapidly drops during diastole, the aortic valve closes to the aorta and opens to the coronary arteries. The back pressure from this pushes blood into the coronary arteries, perfusing the myocardium.

At rest, coronary blood flow is approximately 250 ml/min¹⁹ or 0.8ml/min/g of heart muscle¹⁹, which can increase up to fivefold during exercise. The heart extracts up to 80% of the oxygen in arterial blood, nearly three times the amount consumed by the rest of the body¹⁹. Hence, the energy demand of the myocardium is met primarily by increased blood supply via vasodilation of resistance coronary vessels. The magnitude of the increase in coronary blood flow to accommodate increased demand is often referred to as coronary reserve. Coronary reserve is governed primarily by coronary vascular tone, which in turn is regulated by local metabolic demand, neuronal influences (sympathetic and parasympathetic stimulation) and flow-dependent endothelial control (figure 1.1). For instance, hypoxia directly triggers vasodilation of coronary arteries and also the accumulation of adenosine, a potent vasodilator. At rest, autoregulatory mechanisms maintain a constant coronary blood flow over a range of mean arterial pressures from 45 to 150 mmHg²⁰ and is essentially mediated by the same factors mentioned above that mediate coronary reserve. If pressure changes beyond this range, coronary blood flow becomes directly dependent on perfusion pressure. In general, coronary vascular tone is determined by the coordination of all three control mechanisms (figure 1.1 and 1.2) and the influence of each mechanism varies along the vascular tree. Aging can modify the regulation of coronary circulation inducing gradual reduction in blood flow at rest and with increased demand. Endothelial dysfunction, arterial stiffness and left ventricular

hypertrophy are some of the age-related changes that can affect coronary circulation^{22,23}. CAD, on the other hand, exacerbates age-related dysfunction in regulation of coronary circulation.

Figure 1.1: Vascular disease modulation of vasodilation mechanisms of coronary arteries.



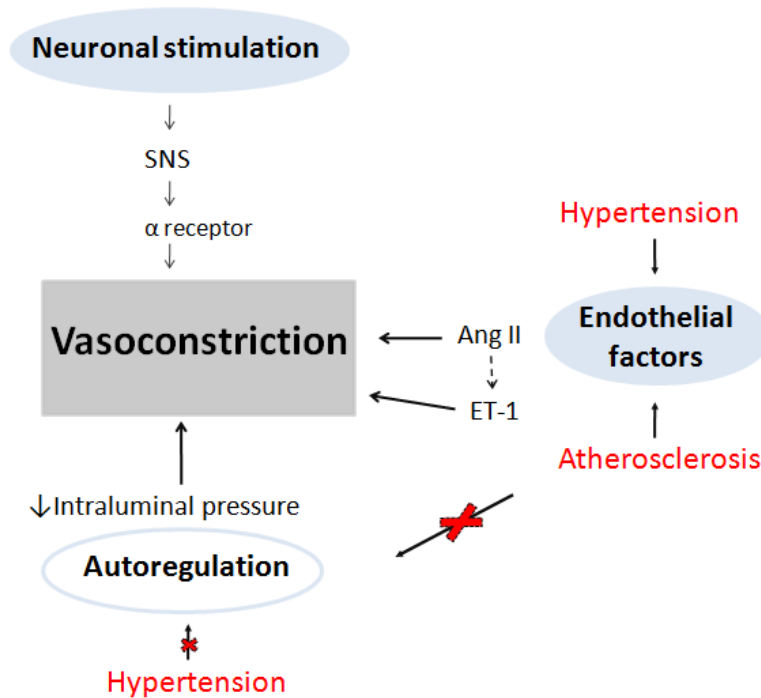
EDRF = Endothelium-derived relaxing factor. Solid lines indicate direct influence, broken lines indicate secondary influence and red diagonal crosses indicates impairment of normal regulation.

Adapted from Ramanathan and Skinner¹⁹

1.2.3 CAD impairment to coronary perfusion

The impact of CAD on coronary circulation is significant to the function of the heart and equally important to the supply of blood to the brain. The brain, much like the heart, does not maintain a reservoir of energy substrates to help meet its energy demand. Hence, an increase in local metabolic demand will result in rapid hyperaemia to the corresponding tissue. As such, the brain and the heart are highly sensitive to insufficient supply of blood flow, that is, ischemia. In the heart, ischemia can be a consequence of narrowed vessels, referred to as coronary stenosis, or impairment in vasodilatory mechanisms due to atherosclerosis, diabetes or hypertension²⁴. Vascular disease processes affect not only the vasodilation mechanisms, but they can impair the normal regulation of coronary circulation at rest and modulate vasoconstriction factors, as shown in figures 1.1 and 1.2. Atherosclerosis facilitates endothelial dysfunction by inhibiting the release of nitric oxide (NO)^{20,21}, blunting vasodilation, and by increasing the production of vasoconstrictor factors such as endothelin^{20,21}. Furthermore atherosclerosis can cause transient narrowing of coronary arteries, known as coronary spasm, by abolishing NO-mediated vasodilation and by increasing vasomotor tone at rest²⁰.

Figure 1.2: Vascular disease modulation of vasoconstriction mechanisms of coronary arteries



ET-1 = Endothelin-1. Solid lines indicate direct influence, broken lines indicate secondary influence and red diagonal crosses indicates impairment of normal regulation.

Adapted from Ramanathan and Skinner¹⁹

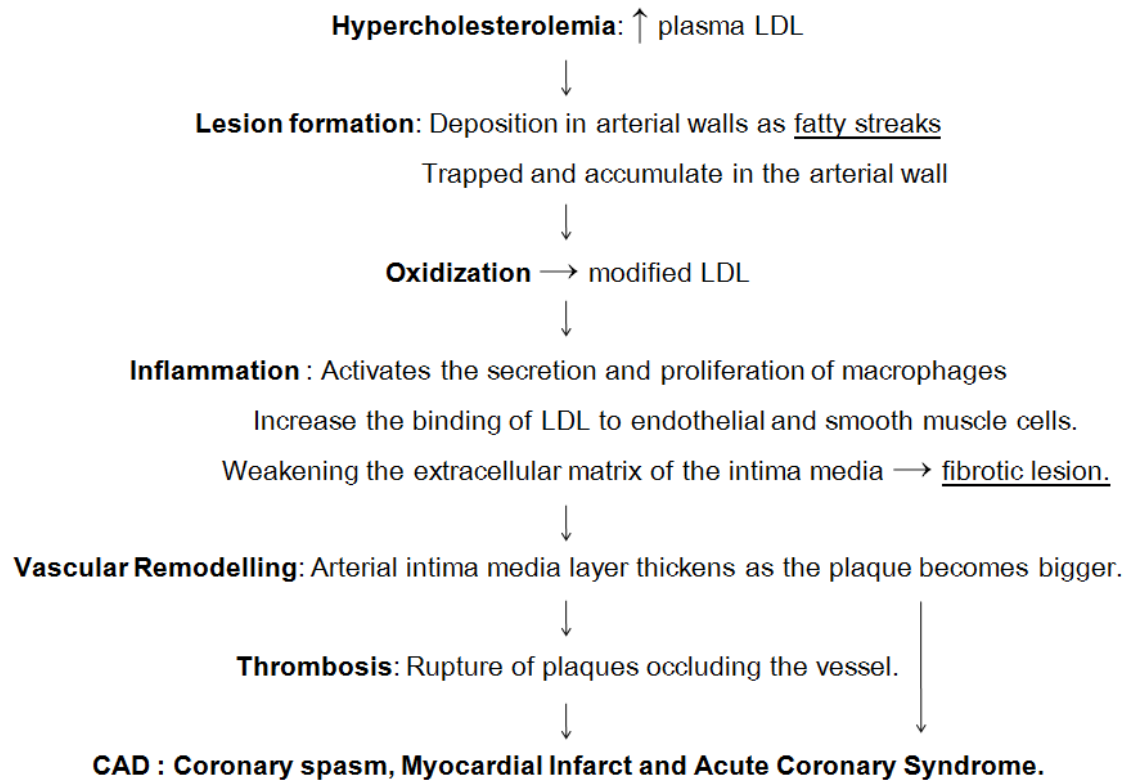
1.2.4 Pathogenesis of coronary artery disease

Atherosclerosis is the primary cause of CAD. It often occurs within the epicardial coronary arteries and is viewed as an inflammatory process in response to vascular injury²⁵. Since the mid-19th century, the accumulation of lipids in arterial wall was known to produce atherosclerotic lesions²⁵, but the notion of vascular injury was only proposed in the mid 1980's²⁵. Atherosclerosis is a progressive syndrome that starts off

with infiltration of lipoproteins in the intima of coronary arteries called fatty streaks, advancing to build up of lipids that adhere to smooth muscle lining forming plaques^{17,25-27}. The plaques disrupt the endothelium, finally triggering an inflammatory response to the fibrous caps of the plaques which then rupture and occlude vessels^{17,25-27}. This process is complex and beyond the scope of this thesis. Below, a schematic of the simplified atherosclerotic process is shown in figure 1.3.

The common clinical outcomes of atherosclerosis in the heart include ischemia, tissue necrosis or myocardial infarction (MI), unstable angina, acute coronary syndrome and sudden death, to name a few, all of which are symptoms associated with CAD²⁷. Typical markers of atherosclerosis include measures that detect downstream effects of atherosclerosis-mediated inflammation/injury such as plasma high-sensitive C-reactive protein (hs-CRP)²⁸, interleukin-6 (due to increased level of cytokines) and tumor necrosis factor- α ²⁹. In addition, non-inflammatory markers associated with arterial stiffness such as aortic pulse wave velocity^{29,30}, ankle-arm index²⁹, arterial (brachial) intima media thickness³¹ are also usually used in assessing atherosclerosis risk and burden.

Figure 1.3: A concise description of the pathogenesis of atherosclerosis



For detailed description consult the following references 17, 25-27.

These markers have been shown to be effective predictors of CAD²⁹. Interestingly, recent evidence have also shown that the common carotid intima media thickness (CIMT) can be used as surrogate marker of generalized atherosclerosis^{31,32}, and adding CIMT measurements to typical risk predictors can improve 10-year CAD risk stratification³³. Atherosclerosis is not only significant in pathology of CAD but it is associated with abnormal changes in the structure and function of the brain, and will be discussed further in section 1.5.

1.2.5 Risk factors for coronary artery disease

Age is the most important predictor of atherosclerotic diseases. Other well known risk factors attributed to CAD are listed in the table 1.1³⁴⁻³⁸. These risk factors are used in identifying individuals at increased risk for CAD. In Canada, a comprehensive program for diagnosis and treatment of atherosclerosis disease, and prevention of cardiovascular disease, based on these risk factors is managed by the Canadian Cardiovascular society³⁴. It is important to note that these risk factors are also associated with structural and functional impairments in brains of older adults, as will be discussed further in section 1.5.

Table 1.1: Major Risk Factors for Coronary Artery Disease

Non-modifiable

Age and Gender: Men \geq 40 years old or women \geq 50 years old

Genetics: Family history of premature CAD in first-degree relative

Modifiable

Hyperlipidemia : LDL $>$ 5.0mmol/L, total cholesterol to HDL ratio $>$ 5

Hypertension: systolic $>$ 140 mmHg or diastolic $>$ 90mm Hg

Diabetes mellitus

Obesity and physical inactivity: increased waist circumference or BMI $>$ 27 kg/m²

Evidence of atherosclerosis: hs-CRP $>$ 2.0 mg/L

Smoking

Compiled from references³⁴⁻³⁸

1.2.6 Current therapeutic interventions

Interventions for CAD can be classified as either primary therapeutic and/or secondary preventative interventions. A list of the main current interventions and promising therapeutic options are listed in table 1.2. The majority of primary interventions are geared towards improving or restoring coronary blood flow, while secondary interventions are employed to minimize risks and maintain coronary function. A number of these interventions have been shown to interact with cerebral blood flow regulation or transiently affect brain functions such as cognitive processing (table 1.2).

Table 1.2: Interventions employed in management of CAD

Pharmacotherapy :can be both primary and preventative

1. Lipid lowering and thrombolytic therapy

a) Statins:

- Reduction of CAD risk³⁹ by inhibiting hepatic production of cholesterol, thereby reducing further thickening of vessel wall diameter^{40,41}.
- Reverse endothelial dysfunction in coronary vessels⁴⁰
- Lower levels of anti-inflammatory markers such as hs-CRP^{40,41}.
- Associated with increase in cerebral blood flow⁴¹ and lower risk for vascular dementia^{41,42}.

b) Anti-inflammatory :

- Include antiplatelets and anticoagulants.
- Inhibit the formation of occlusive thrombus by preventing aggregation of platelets⁴⁰.
- A notable example is salicylates such as aspirin.
- The effect on CAD risk management is still unclear⁴⁰.
- Evidence of less cognitive decline in high-risk CAD patients⁴³ although contradictory.

2. Nitrates: Mediate release of NO and cause vasodilation, improving coronary blood flow⁴⁴.

3. Antihypertensive

a) Calcium channel blockers :

- Used in secondary prevention of CAD⁴⁵
- Cause vasodilation and lower ventricular pressure load⁴⁵

b) Beta-blockers:

- Used in treatment of CAD symptoms including acute coronary syndrome and stable angina
- Block SNS receptors, produce positive inotropic effects (increase myocardial contractility) and prevent left ventricular dysfunction⁴⁶.

c) ACE inhibitors:

- Reduction of MI and left ventricular dysfunction⁴⁷.
- Blocks angiotensin-converting enzyme (ACE) action in the renin-angiotensin-aldosterone system⁴⁷.
- Treatment in hypertensive with ACE inhibitors or similar acting angiotensin receptor blockers have been associated with less decline in cerebral blood flow over time⁴⁸ and less decline in cognitive function⁴⁹.

Coronary revascularization techniques

- Includes percutaneous coronary intervention (PCI) and coronary artery bypass graft (CABG).
- Used in patients with unstable angina or acute MI as primary intervention to reduce the death or MI⁵⁰.
- Transient memory loss and reduction in psychomotor speed have been reported after first few weeks of CABG and resolves 1- 3 months after surgery^{51,52}.

Cardiac rehabilitation (CR): secondary prevention programs aimed at minimizing CAD risks include^{34,53}.

1. Smoking cessation
2. Low sodium and sugar diet
3. Caloric restriction
4. Regular moderate- intensity physical activity and low-impact aerobic exercise (30-60 minutes most days of the week) ⁵⁴.

Prescribed exercise training interventions: combine moderate-to-vigorous intensity aerobic exercise and resistance training as recommended by the American College of Sports Medicine and American Heart Association for older adults⁵⁵.

1. Aerobic exercise: at a frequency of 3-5 days/week and an intensity of 50-80% of exercise capacity lasting for a duration of 20 - 60 minutes using modalities such as walking, treadmill or cycling exercises⁵⁴.
2. Resistance exercise: at a frequency of 2-3 days/week and an intensity of 10-15 repetitions per set lasting a duration of 1-3 sets of 8-10 different upper and lower body exercises using modalities that include various forms of weight lifting and strength training⁵⁴.

Promising future interventions

1. Genomics-based therapy: Molecular targeting of pharmacological agents to pathways associated with proteins that encode genes important for lipid production, to improve responsiveness. For instance clopidogrel is an antiplatelet being investigated in patients with genetic variants in cytochrome P-450, an enzyme required for metabolism of clopidogrel⁵⁶. In these patients the antiplatelet effect of the drug is reduced.
2. Stem Cell therapies: preclinical studies and clinical trials are ongoing to determine the benefit of stem cell therapies in improvement of cardiovascular function by replacement or repair of damaged cardiac tissue with progenitor cells derived from various embryonic sources⁵⁷. Clinical trials have shown some reduction in death and recurrence of MI in stem cell transplants⁵⁷. However there are several challenges to this form of therapy including the potential malignant transformation of the cells⁵⁷.

Cardiac rehabilitation (CR) programs are central to the management of CAD and involve multifaceted behavioural modification interventions aimed at reducing the risk of new MI or recurrence of MI after a coronary event⁵⁸. In Canada, CR programs are largely hospital-based with a median duration of 5 months although home-based programs are also offered as an alternative. Studies have shown that the use of CR led to reductions of 15%⁵⁸ to 50%⁵⁹ in mortality rates associated with cardiovascular disease. The core components of CR include nutritional counselling, risk factors management, psychosocial

interventions and exercise training⁵⁴. Moderate intensity exercise training is a key component of CR programs, and the singular effect of exercise on CAD includes, reduction in cardiac mortality and morbidity, reduced risk for CAD and increased myocardial function⁶⁰. Even, small gains in exercise capacity of 1 ml/kg/min⁻¹ peak oxygen consumption or 1 metabolic equivalent are associated with 10% reduction in cardiac mortality⁶¹. Furthermore there is strong evidence that exercise training can reduce arterial stiffness in patients with CAD. A review of 5 studies relating exercise training to arterial stiffness in CAD patients, reported consistent findings of associations of improved cardiorespiratory fitness and reduced pulse wave velocity and augmentation index, another measure of arterial stiffness, in CAD patients after completion of exercise training programmes⁶². Table 1.3 adapted from the Mayo Clinic proceedings editorial by Franklin and McCullough⁶³, highlights the therapeutic effects of regular physical activity on cardiovascular disease. These effects are potentially the results of improved endothelial function, angiogenesis, proliferation of collateral vessels and regression of coronary atherosclerosis following repeated bouts of exercise⁶⁴⁻⁶⁶. There is increasing evidence that suggests that moderate exercise could have neurorehabilitation effects as well. Section 1.6 will discuss the neuroplastic effects of aerobic exercise training in older adults, and in adults with increased risks for CAD. In chapters 2 and 3, the potential capacity of CR-based exercise programs in reversing brain abnormalities observed in CAD patients are demonstrated.

Table 1.3: Potential benefits of regular exercise for cardiovascular disease patients.

<u>Anti-atherosclerotic</u>	<u>Antithrombotic</u>	<u>Anti-ischemic</u>	<u>Antiarrhythmic</u>
Improve lipids	↓ Platelet aggregation	↓ Myocardial oxygen demand	↑ Vagal tone
↓ Blood pressure	↓ Fibrinogen	↑ Coronary flow	↓ Adrenergic activity
↓ Adiposity	↑ Fibrinolysis	↓ Endothelial dysfunction	↑ HR variability
↓ Inflammation	↓ blood viscosity	↑ Nitric oxide release	

Adapted from reference⁶³

1.3 Cerebral hemodynamics

Brain perfusion is tightly regulated by several complex mechanisms that ensure constant supply of oxygenated blood to meet the brain's energy demand. These mechanisms dynamically adjust cerebral blood flow (CBF) to match changes in neuronal activity (metabolic regulation), cerebral perfusion pressure (autoregulation), sympathetic nerve activation (neurogenic regulation) and/or vasoactive factors (chemoreceptor regulation)⁶⁷. Under normal conditions, the resultant flow (F) is determined by the differential perfusion pressure (ΔP) and resistance (R) to flow in accordance with Poiseuille's law⁶⁸ (Eq. 1):

$$F = \frac{(P_1 - P_2)\pi r^4}{8\mu L} = \frac{\Delta P}{R} \quad (1)$$

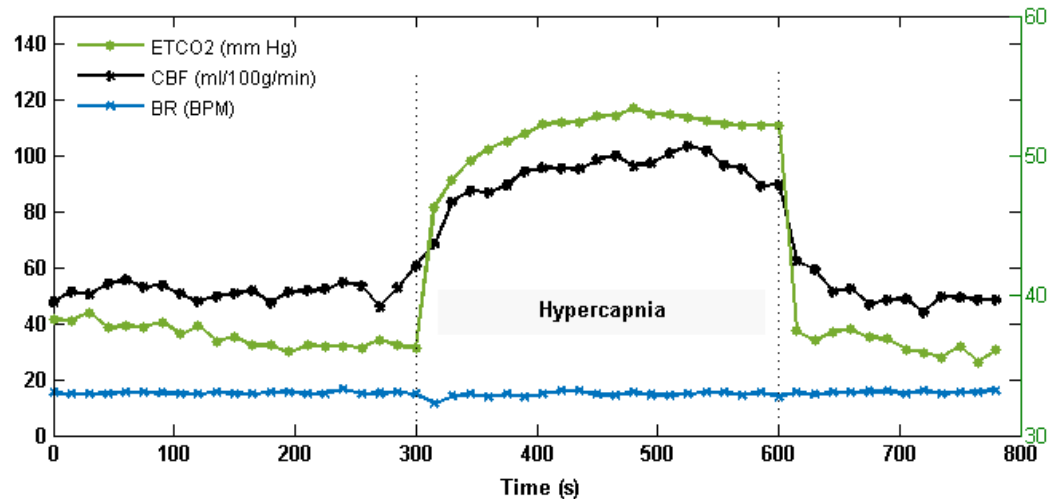
Where P_1 is the inflow pressure or mean arterial blood pressure, P_2 is outflow pressure or intracranial pressure which includes central venous pressure and CSF pressure, while r , L

and μ describe the vessel's resistance to flow and are the radius and length of the vessel, and the viscosity of the fluid within the vessel, respectively. It follows that CBF is determined by the difference in cerebral perfusion pressure and cerebrovascular resistance. Such that alterations to cerebral perfusion pressure or vascular resistance outside the normal basal range will alter CBF levels and activate regulatory mechanisms to preserve constant flow. For instance, cerebral autoregulation maintains a relatively constant CBF over a range of mean arterial pressures from 60 to 150 mm Hg⁶⁹. If perfusion pressure drops beyond the lower limit or increases above the upper limit, CBF will increase or decrease accordingly. All regulatory mechanisms ultimately exert their influence on vascular smooth muscles of the intracranial arterioles, to increase CBF by vasodilation or decrease CBF by vasoconstriction. The magnitude of changes in CBF, and to a lesser extent the corresponding blood volume, is greater during vasodilation than vasoconstriction⁷⁰. As such, regional measurements of basal levels of CBF and vascular resistance of cerebral vessels to a vasodilatory stimuli provide crucial markers of regional cerebrovascular health⁷¹⁻⁷³.

One of the most potent vasoactive stimuli is CO₂. Increased concentration of blood CO₂ increases partial pressure of arterial CO₂ (P_aCO₂) and changes blood tissue pH, inducing relaxation of vascular smooth muscles directly or via secondary mechanisms that release vasoactive agents such as prostaglandins and nitric oxide⁶⁷. Inhalation of CO₂ can trigger changes in pH and vessel diameter within 10s and subsequent changes in CBF within 30s of the beginning of inhalation, with CBF reaching peak values around 2 min⁶⁷. The relative increase in CBF per mm Hg increase in P_aCO₂ is around 5%/mm Hg⁷⁴. This is illustrated in figure 1.4 showing the time courses of end-

tidal CO₂ (ETCO₂), a surrogate marker of P_aCO₂, and CBF for a 60-year-old male inhaling 6% CO₂ for 5 min.

Figure 1.4: Time courses of CBF and ETCO₂ during hypercapnia.



Time courses of ETCO₂, total gray matter CBF and breathing rate (BR) measurements in a 60 year old male acquired every 15s over 13 min. Hypercapnia was induced using 6% CO₂+ 21% O₂+ 73% N₂ for a duration of 5 min. Time-averaged ETCO₂ for normocapnia and hypercapnia were 37 ± 0.8 and 51 ± 3.8 mm Hg, respectively, corresponding to 37% increase in ETCO₂ and 78% increase in CBF relative to baseline. Breathing rate was maintained at around 15 breaths per minute (BPM) during both capnia conditions using paced-breathing (metronome) to prevent hyperventilation.

This rapid response of CBF to CO₂ makes cerebrovascular CO₂ reactivity an excellent means of probing cerebral hemodynamic alterations. Cerebrovascular CO₂ reactivity (CVR) can be described as a measure of the response of the brain's microvasculature to CO₂ stimulus, typically an elevation of arterial CO₂ tension (i.e., hypercapnia). Hypercapnia manipulations using CO₂ inhaled concentrations of 5-8% - resulting in an P_aCO₂ increase of up to 15 mm Hg -are considered safe⁶⁷ and severe adverse respiratory, cardiovascular or neurological effects to short-term exposure are

observed at concentrations $\geq 10\%$ ⁷⁵. Furthermore, mild hypercapnia manipulations are low cost, easy to implement, relatively reproducible and highly sensitive to hemodynamic impairments by 'steal phenomenon', where vessels that are maximally dilated will have reduced capacity to increase CBF⁷⁶. However, it should be noted that the acute effect of mild hypercapnia on brain oxygen metabolism⁷⁷ and neuronal activity⁶⁷ is unclear and being investigated by various groups.

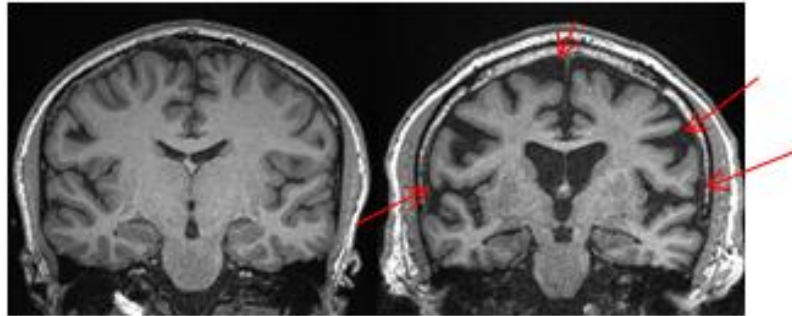
1.4 Brain changes associated with normal aging

Aldred Scott Warthin (1928) described normal aging as a 'syndrome' - a complex period of retrogression that *"consists, therefore, of a combination of organ - and tissue - involutions, shown histologically by well-defined tissue-lesions and manifested clinically by descending function-curves."*⁷⁸ This process he argues, starts gradually after maturation, develops throughout mid-life, accelerates by age 70 at which time tissue involutions start to become 'clinically apparent', and terminates in biological or pathological death⁷⁸. In the brain, various studies using tissue histology and morphometric (CT and MRI) techniques, support Warthin's assertion of age-related tissue involution⁷⁹. All structures in the brain⁸⁰, with the exception of the brainstem⁸⁰⁻⁸² undergo consistent progressive age-related involution⁸⁰. Decline in total and regional volume have been reported for gray matter (GM)⁸³ and white matter (WM)⁷⁹ following maturation around the age of 30 years old, as well as impaired CBF⁸⁴⁻⁸⁶, cerebral metabolic rates of glucose (CMR_{glc})^{85,87} and oxygen (CMRO₂)^{85,86}. The pattern of age-related brain changes vary across the brain with some regions showing a linear trend, while others show a non-linear or curvilinear pattern, and some show preservation or delayed age

effect^{80,88-90}. For instance, the frontal regions particularly the prefrontal, show the earliest and greatest loss of volume with age^{79,91}, while the hippocampus and cerebral WM show an initial increase in volume prior to an accelerated decline much later in life⁸⁰, which could signify compensation⁹², while the limbic structures show significant GM preservation relative to other areas⁸⁹. This reflects the selective vulnerability of certain brain regions to aging, and possibly pathological effects⁷⁹.

It is widely accepted that the topological pattern of normal aging follows an anterior-to-posterior gradient⁹³, affecting first, regions that mature last during postnatal brain development⁸⁹. Myelination, for instance, occurs in the cerebellum prior to the cerebral lobes and in the occipital prior to the frontal lobes, continuing up to fifth decade of life⁹⁴. While loss of myelin sheath have been found predominantly in the anterior regions of the brain of older subjects compared to younger ones^{95,96}. This 'last-in-first-out' principle, also referred to as the 'retrogenesis hypothesis'⁹³ is observed in normal aging, as alterations in GM and WM structure⁹³ and impairments in selective domains of cognitive function⁹⁷. This topological pattern of normal aging is what differentiates it from pathological aging processes such as dementia⁹⁸⁻¹⁰¹. The following sections will outline evidence of age-related retrogenesis in the brain, describe possible neurobiological contributions to normal brain aging, and outline effects of aging on brain function. It is important to note that given the large variation in study samples (age range, exclusion/inclusion criteria, sample size), methodology (i.e. cross-sectional or longitudinal), image acquisition, and image analysis techniques, comparison of observations among studies and overall generalization of results are limited.

Figure 1.5: Illustration of overt age-related brain changes seen on structural MR images.



T1-weighted images of a young (left, 24 years old male) and older (right, 68 years old male) healthy participants, illustrates common differences in brain structures typically attributed to normal aging. Brain atrophy, sulcal widening and enlarged ventricles (shown in red arrows) are evident in the older brain. Images were derived from data collected as part of my thesis project.

1.4.1 Evidence of age-related changes in the brain

Brain atrophy¹⁰⁰, ventricular enlargement¹⁰²⁻¹⁰⁵ and increase in white matter hyperintensity⁹¹ are overt appearances of normal aging easily detectable in structural MR images, as exemplified in figure 1.5, in a young and older subject randomly selected from data acquired during my thesis project. On average, the total GM volume (GMV) decays by 2-3% per decade^{105,106}, where the frontal lobe being one of the highest, decreases at a rate of around 5.5% per decade¹⁰⁷. Reductions in GMV^{87,89,90,103,104,108-110} and cortical thinning^{93,111,112} related to aging are found more often in the frontal and parietal regions¹¹³, with minimal involvement of the cerebellum^{82,114}, temporal lobe¹¹³ and subcortical regions including the limbic⁸⁹ structures, and general preservation of the brainstem^{81,82} and occipital lobe¹¹⁵.

The hippocampus and entorhinal cortex known for their significance in memory processing^{116,117} and vulnerability to Alzheimer's disease (AD), also experience age-

related brain atrophy^{80,93,100,105,118}. However, normal aging of these medial temporal lobe structures are more subtle compared to the drastic changes seen in AD⁹³. Their volumes are relatively stable throughout young adult and midlife, after which they decline exponentially from an annual rate of atrophy of ~0.05% in midlife to ~2% after age 60⁹³. For comparison, the annual rate of atrophy reported for MCI and AD subjects in the hippocampus and entorhinal cortex are 2.39% and 3.64%, respectively⁹³.

Likewise, deficits in WM volume also seem to appear much later in life, after the age of 70 and decline more rapidly than GMV^{88,119,120}, following similar spatial pattern to GMV loss^{119,121}. In healthy elderly adults, loss of WM volume is more prominent in prefrontal regions^{118,121-123}, followed by regions within the parietal cortex^{118,121} and inferior temporal regions^{121,123}. Furthermore, the presence of focal areas of increased signal intensity on T2-weighted MR images, known as white matter hyperintensities (WMH), are common in deep WM and periventricular WM regions of older adult brains^{91,119,124,125}. Subcortical and periventricular WMH are prevalent after the age of 60 years, occurring in nearly 90% and over 60% of individuals, respectively^{124,125}. Although, the severity and extent of WMH lesions are associated with increased age¹²⁴, and linked to cognitive impairments in memory^{125,126} and processing speed^{126,127}, the increased risks for vascular disease associated with aging such as hypertension, are greater indicators of WMH than aging alone¹²⁵.

On the other hand, results of WM microstructural integrity assessed using MRI measurement of WM diffusivity, such as diffusion tensor imaging (DTI), offer more consistent findings of age differences in WM¹¹⁹ and provide better support of the retrogenesis hypothesis^{91,119}. Diffusion-weighted indices including fractional anisotropy

(FA), radial diffusivity and axial diffusivity have been used in numerous studies to quantify white matter structural integrity during brain development, normal aging, and in various disease states¹²⁸⁻¹³⁰. Reductions in FA could signify degradation of WM structure, inflammation, or loss of glial cells, while increased radial and axial diffusivities suggests demyelination and axonal loss or damage¹²⁸⁻¹³⁰. Decreased FA in older adults compared to younger adults have been reported primarily in anterior WM including uncinate fasciculus bundles of frontal WM, cingulum bundle in parietal, WM tracts in anterior portion of temporal lobe, but not in the inferior longitudinal fasciculus of the posterior temporal lobe connecting to the occipital^{101,131-136}. Increased radial and axial diffusivities have also been found in the anterior portion of the corpus callosum (genu)^{134,135,137}. Hasan et al. measured diffusivity in 24 WM fiber tracts in 119 healthy subjects from 6 to 68 years old and demonstrated a U-curve relationship between increasing age and radial diffusivity¹³⁸. An initial decline in diffusivity was observed post-adolescence up to the age of 40, which the authors suggested was reflective of sustained "*progressive*" myelination, followed by rapid increase in diffusivity with advancing age, which was attributed to "*regressive*" and "*degenerative*" natural aging¹³⁸. A similar but inverted U-curve was also observed in tracts measured by FA¹³⁸. These diffusion-weighted MRI observations are supported by histological examinations that have shown myelin and axonal loss in various areas of the brains after midlife, in both human^{95,96,139} and animal¹⁴⁰ studies. When taken together, measurements of WM macro- and micro-structure suggest that brain regions with recent myelination following maturation are more prone to age-related myelin degeneration.

Similar to GM and WM structural deficits, an anterior-to-posterior gradient in GM hypoperfusion have be found with advancing age^{8,9,86,137,141–145}, starting as early as 20 years old and progressing steadily through middle and old age^{8,9,84,86,146}, at an annual global rate of nearly -0.4%^{137,143,144}.The greatest association with normal aging, were found in the frontal and parietal lobes, followed by the temporal cortex, while minimal relative changes are seen in the occipital or portions of the cerebellum^{8,9,86,137,141–144,147}, even after correction for signal dilution from partial volume effects^{137,142,143}. These age-related changes in GM CBF are usually independent of underlying brain atrophy or cortical thinning¹⁴³, suggesting that separate neurobiological mechanisms could mediate brain atrophy and cortical hypoperfusion, such as vascular aging^{23,148}. Aging affects not only resting GM CBF, it can impair the brain's ability to respond rapidly to an increase in task-demand^{9,86,149,150}. This is evident in reduced CVR^{86,149–151}, decreased CMRglc^{85,87,145,147,152}, and in increased oxygen extraction^{85,86} with advanced age. Lu et al demonstrated that age-related decline in CVR observed in the prefrontal cortex, appeared earlier and at a much greater rate of decay compared to CBF⁸⁶. These age-related impairments in cerebrovascular hemodynamics and in metabolism of brain energy substrates could explain associations of aging to cognitive decline in domains of memory and attention^{153–155}. However, age-related changes in CBF, CVR or CMRglc are controversial given that some studies have reported no change^{156–158} (after partial volume correction)^{159,160}, or an increase⁸ with increase in age. Investigations of subtle change in CBF or CMRglc related to aging are largely limited by the ability of current imaging techniques to spatially resolve GM/WM-specific voxel signals and minimize partial volume effects^{161,162}. In general, structural and functional brain changes associated with

normal aging are likely restricted to anterior portions of brain, areas that are involved in memory, executive functioning and attention.

1.4.2 Neurobiology of normal brain aging

The neurobiological processes that mediate the structural and functional changes associated with age are not fully understood. Aldred Scott Warthin (1928) postulated that age-related changes are "*...due to a loss of growth-energy, so that the cell loss exceeds the regenerative powers, and numerical and quantitative atrophies ensue.*"¹⁷⁸ This speaks not only to changes in the brain's energy demand and supply with age⁸⁵, but also to the restorative or plastic capacity of the brain following age-related tissue involution¹⁶³, as will be described in section 1.6. Earlier propositions suggested that normal brain aging was likely a result of neuronal loss^{94,95,164} secondary to cerebral hypoperfusion^{141,165} and subsequent hypometabolism¹⁶⁶. However, recent evidence demonstrates that normal brain aging is more likely to arise from loss of dendrites (spine and arborization), decrease in synaptic pruning and alterations in neurotransmitter response over time as the brain struggles to maintain energy demands in the face of shrinking supply (for review see Dickstein et al¹⁶⁷). Significant reductions in synaptic density and the number of synapses have been reported in the prefrontal¹⁶⁸⁻¹⁷⁰, superior temporal and precentral cortices^{170,171} in older humans compared to young, and in aged nonhuman primates^{172,173}, canines¹⁷⁴ and rats¹⁷⁵. In addition, age-related reductions in glutamatergic¹⁷⁶, serotonergic¹⁷⁷ and cholinergic¹⁷⁸ neuroreceptor density and binding sites of frontal regions, along with reductions in myelination^{95,96}, contribute to disruptions in brain signalling pathways¹⁶⁷, which are observed as alterations in functional connectivity of frontal networks such as

the default mode network^{179–183}. Furthermore, molecular and microvascular changes associated with aging including, increased oxidative stress, atherosclerotic plaque formation, vessel stiffness, increased arterial blood pressure, inflammation and decreased capillary diameter and density, contribute to the attenuation of resting CBF, and create impairments in cerebrovascular tone^{23,148}, further limiting the brain's ability to meet energy demands in task-intensive regions such as in the frontal cortex.

1.4.3 Effect of age on brain function

The cumulative effect of various changes in brain structure, metabolism and cerebrovascular function resulting from normal aging can impact the performance of cognitive function^{184,185}. Poorer performance on tests for verbal fluency, visuospatial function, working memory, executive function and selective attention are associated with increased age^{186,187}. Although brain regions (prefrontal, medial temporal and parietal) negatively associated with aging are also associated with cognitive control, evidence correlating cognitive decline to structural and functional decline in these brain regions is limited¹⁸⁸. Recent meta-analyses of 80 studies, in which brain activity was measured in young and old healthy adults during performance of cognitive tasks, provide a clearer understanding of the brain's response to normal aging^{189,190}. Both reviews point to the compensatory mechanisms employed by the brain of older adults when engaged in cognitive processing^{189,190}, which could be through modes of bilateral prefrontal cortex activation (i.e. Hemispheric Asymmetry Reduction in OLDER Adults, HAROLD) or a combined increase in anterior brain activity and decrease in posterior regions (i.e. Posterior-Anterior Shift in Aging, PASA)¹⁸⁵. Compared to young adults, older adults

have increased activity largely in the prefrontal cortex, less activity in the occipital during perceptual tasks and no difference in the parietal lobe, even when performance was equal between groups¹⁹⁰. In addition, older adults that performed better tend to have an increase in the left prefrontal activity while those who performed poorly activated only the right prefrontal¹⁹⁰. These patterns of cognitive activation in old adults support views of increased recruitment of brain resources (HAROLD or PASA) during demanding tasks to maintain normal performance in the presence of structural and functional deficits^{185,189}. It remains to be seen if over-recruitment of frontal regions in older adults is indicative of successful cognitive aging or a mark of inefficient activation of specialized brain networks (dedifferentiation)¹⁸⁵. It is quite possible that compensatory activations are attempts at re-organizing frontal brain networks that are structurally¹⁹¹ and functionally¹⁹² altered during aging.

1.5 Brain changes associated with CAD and increased risk for CAD

"The secondary pathologic conditions that are made possible and favoured by primary involution process are many and of great clinical importance, because it is usually through some one of these that the senile individual is kept from achieving a biological death. They fall into several well-defined group: 1) secondary to vascular changes...." A S Warthin, 1928⁷⁸.

The decline in regional brain structure and function in older adults with risks factors for CAD is greater than the decline attributed to normal aging⁶, often affecting

posterior brain regions and cognitive domains that are relatively stable during normal aging. A systematic review of neuroimaging findings from 77 studies that investigated brain changes related to CAD risk factors in asymptomatic individuals, concluded that risk factors of hypertension, type II diabetes, obesity and hyperlipidemia, independently contribute to adverse changes in the structure and function of the brain⁶. More importantly, an increase in the number of risk factors appears to increase the magnitude of brain changes⁶. The impact of CAD risk factors appear to be more regional than global⁶. In this section, evidence of regional brain atrophy, impaired hemodynamics and abnormal brain metabolism related to CAD and disease risk factors will be briefly presented.

1.5.1 Changes in brain structure

Regional brain atrophy in the frontal, temporal and parietal gyri are associated with hypertension^{193,194}, type II diabetes¹⁹⁵⁻¹⁹⁷ and obesity⁶. A voxel-based morphometry (VBM) study of 478 adults aged 60-64 years found an association between hypertension and decreased GMV in the medial frontal, superior frontal and superior temporal regions of male subjects, after controlling for effects of age and other vascular disease risk factors¹⁹⁴. In another study of 134 adults from 50-70 years old, higher systolic blood pressure was associated with decrease in GMV in the supplementary motor area, superior frontal gyrus, anterior cingulate and middle temporal regions in male subjects¹⁹³. No association between hypertension and brain volume were found among women subjects in both studies. Novak et al¹⁹⁷ and Last et al¹⁹⁵ reported lower GMV in the parietal and

occipital lobes of type II diabetics compared to non-diabetics, and more recently a VBM study¹⁹⁸ found decreased GMV in the temporal and precentral gyri as well.

An increase in white matter lesions and a decrease in regional WM volume are associated with hypertension^{199–202} and diabetes^{195,197,198,200,203}. Ventricular widening have also been observed in hypertensive^{204,205} and diabetic²⁰⁶ patients compared to age-matched controls. Even in earlier on in life, higher systolic blood pressure have been linked to white matter injury and decreased regional GMV in individuals under the age of 50²⁰⁷. However, it appears that higher systolic blood pressure may not be associated with longitudinal changes in brain volume^{199,208} or in the frequency and severity of white matter lesions^{200,202,203}. Rather, higher diastolic blood pressure in midlife are linked to greater longitudinal decline in GMV²⁰⁸ and increased frequency and severity of white matter lesions^{200,202}.

1.5.2 Changes in brain function

Individuals with uncontrolled or untreated hypertension have been shown to have regional hypoperfusion in the superior, inferior²⁰⁹ or and orbito-frontal cortices, anterior cingulate, and temporal and occipital regions compared to normotensive controls^{210–213}. Accelerated decline in regional CBF over time has also been observed in hypertensive adults compared to older normotensive adults²¹¹ and could be linked to uncontrolled increases in blood pressure⁴⁸ and increased arterial stiffness^{209,214}. One study of type II diabetics reported reductions in CBF under resting conditions and during hypercapnia in the temporal and parieto-occipital regions. Although in the diabetic group, hypertension

was associated with lower CBF including during hypercapnia¹⁹⁵. Another recent study in a larger cohort (541) of middle aged adults, found lower CVR in the cingulate and medial prefrontal lobe in individuals with elevated blood pressure compared to normotensive subjects, but no difference in regional CVR in individuals with elevated blood glucose or blood cholesterol compared to subjects with normal levels⁷³. Hypertension is also associated with significant reductions in CMRglc in the striatum²¹⁵ and with increased insulin resistance in the frontal, cingulate, parietal and temporal lobes²¹⁶.

This abnormality in glucose metabolism in diabetics was linked to poor performance on memory tasks and an activation pattern that seem to demonstrate compensatory attempts during delayed recall tests²¹⁶. Impairments in memory as well as in executive control, psychomotor speed and attention are reported in hypertensive adults^{193,199,204,212} and in individuals diagnosed with cardiovascular disease^{217,218}. In cardiovascular disease patients, one study demonstrated accelerated decline over time in visuospatial skills, memory and overall cognitive function, and a linear decline in language, attention and psychomotor speed²¹⁷. It is quite possible that cognitive dysfunctions associated with vascular disease are related to cerebral hypoperfusion and abnormal distribution of CBF during increased demand. For instance, in hypertensive subjects, decreased CBF in the superior frontal, anterior parietal and temporal was associated with decreased performance in attention and psychomotor processing²¹². In addition, during working memory tasks, hypertensive compared to normotensive subjects had lower increase in posterior parietal CBF²¹⁹, displayed attempts at recruitment of other cortical regions, and increased contralateral flow²²⁰. These regional flow alterations could be mediated by vascular aging that are exacerbated by cardiovascular disease. Cerebral

hypoperfusion is linked to increased arterial stiffness²²¹, and increased evidence of atherosclerosis²¹⁴, and is associated with compromised neuronal viability²²². In addition, higher carotid intima media thickness and increased pulse wave velocity are linked to poorer memory performance and lower scores on processing speed and executive function^{218,223}. However, the pathogenesis of brain alterations associated with cardiovascular disease and disease risk factor are not well known. Equally, it is unclear what impact cardiovascular disease, specifically diseases of atherosclerotic origin such as CAD; have on the structural integrity and functional capacity of aging brains.

1.6 The potential neuroplastic effects of aerobic exercise training

1.6.1 Defining physical fitness training

Physical activity contributes to lower risk for CAD⁵³ and improves brain health even in late adulthood and in chronic sedentary individuals²²⁴. Physical activity can be defined as movements of the body produced by skeletal muscles that results in expenditure of energy²²⁵. Physical exercise is purposeful physical activity that is planned and repetitive²²⁵. While, physical fitness "is a set of attributes that people have or achieve" (Caspersen et al²²⁵, page 128) and can be defined as "the ability to carry out daily tasks with vigor and alertness, without undue fatigue and with ample energy to enjoy leisure-time pursuits and to meet unforeseen emergencies" (Caspersen et al²²⁵, page 128). Cardiorespiratory fitness is a health-related component of physical fitness defined as the ability of the circulatory and respiratory systems to supply oxygen during sustained physical activity²²⁵. Individual exercise capacity and fitness level are determined

primarily by age, sex, exercise habit and cardiovascular health status²²⁶. Capacity and fitness level are measured using graded exercise tests such as treadmill or cycle ergometer, in absolute terms as metabolic equivalent of tasks (METs) meaning the amount of oxygen consumed at rest, where 1 METs approximates 3.5 mL of oxygen per kilogram of body weight per minute²²⁶. However, the gold standard measure of exercise capacity and fitness is the relative measurement of maximal oxygen consumption (VO_2max) during dynamic exercise, a level where the greatest amount of oxygen is consumed despite an increasing workload²²⁶. For example, normal VO_2max of a 50-59 year old male is roughly 36 mL/kg/min or 10 METs²²⁶. The amount of VO_2max in healthy humans is governed largely by the amount of systemic oxygen delivery to skeletal muscles, which is in turn, determined by the maximal cardiac output²²⁷.

The recommended form of physical fitness in older adults and adults with cardiovascular disease are moderate-to-vigorous intensity aerobic exercise and muscle-strength training activities⁵⁵. In absolute and relative terms, moderate-to-vigorous intensity exercises are between 3 to 6 METs⁵⁵ or 50 to 80% of VO_2max ⁵⁵ or a score of 12-16 on the 20-scale Borg rating scale of relative perceived exertion²²⁶. An improvement in cardiorespiratory fitness by 5.4 ± 1.2 ml/kg/min⁶¹ or an increase of 15 to 20%²²⁸ in peak oxygen consumption can be expected by cardiac patients enrolled in CR programs. However, perceived improvements in fitness level reported in various studies are difficult to compare, limited by heterogeneities in training intensities (low-moderate, vs. moderate-high), programme duration (4 -52 weeks), number of exercise sessions (36 or > 36 sessions), exercise modalities (aerobic vs. mixed of aerobics and strength training), patient fitness level on entry and modality of fitness testing (maximal treadmill

or cycle ergometer vs. predictive submaximal testing including modified treadmill tests, or 1-mile track walk test vs. self-reported physical activity questionnaires). These variations in aerobic training regimen and fitness testing also limit comparisons of neurovascular benefits associated with aerobic exercise training. In general, improvements are associated with higher exercise intensity and with programs consisting of 36 or more sessions of aerobic-based exercise or a combination of aerobic and resistance training⁶¹. Majority of the gains in cardiorespiratory fitness are achieved in the first 4-12 weeks of training and little or no further increase are observed after initial gain⁶¹. Submaximal testing using graded exercise protocols with shorter stages and smaller transitions between workloads are preferred for testing fitness level in cardiac disease patients²²⁶.

1.6.2 Effects of moderate intensity aerobic fitness training on brains of older adults

A review of studies examining the relationship between physical activity and brain volume in older adults outlined 9 studies where higher fitness level was associated with greater gray matter volumes in the anterior cingulate cortex, prefrontal, parietal and temporal regions, as well as the hippocampus^{224,229}. Notably, Colcombe et al (2003)²³⁰ showed that age-related decline in the prefrontal, parietal and temporal gray and white matter regions were moderated by higher aerobic fitness level. Compared to other brain areas, these regions also showed greater tissue preservation with increasing fitness level²³⁰, consistent with findings from other studies^{224,229}. It appears that regions that show the greatest rate of age-related decline in brain volume discussed earlier are also the

regions that are highly plastic and respond more readily to modifying effects of exercise. In the hippocampus, for instance, a study found an annual increase in volume of 2% in the anterior hippocampus of aerobically trained older adults compared to an annual decline of 1.5% in a stretching-toning control group²³¹. The increase in volume was associated with increased levels of serum brain-derived neurotrophic factor (BDNF) and improved performance in spatial memory tasks²³¹. In another study, peak VO₂ was positively associated with fractional anisotropy in the middle and posterior cingulum bundle²³² and with fractional anisotropy and radial diffusivity in the body and genu of the corpus callosum²³³ of brains of previously sedentary older adults.

Likewise, increases in CBF have been found in the hippocampus²³⁴, anterior cingulate cortex²³⁵ and posterior cingulate/precuneus²³⁶ of aerobically trained older adults. Four months of aerobic exercise showed increased connectivity between the hippocampus and anterior cingulate cortex in the trained group compared to healthy controls²³⁴. Increased brain network connectivity and improved network efficiency between fronto-temporal regions and within the default mode network and frontal executive networks are also demonstrated in aerobically trained older adults²³⁷. In addition, positive correlation between aerobic fitness and task-induced activation in the anterior cingulate, lateral prefrontal and lateral parietal regions are evident across various tasks for executive function and semantic memory retrieval, potentially mediated by increased regional brain volume²²⁹. However, Colcombe et al²³⁸ reported decreased activity in the anterior cingulate, left medial frontal and middle superior temporal in aerobically trained older adults performing conflicting response tasks, a probe of the attention-driven network. This finding was attributed to improved adaptations in the

attention network following exercise training²³⁸. It is quite clear that most domains of cognitive control in healthy older adults benefit from physical activity, with the greatest improvements seen in domains of executive function, while modest improvements are seen on tasks of attention and spatial memory, and limited effect on tasks for working memory²¹⁴.

In cardiovascular disease, 12-to-18 weeks of cardiac rehabilitation were associated with improved performance on executive function, psychomotor speed, attention and episodic memory tasks, and these improvements were preserved for up to 9 months after completion of a 12-week CR program²³⁹. Although, there is overwhelming evidence of the neuro-protective and neuroplastic effects of aerobic exercise in healthy older adults, the benefits of aerobic exercise, alone or as part of a CR program on brain structure and function in cardiovascular disease patients are not well known. In fact, only one study to date has linked aerobic exercise-based CR programs to regional changes in CBF and GMV in brains of cardiovascular disease patients. In that study, MacIntosh et al²⁴⁰, associated gains in fitness level (VO₂ peak) after 6-month CR program with baseline CBF in the left postcentral gyrus and baseline GM density in the right putamen. The effects of exercise training were not explicitly investigated. This highlights the need for research to investigate the neuroplastic efficacy of exercise-based CR programs.

It is not surprising that exercise can modify regional brain structure and cause selective changes in function as well. A number of studies have shown that skill training and learning modify structures within the adult brain²⁴¹. Learning-induced plasticity, for instance, has been shown in the occipito-temporal cortex of individuals trained to juggle²⁴². London taxi drivers were found to have larger posterior hippocampus volume

compared to controls and the enlargement was correlated to length of time spent driving a taxi cab, demonstrating the effect of navigational skill experience²⁴³. Interestingly, the effects of exercise are not only limited to motor areas, but also effects are significant in cognitive regions of the brain, signifying the potential salutary effects of exercise training in remedying pathological brain aging. It can be said that aerobic exercise training could potentially offer long-term neuroprotective benefits. This was demonstrated in a recent study where walking 72 blocks per week, equivalent to 9-15 km per week, was associated with greater GM volume in the inferior frontal, hippocampus and supplementary motor area nine years after exercise cessation²⁴⁴, and a reduced risk for developing cognitive impairments²⁴⁴. Meta-analyses of exercise training in older adults concluded that short-term exercise training when used as an intervention, offered cognitive benefits in individuals with dementia or cognitive impairments²⁴⁵ but not in older adults free from cognitive impairments²⁴⁶. In all, moderate intensity aerobic exercise is sufficient to elicit significant changes in the structure and function of the adult brain²²⁴.

1.6.3 Plausible neurobiological mechanisms

The neurobiological mechanisms of exercise-induced neuroplasticity or influence of exercise on cognition are unclear. Animal studies points to neurogenesis, angiogenesis, synaptic plasticity and upregulation of neurotrophins²⁴⁷ as possible neurobiological mechanisms. Rodent studies have shown that animals exposed to voluntary running have increased number of new neurons, spine density and higher levels of neurotrophin in the hippocampus compared to sedentary controls, which translated into enhanced learning and memory for Morris water maze tasks and improved performance on avoidance

tasks²⁴⁷. It is more likely that exercise induces synaptogenesis rather than neurogenesis or true increase in neuronal volume²⁴¹. Increased GM volumes observed post exercise training are likely due to expansion of the soma and nucleus of neurons and glial cells as well as increased synaptic density, dendritic branching and dendrite spine proliferation²⁴¹. These microstructural changes are potentially mediated by upregulation of neurotrophins that stimulate cell turnover and neuron proliferation including signal proteins such as BDNF, vascular endothelial growth factor (VEGF) and insulin-like growth factor 1 (IGF-1)²⁴⁷. Increased concentration and expression of BDNF in the hippocampus, frontal cortex, striatum and cerebellum after exercise training have been observed in mice²⁴⁸. When BDNF binding is blocked in mice performing water maze tasks, the effect of exercise is abolished²⁴⁹. Higher serum concentration of BDNF as a function of short-term exercise have been observed in a few studies of young adults²⁵⁰. Increased serum levels of BDNF have been observed in older adults after 1 year of exercise training and was associated with increased hippocampal volume²³¹. However, there is no clear indication that high-intensity exercise or long-term chronic exercise have positive effects on BDNF levels²⁵⁰.

A more immediate effect of exercise is angiogenesis. Exercise is associated with proliferation of new vessels and increase expression of signal proteins such as VEGF and IGF-1 involved in production of new vessels. Exercise-induced increases in capillary density and VEGF transcription have been observed in the motor cortex, hippocampus, striatum and substantia nigra of mice brains¹⁶³. Using magnetic resonance angiography, Bullitt et al²⁵¹ demonstrated that highly fit healthy older adults had an increased number of small vessels compared to low fit individuals. Another recent study found increased

cerebral blood volume (CBV) in the dentate gyrus of the hippocampus of young-to-middle-aged adults after 3 months of exercise training²⁵². Individuals with higher VO₂max had higher dentate gyrus CBV, but no change in performance of verbal learning (all-trial) or delayed recall memory tests²⁵². These observations corroborated observations of increased CBV in dentate gyrus of adult mice that performed 2 weeks of voluntary wheel running compared to non-exercising controls²⁵². Subsequent post-mortem studies found positive correlation between CBV and bromodeoxyuridine, a marker of newly born cells, in the dentate gyrus²⁵².

In general, there is substantial evidence supporting the notion of exercise-induced proliferation of neuronal cells and increased capillary density, synaptic density and expression of neurotrophic factors, all of which contribute to enhanced structural integrity and improved brain network connectivity/function.

1.7 Quantification of regional brain changes using MRI

This section describes the brain imaging techniques used in this thesis to measure differences in regional brain structure and function between coronary artery disease patients and age-matched controls. Regional differences in brain structure were measured on a voxel-by-voxel basis as local differences in gray matter density using a voxel-based morphometry (VBM) approach implemented in the Statistical Parametric Mapping (SPM) software (<http://www.fil.ion.ucl.ac.uk/spm/software/spm8/>), which is described in the first portion of this section. Next, arterial spin labelling (ASL), a non-invasive perfusion MRI technique for assessment of regional differences in CBF and CVR, is discussed. The last portion of this section presents the rationale for the use of ASL-based

hemodynamic measures as suitable substitutes for established markers of brain function such as glucose metabolism, and introduces a study performed to investigate the regional correlation of CBF to cerebral glucose metabolism, which is described in detail in chapter 4.

1.7.1 VBM measurements of gray matter volume changes

VBM is an automated technique for brain segmentation and voxel-by-voxel comparison of local tissue (typically gray matter) concentration/volume between groups of subjects or against a known parameter of interest. It has been widely used in studies of brain atrophy in normal aging⁹⁰ and neurodegenerative conditions²⁵³, as well as in investigations of neuroplasticity²²⁴. Data for VBM analysis are typically high-resolution (1-mm isotropic) three-dimensional T1-weighted anatomical MR images. T1-weighted imaging, which refers to sensitizing MR pulse sequences to the longitudinal relaxation time of water, is used as it is one of the primary means of generating MR contrast in different tissue types. In brain, good soft tissue contrast is achieved because of differences in the T1 values of GM, WM and CSF, which enables classification of the signal intensities of the various tissue types in each voxel. At a magnetic field strength of 3T, the T1 values of GM, WM and CSF are 1445 ± 119 , 791 ± 27 , and 4163 ± 263 ms, respectively²⁵⁴.

At the basic level, VBM involves the registration of individual T1-weighted images to a common space or template, an approach known as spatial normalization, followed by segmentation into GM, WM and CSF tissue classes, and spatial smoothing of GM segments prior to voxel-wise statistical analysis²⁵⁵. The optimized VBM method available in SPM8 employs additional preprocessing steps to exclude non-brain voxels

prior to spatial normalization and subsequent segmentation¹⁰⁸. It also provides options for computing GM volumes by scaling the voxel concentration by the amount of deformation estimated during spatial normalization, a process known as modulation¹⁰⁸. Modulation compensates for the non-linear effect of spatial normalization and preserves the total amount of GM signal in the normalized data¹⁰⁸. An extension of the optimized approach includes GM/WM templates generation for spatial normalization, by iterative averaging all subjects data using the DARTEL tool (diffeomorphic anatomical registration using exponentiated Lie)²⁵⁶.

In SPM, image segmentation is based on a modified mixture of Gaussians where tissue classes (GM, WM or CSF) are modeled by Gaussian distributions of signal intensities combined with *a priori* knowledge of the spatial distribution of different tissues in normal subjects, derived from probability maps²⁵⁷. With this approach, each voxel is assigned a particular tissue class based on the maximum likelihood of belonging to that class. Essentially, the segmentation step generates images where each voxel has *a posteriori* probability ranging from 0 to 1. The GM/WM spatial priors are either the default priors derived from a standard template (ICBM-152 template, Montreal Neurological Institute) or study-specific, generated from averaged data of all subjects in the study using DARTEL²⁵⁶. The default method for spatial normalization in SPM registers T1 images to a standard template by minimizing the residual sum of squared differences between the images and the template using a 12-parameter affine transformation²⁵⁸. Normalization via DARTEL is highly recommended as this increases the accuracy of inter-subject alignment²⁵⁹, especially for older brains where atrophy can bias matching of T1 images to standard template²⁶⁰. In general, SPM provides a complete

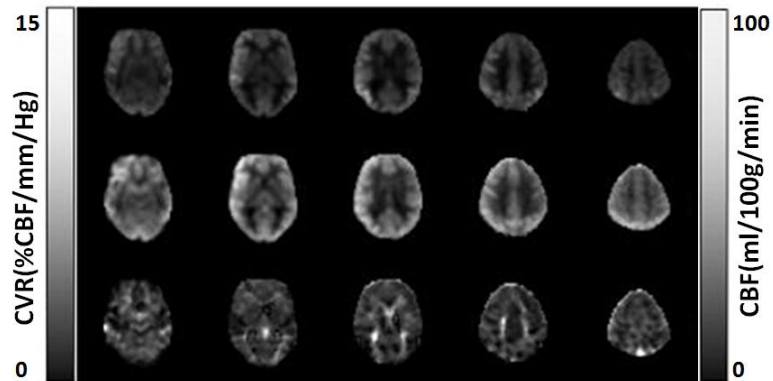
and efficient package for measuring macroscopic differences in GM volume across brain regions, including generation of individual GM volumes, inter-subject alignment to a common space and voxel-by-voxel statistical analysis using general linear models. The optimized VBM approach as implemented in SPM8 was used in this thesis for measurement of GM volume differences. This approach is described in detail in section A1 of the appendix.

1.7.2 Measuring cerebrovascular hemodynamics

The standard tool for assessments of CBF and CVR routinely in clinical practice is transcranial Doppler ultrasonography (TCD). However, TCD measures CBF velocity in large vessels, usually the middle cerebral artery, and equates blood velocity to CBF since the diameter of the vessel is thought to remain constant during vasoactive stimulation²⁶¹. Recently, Coverdale et al⁷⁰ demonstrated that during hypercapnia, the diameter of the middle cerebral artery can dilate by up to 16%, essentially underestimating CBF changes by 25%²⁶¹. In addition, TCD can only provide a global index of changes in CBF velocity, rather than an assessment of regional CBF changes. In contrast to TCD, ASL measures CBF directly and can provide images across the whole brain²⁶². Subsequent assessment of regional CVR can also be made, generally measured as the ratio of the change in CBF to the corresponding change in ETCO_2 ⁶⁷. Figure 1.6 illustrates typical images of CVR and CBF obtained from ASL imaging from a subject. Hypercapnia was induced by inhaling 6% CO_2 mixed in air for 5 min. However, ASL has inherent spatial resolution limitations that can affect regional mapping of hemodynamic changes at a voxel level. An alternative is BOLD functional MRI, which not only has

higher spatial resolution than ASL but also greater signal-to-noise ratio (SNR)²⁶³. However, the BOLD signal depends on multiple physiological parameters, CBF, CMRO₂ and CBV, which can be a confounder²⁶³. In addition, BOLD does not follow a linear relationship with ET_{CO}₂²⁶², unlike ASL (CBF), which only becomes nonlinear when ET_{CO}₂ falls within a hypocapnic range^{262,264}.

Figure 1.6: Axial images of CBF and CVR in a single subject.



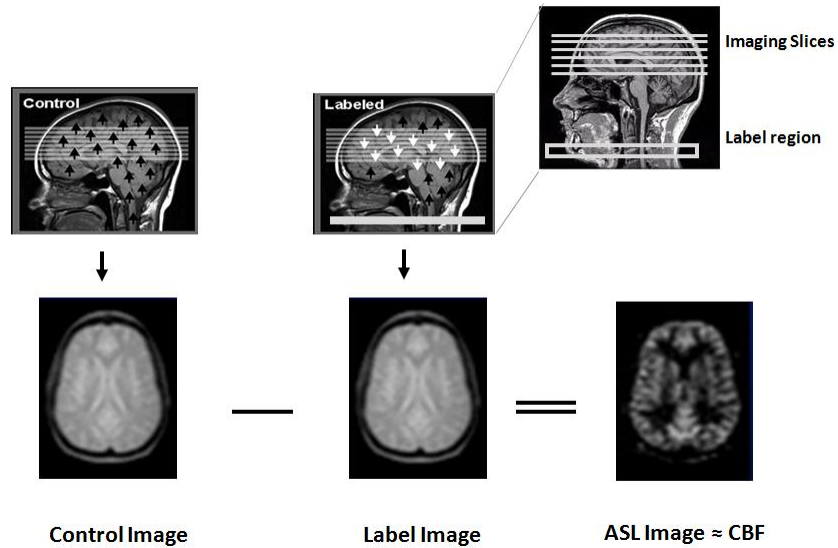
Axial images of CBF at normocapnia (top row), hypercapnia (middle row) and CVR (bottom row) across 5 slices in the brain in a single subject. CBF and CVR measures were derived from ASL imaging²⁶⁵.

1.7.2.1 An overview of ASL

Arterial spin labelling (ASL) is an MRI technique that provides the ability to measure CBF by manipulating the longitudinal magnetization of endogenous arterial blood water²⁶⁶. ASL is akin to PET-H₂¹⁵O²⁶⁷, the gold standard for CBF measurement, since both techniques use water as a flow tracer. For ASL, the flow signal is generated using RF pulses to invert ('label') the longitudinal magnetization of inflowing blood water protons in arteries. The labelled blood water flows into brain tissue, where it alters the local magnetization, resulting in a signal change that is proportional to CBF. A flow-

weighted (ΔM) image is generated by subtracting the labelled image from a control image, which removes signal contributions from ‘static’ brain magnetization (figure 1.7).

Figure 1.7: Continuous ASL label and control conditions.



Perfusion-weighted (ΔM) ASL image is the difference between label images, in which the longitudinal magnetization of arterial blood is inverted, and control images in which the magnetization of arterial blood is fully relaxed.

Because of the direct relationship between CBF and signal change, higher flow values will result in greater signal changes in the labelled image compared to the control image. However, due to the rapid loss of T1 label – blood T1 is approximately 1650 ms at 3T²⁶⁶ – the ASL signal decays rapidly. On the one hand, this enables serial imaging of CBF with temporal resolution of 5-10s, which is sufficient for capturing dynamic changes in CBF. On the other hand, the in-flow of labelled arterial blood only reduces the brain signal by approximately 1% and, therefore, multiple repetitions of label and control

images are acquired to improve SNR. Accurate CBF measurements are dependent on a number of factors including the time for labeled water to reach brain tissue, which is known as the arterial transit time, and labelling efficiency, which refers to the fraction of water magnetization that is inverted during the labelling procedure. These factors are discussed in the following section.

There are two main types of ASL labeling approaches, pulsed²⁶⁸ and continuous²⁶⁹. Pulsed ASL (PASL) inverts the magnetization of a large volume of inflowing arterial blood using a single short (5-10 ms) RF pulse, as such PASL has better temporal resolution and labeling efficiency, but poor SNR. Continuous ASL (CASL) employs long (1-3 s) RF pulses to invert inflowing spins at a single labeling plane. This increases SNR, but due to continuous RF pulse generation, CASL can deposit relatively high RF power into brain tissues. To combine the SNR of CASL and labeling efficiency of PASL with standard transmission RF body-coils available on all commercial MR scanners, a pseudo-continuous ASL (pCASL)²⁷⁰ approach was introduced. With pCASL, the long continuous RF pulse of CASL is replaced by a train of short RF pulses that mimic the adiabatic flow condition of traditional CASL, while minimizing magnetization transfer effects that cause large subtraction errors between the label and control conditions. The advantage of pCASL is it provides whole-brain coverage without the need for an additional labelling coil for CASL or the loss of labeling efficiencies typical of older labeling approach such as amplitude-modulated CASL²⁷¹. A recent white paper on the implementation of ASL for clinical applications recommended the quantification of CBF using a simplified one-compartment flow model with pCASL imaging²⁶⁶. Tancredi et al²⁷² demonstrated that the use of pCASL can provide more robust depiction

of the brain's response to hypercapnia, compared to PASL. A pCASL sequence²⁷³ was used to measure CBF in the studies described in chapters 3 and 4.

1.7.2.2 Quantification of CBF using ASL

CBF in each voxel of pCASL images can be calculated using the standard single compartment tracer kinetic model as outlined in equation(2)²⁷³.

$$CBF(ml/100g/min) = \frac{6000 \cdot \lambda \cdot \Delta M \cdot e^{\left(\frac{\omega}{T1_b}\right)}}{2\alpha \cdot M_0 \cdot T1_b \cdot \left(1 - e^{-\left(\frac{\tau + \omega}{T1_b}\right)}\right)}, \quad (2)$$

where ΔM is the perfusion-weighted signal, M_0 is the equilibrium magnetization, which can be obtained from the control images or by acquiring a separate image with no longitudinal relaxation effects and label condition. λ is the blood/tissue water partition coefficient (0.9 g/mL²⁶⁶), α is the labelling efficiency (85% for pCASL²⁷⁴ multiplied by 94% for background suppression), τ is the label duration, and $T1_b$ is the T1 of blood (~1650 ms at 3T)²⁶⁶. The final parameter, ω , is the post labelling delay (PLD), which refers to the time between the end of labeling period and image acquisition. It is included to enable all of the labeled water to reach the imaging volume, which minimizes the effects of arterial transit times²⁷⁵. This simplified model is based on the assumption that at the time of imaging the labelled water spins remains predominately in the microvasculature and decays with the T1 of blood²⁶⁶.

Although, the simplified one compartment model provides CBF values that correlate well with PET-H₂¹⁵O measurements²⁶⁷, the model assumptions are not likely to be strictly true²⁶⁶. For instance, water exchange between blood and tissue in the capillary

bed is not quite instantaneous, rather water permeability is limited by the tight junctions of the blood-brain barrier²⁷⁶. However, because the T1 values of blood and grey matter are similar at 3T, water exchange effects have minimal effects on the ASL signal^{273,276}, and the general view of the one-compartment model is that inherent errors from model assumptions are relatively small²⁶⁶.

1.7.2.3 Minimizing pCASL-CBF quantification errors

The accuracy of ASL CBF measurements can be degraded by a number of factors, of which the most important is the arterial transit time. For brain, transit times are usually between 1 to 2s²⁶⁶ and vary across brain regions. For instance, the longest transit times are found in WM, the occipital lobe and vascular border zones²⁷⁷. Transit times are affected by blood velocity, age, sex, and cerebrovascular disease, and prolonged times are associated with aging²⁶⁶ and disease²⁷⁸. Individual transit times can be measured by continuous sampling of inflowing blood using multiple inversions times²⁷⁸ or application of flow-sensitive spoiler gradients to separate vascular and tissue signal components, as implemented in the FEAST (flow encoding arterial spin tagging) technique²⁷³. However these efforts are time consuming and in most cases require separate CBF and transit time imaging. Alternatively, a PLD long enough to allow the entire tracer to reach the imaging plane negates the need for transit time mapping. The chosen value is set empirically based on the expected range of transit times within a population and SNR considerations. In older adults and individuals with prolonged transit times, such as in cerebrovascular disease, a PLD of 2s is recommended²⁶⁶.

Measurable errors in CBF quantification can also be attributed to inaccurate label efficiency and blood T1 values. Label efficiency can be affected by flow velocity, RF field inhomogeneity, transit time²⁷⁹, and vessel geometry²⁸⁰. Blood T1 is dependent on hematocrit, temperature and blood oxygenation level, and varies with age and sex²⁸¹. Label efficiency and blood T1 can be measured on each individual subject to minimize their effects²⁷⁵. Phase-contrast MRI can be used to measure global CBF and compared to whole-brain CBF values from ASL to estimate label efficiency²⁷⁹. Efficiency can be optimized if the labeling plane is kept at a distance of ~ 9 cm²⁷⁹ distal to the anterior commissural-posterior commissural line and slightly angled for high flow velocities (> 55 cm/s)^{280,282}. Subject-specific blood T1 values can be obtained using an inversion-recovery steady-state free precession MR imaging sequence to measure the T1 of venous blood²⁸¹.

The SNR can be improved using techniques such as background suppression and retrospective correction of head motion to reduce physiological noise contributions. Background suppression involves the use of inversion pulses during PLD to suppress static brain tissue and intravascular signals. Background suppression has been shown to increase temporal SNR by up to 75%²⁸³ but induces a slight attenuation of ASL signal. Better SNR can also be acquired using newer fast readout approaches. ASL imaging is typically performed with multislice 2D echo-planar imaging (EPI) imaging; however, 3-dimensional gradient-and-spin-echo (3D GRASE) imaging²⁸⁴ has been shown to improve the SNR by nearly 3 times²⁸³. As such, 3D GRASE pCASL images can be acquired with less averaging, *ergo* shorter acquisition times. However, 3D GRASE sequences are prone

to spatial blurring in the slice-encoding/ z-direction and have lower GM-to-WM CBF contrast ratio compared to 2D EPI readouts²⁸³.

Finally, physiological modulators of CBF such as hematocrit, caffeine, time of day, exercise, posture, age, sex, wakefulness and vasoactive pharmacological agents (indomethacin, acetazolamide) can confound hemodynamic measurements⁶⁷. The influence of these factors are minimized by imaging all subjects in the same examination state (supine, eyes-open, caffeine- and pharmacological-free) or during post-processing using covariate analysis methods.

1.8 Do local alterations in hemodynamics signify impairment in neuronal activity?

A long standing notion in functional imaging of neuronal activity is the close spatial correlation of CBF to glucose metabolism and oxygen consumption²⁸⁵, prompting the use of CBF as surrogate markers of function. Changes in CBF are also spatially and temporally correlated to neural activity²⁸⁶. Visual stimulation for instance results in an increase in CBF to the visual cortex, while motor stimulation produces localized hyperaemia in the motor cortex. Given the wide availability of MRI systems and relatively lower cost of performing MRI scans compared to PET, the clinical relevance of adopting ASL-CBF measurements as suitable makers of brain health is appealing. Cerebral glucose metabolism (CMRglc) measured using ¹⁸F-labeled fluorodeoxyglucose (FDG) and PET is considered the gold standard measure of brain function. Good agreement between regional CMRglc and regional CBF measured by PET and ASL respectively have been reported in healthy adults during rest²⁸⁷, and visual stimulation²⁸⁶.

In Alzheimer's disease patients, similar regional pattern of hypoperfusion and hypometabolism were observed when PET-FDG was compared to ASL-CBF²⁸⁸.

However, the extent of CBF and CMRglc coupling is unclear and recent evidence using improved ASL techniques outlined above, suggest that regional variations in correlation of CBF and CMRglc may exist at rest²⁸⁷. It is equally unclear if age and pathological disease disrupt the coupling of CBF with CMRglc. Goyal et al⁸⁵ recently demonstrated that changes in CMRglc and CBF are closely matched during normal development, diverging over time during adulthood. In adults, changes in CBF correlated more with CMRO₂ than CMRglc⁸⁵. A clear pattern emerging from recent correlation studies, is that regions of the brain associated with higher order cognitive processing and perception such as the default mode network including the medial prefrontal, lateral temporal, posterior cingulate cortex and precuneus, show the largest mismatch between flow and glucose metabolism^{147,287,289}. Whether the flow-glucose mismatch in these regions are a normal variant of resting brain function is unknown. It is quite possible that given the significance of these brain regions in fundamental functional organization of the brain, these regions might retain a relatively high CBF-to-CMRglc ratio compared to other brain regions at rest^{287,289}. It is interesting that these brain regions also have higher vulnerability to aging and vascular disease effects (see section on normal and pathological brain aging).

A potential source of variance in correlating regional CBF and CMRglc might be image registration errors. All previous comparison studies were carried out using separate PET and MRI scanners, requiring the need to accurately align images obtained from the two modalities, which were often acquired on different days. Since limitations in spatial

resolution occur in both modalities, errors in image alignment can increase the mismatch between CMRglc and CBF. Novel hybrid PET-MR imaging systems introduced in the last 5 years can offer insights into regional association of blood flow to brain metabolism, and affirm the use of ASL-CBF measures as suitable surrogate for PET-FDG in measurements of brain function.

1.9 Thesis Outline

This thesis work represents a concerted effort at investigating cardiovascular disease contributions to pathological brain aging within a cohort of coronary artery disease patients, and the potential benefits of physical activity. The significance of ASL perfusion imaging as surrogate marker of brain function was also investigated.

1.9.1 An investigation of changes in regional gray matter volume in cardiovascular disease patients, pre and post cardiovascular rehabilitation (Chapter 2).

Regional changes in GM volume associated with cardiovascular disease were assessed in coronary artery disease patients compared to age-matched controls. Evidence of improvements in brain structure with exercise was investigated after 6-month aerobic exercise training. Regional GM volume was measured using voxel-based morphometry. This work was published in *NeuroImage Clinical*, 2013; (3) 388-395 by: U. C. Anazodo, J.K. Shoemaker, N. Suskin, and K. S. St. Lawrence.

1.9.2 Impaired cerebrovascular function in coronary artery disease patients, and recovery following cardiac rehabilitation (Chapter 3).

Cardiovascular disease can impair the brain's hemodynamic function. To investigate regional changes in cerebrovascular hemodynamics, independent of underlying changes in brain structure, pCASL images were acquired at rest and during inhalation of moderate concentrations of CO₂ in the same cohort of coronary artery disease patients and age-matched controls. Regional comparisons in CBF and CVR were performed at baseline between patients and control, and within a subset of patients after 6 months of exercise training. Gray matter volume images from VBM were used as confounding variables to separate changes in structure from function. This work is under review in *Journal of Cerebral Blood Flow and Metabolism* [Manuscript ID: JCBFM-0365-15], submitted by Udunna C Anazodo, J Kevin Shoemaker, Neville Suskin, Tracy Ssali, Danny JJ Wang, and Keith S St. Lawrence.

1.9.3 Simultaneous whole-brain imaging of cerebral perfusion and glucose metabolism on a hybrid PET-MRI scanner (Chapter 4)

In this chapter, regional association of resting CBF and CMRglc were performed in healthy brains of older adults, using the novel integrated PET-MRI scanner. This hybrid scanner allowed simultaneous imaging of ASL-CBF and PET-FDG, minimizing potential misalignment errors. To improve the accuracy of the PET signals measured, a novel method for correcting PET signal loss (attenuation) due to absorption in the body or scatter by MR hardware is also presented. This chapter is based on the paper entitled "Feasibility of simultaneous whole-brain imaging on an integrated PET-MRI system

using an enhanced 2-point Dixon attenuation correction method" published in *Frontiers in Neuroscience*, 2015; (8): 434, by: Udunda C Anazodo, Jonathan D Thiessen, Tracy Ssali, Jonathan Mandel, Matthias Günther, John Butler, William Pavlosky, Frank S Prato, R Terry Thompson, and Keith S St. Lawrence.

1.9.4 Conclusion and Future Work (Chapter 5)

A summary of significant findings of the thesis are presented in this chapter. Clinical relevance and areas for further exploration are described.

1.10 References

1. Smith, J. *Chronic Diseases Related to Aging and Health Promotion and Disease Prevention: Report of the Standing Committee on Health*. (2012). at <<http://www.parl.gc.ca/content/hoc/Committee/411/HESA/Reports/RP5600467/hesarp08/hesarp08-e.pdf>>
2. *Tracking Heart Disease and Stroke in Canada*. (2009). at <www.phac-aspc.gc.ca>
3. Grace, S. L., Bennett, S., Ardern, C. I. & Clark, A. M. Cardiac rehabilitation series: Canada. *Prog. Cardiovasc. Dis.* **56**, 530–5 (2014).
4. World Health Organization. in (Mendis, S., Puska, P. & Norrving, B.) (2011).
5. Rowe, J. W. & Kahn, R. L. Successful Aging. *Gerontologist* **37**, 433–440 (1997).
6. Friedman, J. I. *et al.* Brain Imaging Changes Associated With Risk Factors for Cardiovascular and Cerebrovascular Disease in Asymptomatic Patients. *JACC Cardiovasc. Imaging* **7**, 1039–1053 (2014).

7. Beason-Held, L. L. *et al.* Baseline cardiovascular risk predicts subsequent changes in resting brain function. *Stroke*. **43**, 1542–7 (2012).
8. Beason-Held, L. L., Kraut, M. a & Resnick, S. M. II. Temporal patterns of longitudinal change in aging brain function. *Neurobiol. Aging* **29**, 497–513 (2008).
9. Beason-Held, L. L., Kraut, M. a & Resnick, S. M. I. Longitudinal changes in aging brain function. *Neurobiol. Aging* **29**, 483–96 (2008).
10. De Toledo Ferraz Alves, T. C. *et al.* Subtle gray matter changes in temporo-parietal cortex associated with cardiovascular risk factors. *J. Alzheimer's Dis.* **27**, 575–89 (2011).
11. Seo, S. W. *et al.* Cardiovascular Risk Factors Cause Cortical Thinning in Cognitively Impaired Patients : relationships among cardiovascular risk factors, white matter hyperintensities, and cortical atrophy. *Alzheimer Dis Assoc Disord.* **2**, 106–12 (2012).
12. Van Harten B, de Leeuw FE, Weinstein HC, Scheltens P, B. G. Brain Imaging in Patients With Diabetes: A systemic review. *Diabetes Care* **29**, 2539–2548 (2006).
13. Zlokovic, B. V. Neurovascular pathways to neurodegeneration in Alzheimer's disease and other disorders. *Nat. Rev. Neurosci.* **12**, 723–38 (2011).
14. De la Torre, J. . Critically attained threshold of cerebral hypoperfusion: the CATCH hypothesis of Alzheimer's pathogenesis. *Neurobiol. Aging* **21**, 331–342 (2000).
15. Tarride, J. *et al.* A review of the cost of cardiovascular disease. *Can. J. Cardiol.* **25**, 195–202 (2009).
16. IOM. in (Fuster, V. & Kelly, B.) (The National Academies Press, 2010). at <www.iom.edu>

17. Chilton, R. J. Pathophysiology of coronary heart disease: a brief review. *J. Am. Osteopath. Assoc.* **104**, S5–8 (2004).
18. Tortora, G. J. & Derrickson, B. *Principles of anatomy and physiology*. (Wiley, 2011).
19. Ramanathan, T. & Skinner, H. Coronary blood flow. *Contin. Educ. Anaesthesia, Crit. Care Pain* **5**, 61–64 (2005).
20. Feliciano, L. & Henning, R. J. Coronary Artery Blood Flow : Physiologic and Pathophysiologic Regulation. *Clin. Cardiol.* **786**, 775–786 (1999).
21. Muller-Delp, J. M. The Coronary Microcirculation in Health and Disease. *ISRN Physiol.* **2013**, 1–24 (2013).
22. Bolton, E. & Rajkumar, C. The ageing cardiovascular system. *Rev. Clin. Gerontol.* **21**, 99–109 (2011).
23. Ungvari, Z., Kaley, G., de Cabo, R., Sonntag, W. E. & Csiszar, A. Mechanisms of vascular aging: new perspectives. *J. Gerontol. A. Biol. Sci. Med. Sci.* **65**, 1028–41 (2010).
24. Endemann, D. H. & Schiffrin, E. L. Endothelial dysfunction. *J. Am. Soc. Nephrol.* **15**, 1983–92 (2004).
25. Fuster, V., Badimon, L., Badimon, J. J. & Chesebro, J. H. The Pathogenesis of Coronary Artery Disease and the Acute Coronary Syndromes. *N. Engl. J. Med.* **326**, 242–250 (1992).
26. Hansson, G. Mechanisms of Disease: Inflammation, atherosclerosis, and coronary artery disease. *N. Engl. J. Med.* **352**, 1685–1695 (2005).
27. Libby, P. & Theroux, P. Pathophysiology of coronary artery disease. *Circulation* **111**, 3481–8 (2005).

28. McCormack, J. P. & Allan, G. M. Measuring hsCRP--an important part of a comprehensive risk profile or a clinically redundant practice? *PLoS Med.* **7**, e1000196 (2010).
29. Rodondi, N. *et al.* Markers of atherosclerosis and inflammation for prediction of coronary heart disease in older adults. *Am. J. Epidemiol.* **171**, 540–9 (2010).
30. Sutton-Tyrrell, K. *et al.* Elevated aortic pulse wave velocity, a marker of arterial stiffness, predicts cardiovascular events in well-functioning older adults. *Circulation* **111**, 3384–90 (2005).
31. Iwamoto, Y. *et al.* Intima-media thickness of brachial artery, vascular function, and cardiovascular risk factors. *Arterioscler. Thromb. Vasc. Biol.* **32**, 2295–303 (2012).
32. Iwakiri, T. *et al.* Usefulness of carotid intima-media thickness measurement as an indicator of generalized atherosclerosis: Findings from autopsy analysis. *Atherosclerosis* 21–24 (2012). doi:10.1016/j.atherosclerosis.2012.10.033
33. Negi, S. I. & Nambi, V. The role of carotid intimal thickness and plaque imaging in risk stratification for coronary heart disease. *Curr. Atheroscler. Rep.* **14**, 115–23 (2012).
34. Genest, J. *et al.* 2009 Canadian Cardiovascular Society / Canadian guidelines for the diagnosis and treatment of dyslipidemia and prevention of cardiovascular disease in the adult – 2009 recommendations. *Can. J. Cardiol.* **25**, 567–579 (2009).
35. D’Agostino, R. B., Pencina, M. J., Massaro, J. M. & Coady, S. Cardiovascular Disease Risk Assessment: Insights from Framingham. *Glob. Heart* **8**, 11–23 (2013).
36. Wilson, P. W. F. *et al.* Prediction of Coronary Heart Disease Using Risk Factor Categories. *Circulation* **97**, 1837–1847 (1998).

37. Yusuf, S. *et al.* Effect of potentially modifiable risk factors associated with myocardial infarction in 52 countries (the INTERHEART study): case-control study. *Lancet* **364**, 937–52 (2004).
38. Kannel, W. B., Feinleib, M., McNamara, P. M., Garrison, R. J. & Castelli, W. P. An investigation of coronary heart disease in families. *Am. J. Epidemiol.* **110**, 281–290 (1979).
39. Law, M. R., Wald, N. J. & Rudnicka, A. R. Quantifying effect of statins on low density lipoprotein cholesterol, ischaemic heart disease, and stroke: systematic review and meta-analysis. *BMJ* **326**, 1423 (2003).
40. Ridker, P. M. & Lüscher, T. F. Anti-inflammatory therapies for cardiovascular disease. *Eur. Heart J.* **35**, 1782–91 (2014).
41. Liao, J. & Laufs, U. Pleiotropic effects of statins. *Annu. Rev. Pharmacol. Toxicol.* **45**, 89–118 (2005).
42. Giannopoulos, S., Katsanos, A. H., Kosmidou, M. & Tsivgoulis, G. Statins and vascular dementia: a review. *J. Alzheimers. Dis.* **42 Suppl 3**, S315–20 (2014).
43. Kern, S., Skoog, I., Ostling, S., Kern, J. & Börjesson-Hanson, A. Does low-dose acetylsalicylic acid prevent cognitive decline in women with high cardiovascular risk? A 5-year follow-up of a non-demented population-based cohort of Swedish elderly women. *BMJ Open* **2**, (2012).
44. Abrams, J. The role of nitrates in coronary heart disease. *Arch. Intern. Med.* **155**, 357–364 (1995).
45. Inzitari, M., Di Bari, M. & Marchionni, N. Calcium channel blockers and coronary heart disease. *Aging Clin. Exp. Res.* **17**, 6–15 (2005).
46. Boudonas, G. E. β -Blockers in coronary artery disease management. *Hippokratia* **14**, 231–235 (2010).

47. The PEACE Trial Investigators. Angiotensin-Converting-Enzyme Inhibition in Stable Coronary Artery Disease. *N. Engl. J. Med.* **351**, 2058–2068 (2004).
48. Muller, M. *et al.* Hypertension and longitudinal changes in cerebral blood flow: The SMART-MR study. *Ann. Neurol.* **71**, 825–833 (2012).
49. Sink, K., Leng, X., Williamson, J. & Al, E. Angiotensin-converting enzyme inhibitors and cognitive decline in older adults with hypertension: results from the Cardiovascular Health Study. *Arch. Intern. Med.* **169**, 1195–1202 (2009).
50. Foussas, S. G. & Tsiaousis, G. Z. Revascularization treatment in patients with coronary artery disease. *Hippokratia* **12**, 3–10 (2008).
51. Bokeriia, L. a, Golukhova, E. Z., Polunina, A. G., Davydov, D. M. & Begachev, A. V. Neural correlates of cognitive dysfunction after cardiac surgery. *Brain Res. Brain Res. Rev.* **50**, 266–74 (2005).
52. Selnes, O. a & McKhann, G. M. Neurocognitive complications after coronary artery bypass surgery. *Ann. Neurol.* **57**, 615–21 (2005).
53. Clark, A. M., Hartling, L., Vandermeer, B. & McAlister, F. A. Meta-Analysis: Secondary Prevention Programs for Patients with Coronary Artery Disease. *Ann. Intern. Med.* **143**, 659–672 (2005).
54. Balady, G. J. *et al.* Core Components of Cardiac Rehabilitation/Secondary Prevention Programs: 2007 Update: A Scientific Statement From the American Heart Association Exercise, Cardiac Rehabilitation, and Prevention Committee, the Council on Clinical Cardiology; the Councils o. *Circ.* **115**, 2675–2682 (2007).
55. Nelson, M. E. *et al.* Physical activity and public health in older adults: Recommendation from the American College of Sports Medicine and the American Heart Association. *Circulation* **116**, 1094–1105 (2007).
56. Mega, J. L. *et al.* Cytochrome P-450 Polymorphisms and Response to Clopidogrel. *N. Engl. J. Med.* **360**, 354–362 (2009).

57. Duran, J. & George, J. A Review of the Basis of Autologous Stem Cell Therapy for Coronary Artery Disease. *J Clin. Exp. Cardiol.* **2**, 130 (2011).
58. Martin, B.-J. *et al.* Cardiac Rehabilitation Attendance and Outcomes in Coronary Artery Disease Patients. *Circ.* **126** , 677–687 (2012).
59. Alter, D. A., Oh, P. I. & Chong, A. Relationship between cardiac rehabilitation and survival after acute cardiac hospitalization within a universal health care system. *Eur. J. Cardiovasc. Prev. Rehabil.* **16** , 102–113 (2009).
60. Koutroumpi, M., Pitsavos, C. & Stefanadis, C. The role of exercise in cardiovascular rehabilitation: A review. *Acta Cardiol.* **63**, 73–79 (2008).
61. Sandercock, G., Hurtado, V. & Cardoso, F. Changes in cardiorespiratory fitness in cardiac rehabilitation patients: A meta-analysis. *Int. J. Cardiol.* **167**, 894–902 (2013).
62. Oliveira, N. L., Ribeiro, F., Alves, A. J., Campos, L. & Oliveira, J. The effects of exercise training on arterial stiffness in coronary artery disease patients: a state-of-the-art review. *Clin. Physiol. Funct. Imaging* **34**, 254–62 (2014).
63. Franklin, B. a & McCullough, P. a. Cardiorespiratory fitness: an independent and additive marker of risk stratification and health outcomes. *Mayo Clin. Proc.* **84**, 776–9 (2009).
64. Brown, M. Exercise and coronary vascular remodelling in the healthy heart. *Exp. Physiol.* **88**, 645–658 (2003).
65. Linke, A., Erbs, S. & Hambrecht, R. Exercise and the coronary circulation- alterations and adaptations in coronary artery disease. *Prog. Cardiovasc. Dis.* **48**, 270–84 (2006).
66. Wienbergen, H. & Hambrecht, R. Physical exercise and its effects on coronary artery disease. *Curr. Opin. Pharmacol.* 8–15 (2013).
doi:10.1016/j.coph.2012.12.003

67. Ainslie, P. N. & Duffin, J. Integration of cerebrovascular CO₂ reactivity and chemoreflex control of breathing: mechanisms of regulation, measurement, and interpretation. *Am. J. Physiol. Regul. Integr. Comp. Physiol.* **296**, R1473–95 (2009).
68. Pfitzner, J. Poiseuille and his law. *Anaesthesia* **31**, 273–275 (1976).
69. Paulson, O. B., Strandgaard, S. & Edvinsson, L. Cerebral autoregulation. *Cerebrovasc. Brain Metab. Rev.* **2**, 161–192 (1990).
70. Coverdale, N. S., Gati, J. S., Opalevych, O., Perrotta, a. & Shoemaker, J. K. Cerebral blood flow velocity underestimates cerebral blood flow during modest hypercapnia and hypocapnia. *J. Appl. Physiol.* (in press) (2014).
doi:10.1152/jappphysiol.00285.2014
71. Yezhuvath, U. S., Lewis-Amezcu, K., Varghese, R., Xiao, G. & Lu, H. On the assessment of cerebrovascular reactivity using hypercapnia BOLD MRI. *NMR Biomed.* **22**, 779–86 (2009).
72. Wells, J. a *et al.* Increased cerebral vascular reactivity in the tau expressing rTg4510 mouse: evidence against the role of tau pathology to impair vascular health in Alzheimer's disease. *J. Cereb. Blood Flow Metab.* 1–4 (2014).
doi:10.1038/jcbfm.2014.224
73. Haight, T. J. *et al.* Vascular risk factors, cerebrovascular reactivity, and the default-mode brain network. *Neuroimage* **115**, 7–16 (2015).
74. St Lawrence, K. S., Ye, F. Q., Lewis, B. K., Frank, J. a & McLaughlin, a C. Measuring the effects of indomethacin on changes in cerebral oxidative metabolism and cerebral blood flow during sensorimotor activation. *Magn. Reson. Med.* **50**, 99–106 (2003).
75. Langford, N. J. Carbon dioxide poisoning. *Toxicol. Rev.* **24**, 229–235 (2005).

76. Kassner, A., Roberts, T. P. Beyond Perfusion: Cerebral Vascular Reactivity and Assessment of Microvascular Permeability. *Top Magn Reson Imaging* **15**, 58–65 (2004).
77. Yablonskiy, D. A. Cerebral metabolic rate in hypercapnia: controversy continues. *J. Cereb. blood flow Metab.* **31**, 1502–1503 (2011).
78. Warthin, A. S. The Wesley M Carpenter Lecture: The Pathology of the Aging Process. *Bull. N. Y. Acad. Med.* **4**, 1006–1046 (1928).
79. Raz, N. & Rodrigue, K. M. Differential aging of the brain: patterns, cognitive correlates and modifiers. *Neurosci. Biobehav. Rev.* **30**, 730–48 (2006).
80. Walhovd, K. B. *et al.* Consistent neuroanatomical age-related volume differences across multiple samples. *Neurobiol. Aging* **32**, 916–932 (2011).
81. Lambert, C. *et al.* Characterizing aging in the human brainstem using quantitative multimodal MRI analysis. *Front. Hum. Neurosci.* **7**, 462 (2013).
82. Luft, a R. *et al.* Patterns of age-related shrinkage in cerebellum and brainstem observed in vivo using three-dimensional MRI volumetry. *Cereb. Cortex* **9**, 712–21 (1999).
83. Akiyama, H. *et al.* Normal human aging: factors contributing to cerebral atrophy. *J. Neurol. Sci.* **152**, 39–49 (1997).
84. Kety, S. S. Human cerebral blood flow and oxygen consumption as related to aging. *J. Chronic Dis.* **3**, 478–486 (1956).
85. Goyal, M. S., Hawrylycz, M., Miller, J. A., Snyder, A. Z. & Raichle, M. E. Aerobic Glycolysis in the Human Brain Is Associated with Development and Neotenus Gene Expression. *Cell Metab.* **19**, 49–57 (2014).
86. Lu, H. *et al.* Alterations in cerebral metabolic rate and blood supply across the adult lifespan. *Cereb. cortex* **21**, 1426–34 (2011).

87. Kalpouzos, G. *et al.* Voxel-based mapping of brain gray matter volume and glucose metabolism profiles in normal aging. *Neurobiol. Aging* **30**, 112–124 (2009).
88. Walhovd, K. B. *et al.* Effects of age on volumes of cortex, white matter and subcortical structures. *Neurobiol. Aging* **26**, 1261–1270 (2005).
89. Grieve, S. M., Clark, C. R., Williams, L. M., Peduto, A. J. & Gordon, E. Preservation of limbic and paralimbic structures in aging. *Hum. Brain Mapp.* **25**, 391–401 (2005).
90. Terribilli, D. *et al.* Age-related gray matter volume changes in the brain during non-elderly adulthood. *Neurobiol. Aging* **32**, 354–68 (2011).
91. Brickman, A. M., Muraskin, J. & Zimmerman, M. E. Structural neuroimaging in Alzheimer’s disease: do white matter hyperintensities matter? *Dialogues Clin. Neurosci.* **11**, 181–190 (2009).
92. Cabeza, R., Anderson, N. D., Locantore, J. K. & McIntosh, A. R. Aging Gracefully: Compensatory Brain Activity in High-Performing Older Adults. *Neuroimage* **17**, 1394–1402 (2002).
93. Fjell, A. M., McEvoy, L., Holland, D., Dale, A. M. & Walhovd, K. B. What is normal in normal aging? Effects of aging, amyloid and Alzheimer’s disease on the cerebral cortex and the hippocampus. *Prog. Neurobiol.* **117**, 20–40 (2014).
94. Sowell, E. R., Thompson, P. M. & Toga, A. W. Mapping changes in the human cortex throughout the span of life. *Neuroscientist* **10**, 372–92 (2004).
95. Pakkenberg, B. & Gundersen, H. J. G. Neocortical neuron number in humans: Effect of sex and age. *J. Comp. Neurol.* **384**, 312–320 (1997).
96. Bartzokis, G. Age-related myelin breakdown: a developmental model of cognitive decline and Alzheimer’s disease. *Neurobiol. Aging* **25**, 5–18 (2004).

97. Greenwood, P. M. The frontal aging hypothesis evaluated. *J. Int. Neuropsychol. Soc.* **6**, 705–726 (2000).
98. Alves, G. S. *et al.* Integrating Retrogenesis Theory to Alzheimer ' s Disease Pathology : Insight from DTI-TBSS Investigation of the White Matter Microstructural Integrity. *Biomed. Res. Int.* **Article ID**, 11 (2015).
99. Reisberg, B. *et al.* Evidence and mechanisms of retrogenesis in Alzheimer's and other dementias: Management and treatment import. *Am. J. Alzheimer's Dis. Other Dementias* **17** , 202–212 (2002).
100. Fjell, A. M. *et al.* One-year brain atrophy evident in healthy aging. *J. Neurosci.* **29**, 15223–15231 (2009).
101. Davis, S. W. *et al.* Assessing the effects of age on long white matter tracts using diffusion tensor tractography. *Neuroimage* **46**, 530–541 (2009).
102. Foundas, A. L., Zipin, D. & Browning, C. A. Age-related changes of the insular cortex and lateral ventricles: conventional MRI volumetric measures. *J. Neuroimaging* **8**, 216—221 (1998).
103. Pfefferbaum, A. *et al.* Variation in longitudinal trajectories of regional brain volumes of healthy men and women (ages 10 to 85years) measured with atlas-based parcellation of MRI. *Neuroimage* **65**, 176–193 (2012).
104. Resnick, S. M. *et al.* One-year age changes in MRI brain volumes in older adults. *Cereb. cortex* **10**, 464–72 (2000).
105. Scahill, R. *et al.* A longitudinal study of brain volume changes in normal aging using serial registered magnetic resonance imaging. *Arch. Neurol.* **60**, 989–994 (2003).
106. Takao, H., Hayashi, N. & Ohtomo, K. A longitudinal study of brain volume changes in normal aging. *Eur. J. Radiol.* **81**, 2801–2804 (2012).

107. Sullivan, E. & Pfefferbaum, A. Neuroradiological characterization of normal adult ageing. *Br. J. Radiol.* **80**, S99–S108 (2007).
108. Good, C. D. *et al.* A voxel-based morphometric study of ageing in 465 normal adult human brains. *Neuroimage* **14**, 21–36 (2001).
109. Tisserand, D. J. *et al.* A voxel-based morphometric study to determine individual differences in gray matter density associated with age and cognitive change over time. *Cereb. Cortex* **14**, 966–73 (2004).
110. Raz, N. *et al.* Aging, sexual dimorphism, and hemispheric asymmetry of the cerebral cortex: replicability of regional differences in volume. *Neurobiol. Aging* **25**, 377–96 (2004).
111. Salat, D. H. *et al.* Thinning of the cerebral cortex in aging. *Cereb. Cortex* **14**, 721–30 (2004).
112. Fjell, A. M. *et al.* Accelerating Cortical Thinning: Unique to Dementia or Universal in Aging? *Cereb. Cortex* **24**, 919–934 (2014).
113. Resnick, S. M., Pham, D. L., Kraut, M. a, Zonderman, A. B. & Davatzikos, C. Longitudinal magnetic resonance imaging studies of older adults: a shrinking brain. *J. Neurosci.* **23**, 3295–301 (2003).
114. Raz, N., Dupuis, J. H., Briggs, S. D., McGavran, C. & Acker, J. D. Differential effects of age and sex on the cerebellar hemispheres and the vermis: a prospective MR study. *AJNR. Am. J. Neuroradiol.* **19**, 65–71 (1998).
115. Salthouse, T. a. Neuroanatomical substrates of age-related cognitive decline. *Psychol. Bull.* **137**, 753–784 (2011).
116. Squire, L. R. & Zola-Morgan, S. The medial temporal lobe memory system. *Sci.* **253**, 1380–1386 (1991).

117. Fortin, N. J., Agster, K. L. & Eichenbaum, H. B. Critical role of the hippocampus in memory for sequences of events. *Nat. Neurosci.* **5**, 458–462 (2002).
118. Raz, N. *et al.* Regional brain changes in aging healthy adults: general trends, individual differences and modifiers. *Cereb. Cortex* **15**, 1676–89 (2005).
119. Gunning-Dixon, F. M., Brickman, A. M., Cheng, J. C. & Alexopoulos, G. S. Aging of cerebral white matter: a review of MRI findings. *Int. J. Geriatr. Psychiatry* **24**, 109–117 (2009).
120. Guttmann, C. R. G. *et al.* White matter changes with normal aging. *Neurology* **50**, 972–978 (1998).
121. Salat, D. *et al.* Age-associated alterations in cortical gray and white matter signal intensity and gray to white matter contrast. *Neuroimage* **48**, 21–28 (2009).
122. Salat, D., Kaye, J. & Janowsky, J. Prefrontal Gray and White Matter Volumes in Healthy Aging and Alzheimer Disease. *Arch. Neurol.* **56**, 338–344 (1999).
123. Salat, D. H. *et al.* Regional white matter volume differences in nondemented aging and Alzheimer’s disease. *Neuroimage* **44**, 1247–1258 (2009).
124. De Leeuw, F.-E. *et al.* Prevalence of cerebral white matter lesions in elderly people: a population based magnetic resonance imaging study. The Rotterdam Scan Study. *J. Neurol. Neurosurg. Psychiatry* **70**, 9–14 (2001).
125. Soderlund, H., Nyberg, L., Adolfsson, R., Nilsson, L. G. & Launer, L. J. High Prevalence of White Matter Hyperintensities in Normal Aging: Relation to Blood Pressure and Cognition. *Cortex* **39**, 1093–1105 (2003).
126. Papp, K. V *et al.* Processing speed in normal aging: Effects of white matter hyperintensities and hippocampal volume loss. *Aging, Neuropsychol. Cogn.* **21**, 197–213 (2014).

127. Birdsill, A. C. *et al.* Regional white matter hyperintensities: aging, Alzheimer's disease risk, and cognitive function. *Neurobiol. Aging* **35**, 769–776
128. Taylor, W. Diffusion tensor imaging: background, potential, and utility in psychiatric research. *Biol. Psychiatry* **3223**, 201–207 (2003).
129. Sundgren, P. C. *et al.* Diffusion tensor imaging of the brain: review of clinical applications. *Neuroradiology* **46**, 339–50 (2004).
130. Alexander, A. L., Lee, J. E., Lazar, M. & Field, A. S. Diffusion tensor imaging of the brain. *Neurotherapeutics* **4**, 316–329 (2007).
131. Damoiseaux, J. S. *et al.* White matter tract integrity in aging and Alzheimer's disease. *Hum. Brain Mapp.* **30**, 1051–9 (2009).
132. Head, D. *et al.* Differential Vulnerability of Anterior White Matter in Nondemented Aging with Minimal Acceleration in Dementia of the Alzheimer Type: Evidence from Diffusion Tensor Imaging. *Cereb. Cortex* **14**, 410–423 (2004).
133. Salat, D. H. *et al.* Age-related changes in prefrontal white matter measured by diffusion tensor imaging. *Ann. N. Y. Acad. Sci.* **1064**, 37–49 (2005).
134. Bennett, I. J., Madden, D. J., Vaidya, C. J., Howard, D. V & Howard, J. H. Age-related differences in multiple measures of white matter integrity: A diffusion tensor imaging study of healthy aging. *Hum. Brain Mapp.* **31**, 378–90 (2010).
135. Burzynska, A. Z. *et al.* Age-related differences in white matter microstructure: Region-specific patterns of diffusivity. *Neuroimage* **49**, 2104–2112 (2010).
136. Pfefferbaum, A. *et al.* Age-related decline in brain white matter anisotropy measured with spatially corrected echo-planar diffusion tensor imaging. *Magn. Reson. Med.* **44**, 259–268 (2000).

137. Chen, J. J., Rosas, H. D. & Salat, D. H. The Relationship between Cortical Blood Flow and Sub-Cortical White-Matter Health across the Adult Age Span. *PLoS One* **8**, e56733 (2013).
138. Hasan, K. M. *et al.* Quantification of the spatiotemporal microstructural organization of the human brain association, projection and commissural pathways across the lifespan using diffusion tensor tractography. *Brain Struct. Funct.* **214**, 361–373 (2010).
139. Lintl, P. & Braak, H. Loss of intracortical myelinated fibers: A distinctive age-related alteration in the human striate area. *Acta Neuropathol.* **61**, 178–182 (1983).
140. Knox, C. A., Kokmen, E. & Dyck, P. J. Morphometric Alteration of Rat Myelinated Fibers with Aging. *J. Neuropathol. Exp. Neurol.* **48**, 119–139 (1989).
141. Martin, A. J., Friston, K. J., Colebatch, J. G. & Frackowiak, R. S. J. Decreases in regional cerebral blood flow with normal aging. *J. Cereb. blood flow Metab.* **11**, 684–689 (1991).
142. Asllani, I. *et al.* Separating function from structure in perfusion imaging of the aging brain. *Hum. Brain Mapp.* **30**, 2927–35 (2009).
143. Chen, J. J., Rosas, H. D. & Salat, D. H. Age-associated reductions in cerebral blood flow are independent from regional atrophy. *Neuroimage* **55**, 468–78 (2011).
144. Parkes, L. M., Rashid, W., Chard, D. T. & Tofts, P. S. Normal cerebral perfusion measurements using arterial spin labeling: reproducibility, stability, and age and gender effects. *Magn. Reson. Med.* **51**, 736–43 (2004).
145. Mielke, R. *et al.* Normal and pathological aging - findings of positron-emission-tomography. *J. Neural Transm.* **105**, 821–837 (1998).

146. Biagi, L. *et al.* Age dependence of cerebral perfusion assessed by magnetic resonance continuous arterial spin labeling. *J. Magn. Reson. Imaging* **25**, 696–702 (2007).
147. Bentourkia, M. *et al.* Comparison of regional cerebral blood flow and glucose metabolism in the normal brain: effect of aging. *J. Neurol. Sci.* **181**, 19–28 (2000).
148. Desjardins, M. Vascular correlates of aging in the brain : Evidence from imaging data. *IRBM* **1**, 1–8 (2015).
149. Riecker, A. *et al.* Relation between regional functional MRI activation and vascular reactivity to carbon dioxide during normal aging. *J. Cereb. Blood Flow Metab.* **23**, 565–573 (2003).
150. Park, L., Anrather, J., Girouard, H., Zhou, P. & Iadecola, C. Nox2-derived reactive oxygen species mediate neurovascular dysregulation in the aging mouse brain. *J Cereb Blood Flow Metab* **27**, 1908–1918 (2007).
151. Lipsitz, L. A., Mukai, S., Hamner, J., Gagnon, M. & Babikian, V. Dynamic Regulation of Middle Cerebral Artery Blood Flow Velocity in Aging and Hypertension. *Stroke* **31** , 1897–1903 (2000).
152. Kuhl, D. E., Metter, E. J., Riege, W. H. & Phelps, M. E. Effects of human aging on patterns of local cerebral glucose utilization determined by the [18F]fluorodeoxyglucose method. *J. Cereb. Blood Flow Metab.* **2**, 163–71 (1982).
153. Gauthier, C. J. *et al.* Hearts and minds: linking vascular rigidity and aerobic fitness with cognitive aging. *Neurobiol. Aging* **36**, 304–14 (2015).
154. Heo, S. *et al.* Resting hippocampal blood flow, spatial memory and aging. *Brain Res.* **1315**, 119–127 (2010).
155. Gage, F. H., Kelly, P. A. & Bjorklund, A. Regional changes in brain glucose metabolism reflect cognitive impairments in aged rats. *J. Neurosci.* **4** , 2856–2865 (1984).

156. Schwertfeger, N. *et al.* Cerebrovascular reactivity over time course in healthy subjects. *J. Neurol. Sci.* **249**, 135–139
157. Kastrup, A., Dichgans, J., Niemeier, M. & Schabet, M. Changes of Cerebrovascular CO₂ Reactivity During Normal Aging. *Stroke* **29**, 1311–1314 (1998).
158. Duara, R. *et al.* Human brain glucose utilization and cognitive function in relation to age. *Ann. Neurol.* **16**, 702–713 (1984).
159. Meltzer, C. C. *et al.* Does Cerebral Blood Flow Decline in Healthy Aging? A PET Study with Partial-Volume Correction. *J. Nucl. Med.* **41**, 1842–1848 (2000).
160. Curiati, P. K. *et al.* Age-Related Metabolic Profiles in Cognitively Healthy Elders: Results from a Voxel-Based [18F]Fluorodeoxyglucose–Positron-Emission Tomography Study with Partial Volume Effects Correction. *Am. J. Neuroradiol.* **32**, 560–565 (2011).
161. Asllani, I., Borogovac, A. & Brown, T. R. Regression algorithm correcting for partial volume effects in arterial spin labeling MRI. *Magn. Reson. Med.* **60**, 1362–71 (2008).
162. Asllani, I., Borogovac, A., Brown, T. R., Hirsch, J. & Krakuer, J. Limit of Detection of Localized Absolute Changes in CBF Using Arterial Spin Labeling (ASL) MRI. in *Proc. Int. Soc. Magn. Reson. Med.* 262 (2009).
163. Anderson, B. J., Greenwood, S. J. & McCloskey, D. Exercise as an intervention for the age-related decline in neural metabolic support. *Front. Aging Neurosci.* **2**, 1–9 (2010).
164. Terry, R. D., DeTeresa, R. & Hansen, L. A. Neocortical cell counts in normal human adult aging. *Ann. Neurol.* **21**, 530–539 (1987).

165. Brickman, A. M. *et al.* Reduction in cerebral blood flow in areas appearing as white matter hyperintensities on magnetic resonance imaging. *Psychiatry Res.* **172**, 117–20 (2009).
166. Loessner, A. *et al.* Regional Cerebral Function Determined by FDG-PET in Healthy Volunteers: Normal Patterns and Changes with Age. *J. Nucl. Med.* **36**, 1141–1149 (1995).
167. Dickstein, D. L. *et al.* Changes in the structural complexity of the aged brain. *Aging Cell* **6**, 275–84 (2007).
168. Gibson, P. H. EM study of the numbers of cortical synapses in the brains of ageing people and people with Alzheimer-type dementia. *Acta Neuropathol.* **62**, 127–133 (1983).
169. Jacobs, B., Driscoll, L. & Schall, M. Life-span dendritic and spine changes in areas 10 and 18 of human cortex: A quantitative golgi study. *J. Comp. Neurol.* **386**, 661–680 (1997).
170. De Brabander, Kramers & Uylings. Layer-specific dendritic regression of pyramidal cells with ageing in the human prefrontal cortex. *Eur. J. Neurosci.* **10**, 1261–1269 (1998).
171. Nakamura, S., Akiguchi, I., Kameyama, M. & Mizuno, N. Age-related changes of pyramidal cell basal dendrites in layers III and V of human motor cortex: A quantitative Golgi study. *Acta Neuropathol.* **65**, 281–284 (1985).
172. Peters, A., Sethares, C. & Moss, M. B. The effects of aging on layer 1 in area 46 of prefrontal cortex in the rhesus monkey. *Cereb. Cortex* **8**, 671–684 (1998).
173. Duan, H. *et al.* Age-related Dendritic and Spine Changes in Corticocortically Projecting Neurons in Macaque Monkeys. *Cereb. Cortex* **13**, 950–961 (2003).
174. Mervis, R. Structural alterations in neurons of aged canine neocortex: A Golgi study. *Exp. Neurol.* **62**, 417–432 (1978).

175. Geinisman, Y., de Toledo-Morrell, L. & Morrell, F. Loss of perforated synapses in the dentate gyrus: morphological substrate of memory deficit in aged rats. *Proc. Natl. Acad. Sci.* **83**, 3027–3031 (1986).
176. Hof, P. R. *et al.* Age-related changes in GluR2 and NMDAR1 glutamate receptor subunit protein immunoreactivity in corticocortically projecting neurons in macaque and patas monkeys. *Brain Res.* **928**, 175–186 (2002).
177. Meltzer, C. C. *et al.* Serotonin in Aging, Late-Life Depression, and Alzheimer's Disease: The Emerging Role of Functional Imaging. *Neuropsychopharmacology* **18**, 407–430 (1998).
178. Wenk, G. L., Pierce, D. J., Struble, R. G., Price, D. L. & Cork, L. C. Age-related changes in multiple neurotransmitter systems in the monkey brain. *Neurobiol. Aging* **10**, 11–19 (1989).
179. Tomasi, D. & Volkow, N. D. Aging and functional brain networks. *Mol. Psychiatry* **17**, 549–558 (2012).
180. Hampson, M. *et al.* Intrinsic brain connectivity related to age in young and middle aged adults. *PLoS One* **7**, e44067 (2012).
181. Onoda, K., Ishihara, M. & Yamaguchi, S. Decreased functional connectivity by aging is associated with cognitive decline. *J. Cogn. Neurosci.* **24**, 2186–98 (2012).
182. Sambataro, F. *et al.* Age-related alterations in default mode network: impact on working memory performance. *Neurobiol. Aging* **31**, 839–52 (2010).
183. Damoiseaux, J. S. *et al.* Reduced resting-state brain activity in the 'default network' in normal aging. *Cereb. cortex* **18**, 1856–64 (2008).
184. Raz, N. in *Handb. Aging Cogn.* (Craik, F. I. M. & Salthouse, T. A.) 1–90 (Lawrence Erlbaum Associates Publishers, 2000).

185. Dennis, N. A. & Cabeza, R. in *Handb. Aging Cogn.* (Craik, F. I. . & Salthouse, T. A.) 1–54 (Psychology Press, 2011).
186. Drag, L. L. & Bieliauskas, L. a. Contemporary review 2009: cognitive aging. *J. Geriatr. Psychiatry Neurol.* **23**, 75–93 (2010).
187. Gunstad, J. *et al.* Patterns of cognitive performance in middle-aged and older adults: A cluster analytic examination. *J. Geriatr. Psychiatry Neurol.* **19**, 59–64 (2006).
188. Raz, N. & Kennedy, K. M. in *Imaging the aging brain* (Jagust, W. & D’Esposito, M.) 43–70 (Oxford University Press, 2009).
189. Eyler, L. T., Sherzai, A., Kaup, A. R. & Jeste, D. V. A review of functional brain imaging correlates of successful cognitive aging. *Biol. Psychiatry* **70**, 115–122 (2011).
190. Spreng, R. N., Wojtowicz, M. & Grady, C. L. Reliable differences in brain activity between young and old adults: A quantitative meta-analysis across multiple cognitive domains. *Neurosci. Biobehav. Rev.* **34**, 1178–1194 (2010).
191. Chen, Z. J., He, Y., Rosa-Neto, P., Gong, G. & Evans, A. C. Age-related alterations in the modular organization of structural cortical network by using cortical thickness from MRI. *Neuroimage* **56**, 235–245 (2011).
192. Ferreira, L. K. & Busatto, G. F. Resting-state functional connectivity in normal brain aging. *Neurosci. Biobehav. Rev.* **37**, 384–400 (2013).
193. Gianaros, P. J., Greer, P. J., Ryan, C. M. & Jennings, J. R. Higher blood pressure predicts lower regional grey matter volume: Consequences on short-term information processing. *Neuroimage* **31**, 754–65 (2006).
194. Chen, X., Wen, W., Anstey, K. J. & Sachdev, P. S. Effects of cerebrovascular risk factors on gray matter volume in adults aged 60-64 years: a voxel-based morphometric study. *Psychiatry Res.* **147**, 105–14 (2006).

195. Last, D. *et al.* Global and Regional Effects of Type 2 Diabetes on Brain Tissue Volumes and Cerebral Vasoreactivity. *Diabetes Care* **30**, 1193–1199 (2007).
196. Brundel, M., van den Heuvel, M., de Bresser, J., Kappelle, L. J. & Biessels, G. J. Cerebral cortical thickness in patients with type 2 diabetes. *J. Neurol. Sci.* **299**, 126–30 (2010).
197. Novak, V. *et al.* Adhesion molecules, altered vasoreactivity, and brain atrophy in type 2 diabetes. *Diabetes Care* **34**, 2438–2441 (2011).
198. Chen, Z., Li, L., Sun, J. & Ma, L. Mapping the brain in type II diabetes: Voxel-based morphometry using DARTEL. *Eur. J. Radiol.* **81**, 1870–1876 (2012).
199. Debette, S. *et al.* Midlife vascular risk factor exposure accelerates structural brain aging and cognitive decline. *Neurology* **77**, 461–468 (2011).
200. Guo, X. *et al.* Blood Pressure Components and Changes in Relation to White Matter Lesions: A 32-Year Prospective Population Study. *Hypertens.* **54**, 57–62 (2009).
201. Raz, N., Rodrigue, K. M. & Acker, J. D. Hypertension and the brain: vulnerability of the prefrontal regions and executive functions. *Behav. Neurosci.* **117**, 1169–1180 (2003).
202. Firbank, M. *et al.* Brain atrophy and white matter hyperintensity change in older adults and relationship to blood pressure. *J. Neurol.* **254**, 713–721 (2007).
203. Veldink, J. H., Scheltens, P., Jonker, C. & Launer, L. J. Progression of cerebral white matter hyperintensities on MRI is related to diastolic blood pressure. *Neurology* **51**, 319–320 (1998).
204. Strassburger, T. L. *et al.* Interactive Effects of Age and Hypertension on Volumes of Brain Structures. *Stroke* **28**, 1410–1417 (1997).

205. Salerno, J. a. *et al.* Brain atrophy in hypertension. A volumetric magnetic resonance imaging study. *Hypertension* **20**, 340–348 (1992).
206. Knopman, D. S., Mosley, T. H., Catellier, D. J. & Sharrett, a R. Cardiovascular risk factors and cerebral atrophy in a middle-aged cohort. *Neurology* **65**, 876–81 (2005).
207. Maillard, P. *et al.* Eff ects of systolic blood pressure on white-matter integrity in young adults in the Framingham Heart Study : a cross-sectional study. *Lancet Neurol.* **4422**, 1–9 (2012).
208. Den Heijer, T. *et al.* Association between blood pressure levels over time and brain atrophy in the elderly. *Neurobiol. Aging* **24**, 307–313 (2003).
209. Johansson, B. B. Cerebral vascular bed in hypertension and consequences for the brain. *Hypertension* **6**, III82–6 (1984).
210. Dai, W. *et al.* Abnormal regional cerebral blood flow in cognitively normal elderly subjects with hypertension. *Stroke.* **39**, 349–54 (2008).
211. Beason-Held, L. L., Moghekar, A., Zonderman, A. B., Kraut, M. a & Resnick, S. M. Longitudinal changes in cerebral blood flow in the older hypertensive brain. *Stroke.* **38**, 1766–73 (2007).
212. Efimova, I. Y., Efimova, N. Y., Triss, S. V & Lishmanov, Y. B. Brain Perfusion and Cognitive Function Changes in Hypertensive Patients. *Hypertens Res* **31**, 673–678 (2008).
213. Alosco, M. L. *et al.* The impact of hypertension on cerebral perfusion and cortical thickness in older adults. *J. Am. Soc. Hypertens.* **8**, 561–70 (2014).
214. Sojkova, J. *et al.* Intima-media thickness and regional cerebral blood flow in older adults. *Stroke.* **41**, 273–9 (2010).

215. Salerno, J. A. *et al.* Brain Metabolic Function in Older Men With Chronic Essential Hypertension. *Journals Gerontol. Ser. A Biol. Sci. Med. Sci.* **50A**, M147–M154 (1995).
216. Baker, L. D. *et al.* Insulin resistance and Alzheimer-like reductions in regional cerebral glucose metabolism for cognitively normal adults with prediabetes or early type 2 diabetes. *Arch. Neurol.* **68**, 51–7 (2011).
217. Okonkwo, O. C. *et al.* Longitudinal trajectories of cognitive decline among older adults with cardiovascular disease. *Cerebrovasc. Dis.* **30**, 362–73 (2010).
218. Muller, M., Grobbee, D. E., Aleman, a, Bots, M. & van der Schouw, Y. T. Cardiovascular disease and cognitive performance in middle-aged and elderly men. *Atherosclerosis* **190**, 143–9 (2007).
219. Jennings, J. R. *et al.* Reduced cerebral blood flow response and compensation among patients with untreated hypertension. *Neurology* **64**, 1358–1365 (2005).
220. Jennings, J. R. *et al.* Cerebral Blood Flow in Hypertensive Patients: An Initial Report of Reduced and Compensatory Blood Flow Responses During Performance of Two Cognitive Tasks . *Hypertens.* **31** , 1216–1222 (1998).
221. Tarumi, T., Shah, F., Tanaka, H. & Haley, A. P. Association Between Central Elastic Artery Stiffness and Cerebral Perfusion in Deep Subcortical Gray and White Matter. *Am. J. Hypertens.* **24** , 1108–1113 (2011).
222. Haley, A. P., Tarumi, T., Gonzales, M. M., Suwagara, J. & Tanaka, H. Subclinical Atherosclerosis is Related to Lower Neuronal Viability in Middle-aged Adults: A (1)H MRS Study. *Brain Res.* **1344**, 54–61 (2010).
223. Wendell, C. R., Zonderman, A. B., Metter, E. J., Najjar, S. S. & Waldstein, S. R. Carotid intimal medial thickness predicts cognitive decline among adults without clinical vascular disease. *Stroke* **40**, 3180–5 (2009).

224. Erickson, K. I., Miller, D. L., Weinstein, A. M., Akl, S. L. & Banducci, S. Physical activity and brain plasticity in late adulthood: a conceptual and comprehensive review. *Ageing Res.* **4**, 34–47 (2012).
225. Caspersen, C. J., Powell, K. E. & Christenson, G. M. Physical activity, exercise, and physical fitness: definitions and distinctions for health-related research. *Public Health Rep.* **100**, 126–131 (1985).
226. Fletcher, G. F. *et al.* Exercise Standards for Testing and Training: A Statement for Healthcare Professionals From the American Heart Association. *Circulation* **104**, (2001).
227. Bengt, S. & Calbet, J. AL. Point: In health and in a normoxic environment, Vo₂max is limited primarily by cardiac output and locomotor muscle blood flow. *J. Appl. Physiol.* **100**, 744–745 (2006).
228. Ades, P. Cardiac rehabilitation and secondary prevention of coronary heart disease. *N. Engl. J. Med.* **345**, 892–902 (2001).
229. Hayes, S. M., Hayes, J. P., Cadden, M. & Verfaellie, M. A review of cardiorespiratory fitness-related neuroplasticity in the aging brain. *Front. Aging Neurosci.* **5**, 31 (2013).
230. Colcombe, S. J. *et al.* Aerobic Fitness Reduces Brain Tissue Loss in Aging Humans. *Journals Gerontol. Ser. A Biol. Sci. Med. Sci.* **58**, M176–M180 (2003).
231. Erickson, K. I. *et al.* Exercise training increases size of hippocampus and improves memory. *Proc. Natl. Acad. Sci.* **108**, 3017–3022 (2011).
232. Marks, B. L., Katz, L. M., Styner, M. & Smith, J. K. Aerobic fitness and obesity: relationship to cerebral white matter integrity in the brain of active and sedentary older adults. *Br. J. Sport. Med.* **45**, 1208–1215 (2011).

233. Johnson, N. F., Kim, C., Clasey, J. L., Bailey, A. & Gold, B. T. Cardiorespiratory fitness is positively correlated with cerebral white matter integrity in healthy seniors. *Neuroimage* **59**, 1514–1523 (2012).
234. Burdette, J. H. *et al.* Using network science to evaluate exercise-associated brain changes in older adults. *Front. Aging Neurosci.* **2**, 23 (2010).
235. Chapman, S. B. *et al.* Shorter term aerobic exercise improves brain, cognition, and cardiovascular fitness in aging. *Front. Aging Neurosci.* **5**, 75 (2013).
236. Thomas, B. P. *et al.* Life-long aerobic exercise preserved baseline cerebral blood flow but reduced vascular reactivity to CO₂. *J. Magn. Reson. Imaging* **38**, 1177–83 (2013).
237. Voss, M. W. *et al.* Plasticity of brain networks in a randomized intervention trial of exercise training in older adults. *Front. Aging Neurosci.* **2**, 1–17 (2010).
238. Colcombe, S. J. *et al.* Cardiovascular fitness, cortical plasticity, and aging. *Proc. Natl. Acad. Sci. U. S. A.* **101**, 3316–21 (2004).
239. Hayes, S. M., Alosco, M. L. & Forman, D. E. The Effects of Aerobic Exercise on Cognitive and Neural Decline in Aging and Cardiovascular Disease. *Curr. Geriatr. Reports* **3**, 282–290 (2014).
240. MacIntosh, B. J. *et al.* Cardiopulmonary fitness correlates with regional cerebral grey matter perfusion and density in men with coronary artery disease. *PLoS One* **9**, e91251 (2014).
241. May, A. Experience-dependent structural plasticity in the adult human brain. *Trends Cogn. Sci.* **15**, 475–482 (2011).
242. Driemeyer, J., Boyke, J., Gaser, C., Büchel, C. & May, A. Changes in Gray Matter Induced by Learning—Revisited. *PLoS One* **3**, e2669 (2008).

243. Maguire, E. A. *et al.* Navigation expertise and the human hippocampus: A structural brain imaging analysis. *Hippocampus* **13**, 250–259 (2003).
244. Erickson, K. I. *et al.* Physical activity predicts gray matter volume in late adulthood: the Cardiovascular Health Study. *Neurology* **75**, 1415–22 (2010).
245. Heyn, P., Abreu, B. C. & Ottenbacher, K. J. The effects of exercise training on elderly persons with cognitive impairment and dementia: A meta-analysis1. *Arch. Phys. Med. Rehabil.* **85**, 1694–1704 (2004).
246. Young, J., Angevaren, M., Rusted, J. & Tabet, N. Aerobic exercise to improve cognitive function in older people without known cognitive impairment. *Cochrane Database Syst. Rev.* CD005381 (2015).
doi:10.1002/14651858.CD005381.pub4.Copyright
247. Voss, M. W., Vivar, C., Kramer, A. F. & van Praag, H. Bridging animal and human models of exercise-induced brain plasticity. *Trends Cogn. Sci.* 1–20 (2013).
doi:10.1016/j.tics.2013.08.001
248. Neeper, S. A., Goautomez-Pinilla, F., Choi, J. & Cotman, C. Exercise and brain neurotrophins. *Nature* **373**, 109 (1995).
249. Waynman, S., Ying, Z. & Gomez-Pinilla, F. Hippocampal BDNF mediates the efficacy of exercise on synaptic plasticity and cognition. *Eur. J. Neurosci.* **20**, 2580–2590 (2004).
250. Ahlskog, J. E., Geda, Y. E., Graff-Radford, N. R. & Petersen, R. C. Physical exercise as a preventive or disease-modifying treatment of dementia and brain aging. *Mayo Clin. Proc.* **86**, 876–84 (2011).
251. Bullitt, E. *et al.* The Effect of Exercise on the Cerebral Vasculature of Healthy Aged Subjects as Visualized by MR Angiography. *Am. J. Neuroradiol.* **30** , 1857–1863 (2009).

252. Pereira, A. C. *et al.* An in vivo correlate of exercise-induced neurogenesis in the adult dentate gyrus. *Proc. Natl. Acad. Sci. U. S. A.* **104**, 5638–5643 (2007).
253. Whitwell, J. L. Voxel-based morphometry: an automated technique for assessing structural changes in the brain. *J. Neurosci.* **29**, 9661–4 (2009).
254. Chen, L., Bernstein, M., Huston, J. & Fain, S. Measurements of T1 relaxation times at 3.0 T: implications for clinical MRA. in *Proc. 9th ...* **9**, 1391 (2001).
255. Ashburner, J. & Friston, K. J. Voxel-based morphometry--the methods. *Neuroimage* **11**, 805–21 (2000).
256. Ashburner, J. A fast diffeomorphic image registration algorithm. *Neuroimage* **38**, 95–113 (2007).
257. Ashburner, J. & Friston, K. J. Unified segmentation. *Neuroimage* **26**, 839–51 (2005).
258. Ashburner, J., Neelin, P., Collins, D. L., Evans, A. & Friston, K. Incorporating Prior Knowledge into Image Registration. *Neuroimage* **6**, 344–352 (1997).
259. Klein, A. *et al.* Evaluation of 14 nonlinear deformation algorithms applied to human brain MRI registration. *Neuroimage* **46**, 786–802 (2009).
260. Ashburner, J. & Friston, K. J. Why Voxel-Based Morphometry Should Be Used. *Neuroimage* **14**, 1238–1243 (2001).
261. Ainslie, P. N. & Hoiland, R. L. Transcranial Doppler ultrasound: Valid, invalid, or both? *J. Appl. Physiol.* **117**, 1081–1083 (2014).
262. Halani, S., Kwinta, J. B., Golestani, A. M., Khatamian, Y. B. & Chen, J. J. Comparing Cerebrovascular Reactivity Measured using BOLD and Cerebral Blood Flow MRI: The Effect of Basal Vascular Tension on Vasodilatory and Vasoconstrictive Reactivity. *Neuroimage* **110**, 110–123 (2015).

263. Brown, G. G., Perthen, J. E., Liu, T. T. & Buxton, R. B. A primer on functional magnetic resonance imaging. *Neuropsychol. Rev.* **17**, 107–25 (2007).
264. Tancredi, F. B. & Hoge, R. D. Comparison of cerebral vascular reactivity measures obtained using breath-holding and CO₂ inhalation. *J. Cereb. Blood Flow Metab.* 1–9 (2013). doi:10.1038/jcbfm.2013.48
265. Anazodo, U., Shoemaker, J. K., Suskin, N., Wang, D. J. J. & St. Lawrence, K. S. Correlation of brain atrophy to decreased CBF and CVR in coronary artery disease patients. in *Proc. Intl. Soc. Mag. Reson. Med* 2974 (2015).
266. Alsop, D. C. *et al.* Recommended Implementation of arterial spin-labeled perfusion MRI for clinical applications: A consensus of the ISMRM perfusion study group and the European consortium for ASL in dementia. *Magn. Reson. Med.* **73**, 102–116 (2015).
267. Ye, F. Q. *et al.* H₂(¹⁵O) PET validation of steady-state arterial spin tagging cerebral blood flow measurements in humans. *Magn. Reson. Med.* **44**, 450–6 (2000).
268. Wong, E. C., Buxton, R. B. & Frank, L. R. Implementation of quantitative perfusion imaging techniques for functional brain mapping using pulsed arterial spin labeling. *NMR Biomed.* **10**, 237–249 (1997).
269. Williams, D. S., Detre, J. a, Leigh, J. S. & Koretsky, a P. Magnetic resonance imaging of perfusion using spin inversion of arterial water. *Proc. Natl. Acad. Sci. U. S. A.* **89**, 212–6 (1992).
270. Dai, W., Garcia, D., de Bazelaire, C. & Alsop, D. C. Continuous flow-driven inversion for arterial spin labeling using pulsed radio frequency and gradient fields. *Magn. Reson. Med.* **60**, 1488–1497 (2008).
271. Wong, E. C. An Introduction to ASL Labeling Techniques. *J. Magn. Reson. Imaging* **00**, 1–10 (2014).

272. Tancredi, F. B. *et al.* Comparison of pulsed and pseudocontinuous arterial spin-labeling for measuring CO₂-induced cerebrovascular reactivity. *J. Magn. Reson. Imaging* **36**, 312–21 (2012).
273. Wang, J. *et al.* Arterial transit time imaging with flow encoding arterial spin tagging (FEAST). *Magn. Reson. Med.* **50**, 599–607 (2003).
274. Xu, G. *et al.* Reliability and precision of pseudo-continuous arterial spin labeling perfusion MRI on 3.0 T and comparison with 15O-water PET in elderly subjects at risk for Alzheimer's disease. *NMR Biomed.* **23**, 286–293 (2010).
275. Wu, W., St Lawrence, K. S., Licht, D. J. & Wang, D. J. J. Quantification Issues in Arterial Spin Labeling Perfusion. *Top Magn Reson Imaging* **21**, 65–73 (2011).
276. St. Lawrence, K. S., Owen, D. & Wang, D. J. J. A Two-Stage Approach to Measuring Vascular Water Exchange and Arterial Transit Time by Diffusion-Weighted Perfusion MRI. *Magn. Reson. Med.* **67**, 1275–1284 (2012).
277. MacIntosh, B. J. *et al.* Assessment of arterial arrival times derived from multiple inversion time pulsed arterial spin labeling MRI. *Magn. Reson. Med.* **63**, 641–7 (2010).
278. Martin, S. Z. *et al.* 3D GRASE pulsed arterial spin labeling at multiple inflow times in patients with long arterial transit times: comparison with dynamic susceptibility-weighted contrast-enhanced MRI at 3 Tesla. *J. Cereb. Blood Flow Metab.* 1–10 (2014). doi:10.1038/jcbfm.2014.200
279. Aslan, S. *et al.* Estimation of labeling efficiency in pseudocontinuous arterial spin labeling. *Magn. Reson. Med.* **63**, 765–71 (2010).
280. Petr, J., Schramm, G. & van den Hoff, J. Measuring the influence of vessel geometry on PCASL labeling efficiency. in *Proc. Intl. Soc. Mag. Reson. Med.* **23**, 2952 (2015).

281. Wu, W.-C. *et al.* In vivo Venous Blood T1 Measurement using Inversion Recovery TrueFISP in Children and Adults. *Magn. Reson. Med.* **64**, 1140–1147 (2010).
282. Sokolska, M., Golay, X. & Thomas, D. Effect of labelling plane angulation on pCASL labelling efficiency – does it really matter ? in *Proc. Intl. Soc. Mag. Reson. Med* **23**, 2331 (2015).
283. Vidorreta, M. *et al.* Comparison of 2D and 3D single-shot ASL perfusion fMRI sequences. *Neuroimage* **66**, 662–671 (2013).
284. Günther, M., Oshio, K. & Feinberg, D. a. Single-shot 3D imaging techniques improve arterial spin labeling perfusion measurements. *Magn. Reson. Med.* **54**, 491–8 (2005).
285. Fox, P. T., Raichle, M. E., Mintun, M. A. & Dence, C. Nonoxidative Glucose Consumption during Focal Physiologic Neural Activity. *Science (80-.)*. **241**, 462–464 (1988).
286. Newberg, A. B. *et al.* Concurrent CBF and CMRGlC changes during human brain activation by combined fMRI-PET scanning. *Neuroimage* **28**, 500–6 (2005).
287. Cha, Y.-H. K. *et al.* Regional correlation between resting state FDG PET and pCASL perfusion MRI. *J. Cereb. Blood Flow Metab.* **33**, 1909–1914 (2013).
288. Chen, Y. *et al.* Voxel-level comparison of arterial spin-labeled perfusion MRI and FDG-PET in Alzheimer disease. *Neurology* **77**, 1977–85 (2011).
289. Vaishnavi, S. N. *et al.* Regional aerobic glycolysis in the human brain. *Proc. Natl. Acad. Sci. U. S. A.* **107**, 17757–62 (2010).

2 Chapter 2

An investigation of changes in regional gray matter volume in cardiovascular disease patients, pre and post cardiovascular rehabilitation.

2.1 Introduction

According to the Institute of Medicine, the age standardized mortality rate from cardiovascular disease has declined steadily over the past 50 years in industrialized nations¹. Much of the decline can be attributed to effective management of risk factors associated with the disease. However, in the developed world, cardiovascular disease still remains the most prevalent chronic disease in individuals over the age of 50, and the debilitating effects of the disease are evident by the high rate of hospitalization amongst this patient group². Therefore, there is heightened urgency to understanding the impact of cardiovascular disease on 'successful aging', particularly given that the number of adults over the age of 60 is steadily increasing.

One growing concern is the potential link between cardiovascular disease risk factors and neurological impairment in older adults. Hypertension, diabetes and hyperlipidemia have been independently linked to abnormal changes in morphology and function of the aging brain³. Older individuals with higher estimated risk of coronary artery disease (CAD) tend to have decreased brain volume, cerebral blood flow, and glucose metabolism in regions of the brain associated with cognitive function and, as such, are at a greater risk of dementia³. Even in older adults with no clinical diagnosis of

cardiovascular disease, decline in cardiac function is associated with deficits in cognitive function⁴, brain atrophy⁵ and white matter hyperintensity⁶.

Despite the above studies involving cardiovascular risk factors, there have been no similar studies on the impact of cardiovascular disease, more specifically CAD, on normal age-related changes in regional brain morphology. Coronary artery disease is the most common form of cardiovascular disease in adults over 50 years old with known pathophysiology⁷ and effective management strategies⁸. Physical activity is one of the most powerful and readily available interventions with proven efficacy in preventing secondary CAD. Physical activity, specifically aerobic fitness has been shown to improve coronary flow, lower the risk of myocardial reinfarction, lower mortality rates, and improve overall cardiac function⁹. Consequently, increased levels of physical activity are increasingly prescribed as part of the clinical management for CAD¹⁰. In older adults, physical activity has also been associated with improved cognitive function¹¹, decreased risk for dementia¹² and reversal of cortical decline¹³.

These observations highlight the need to investigate the association between CAD and brain structure and whether interventions, such as physical activity, can reverse any adverse disease-related effects. The objectives of this study were twofold: 1) to investigate potential differences in regional gray matter volume in patients recently diagnosed with CAD compared to controls, and 2) to determine if a standard cardiac rehabilitation regimen would reverse CAD-related structural changes.

2.2 Methods

2.2.1 Participants

This study was approved by the Western University Health Sciences Research Ethics Board, and written informed consent was obtained from all subjects. CAD patients were recruited from the London Health Sciences Centre for Cardiac Rehabilitation and Secondary Prevention program following recent diagnosis of one of the following: acute coronary syndrome (ST elevation or non-ST elevation myocardial infarct), angina, percutaneous coronary intervention, or coronary artery bypass surgery. Patients were excluded if they had congenital coronary abnormality, cardiomyopathy, severe congestive heart failure, second or third-degree atrioventricular block, more than two myocardial infarcts, sick sinus syndrome, or major arrhythmias. Patients with uncontrolled hypertension or a history of diabetes for more than 5 years were also excluded. Age-matched control subjects included in this study had no clinical diagnosis of cardiovascular disease, were non-smokers, and did not have hypertension or diabetes. Both patients and controls were free of any neurological condition or disease.

2.2.2 Clinical assessments of health

The relevant clinical markers of CAD measured in all subjects are described below. A standard three-lead electrocardiogram was conducted after 20 minutes of supine rest. Blood pressure was continuously measured during electrocardiogram using a Finometer, which was calibrated against periodic sphygmomanometric measurements (Dinamp, GE Healthcare, Finland). Blood-borne markers of vascular disease namely; plasma lipids, cholesterol, high-sensitivity C-reactive protein (hs-CRP) and glucose, were

collected under fasting conditions. A Doppler echocardiography (GE/Vingmed System FiVe Doppler) was completed prior to cardio-respiratory exercise stress testing to assess left ventricular ejection fraction, left ventricular mass and left ventricular contractility. A test of global or overall cognitive function was performed with the Montreal Cognitive Assessment, MoCA (<http://www.mocatest.org/>). Cardiorespiratory fitness was measured by a graded exercise test in which subjects were tested to volitional exhaustion under standard clinical observation (ACSM 1995)¹⁴. Breath-by-breath measurements of oxygen consumption (VO_2), heart rate and blood pressure were recorded throughout the test. Maximal oxygen consumption ($\text{VO}_{2\text{max}}$) is an established marker of cardiorespiratory fitness and a clinically accepted surrogate marker for left ventricular function¹⁵. Each subject's $\text{VO}_{2\text{max}}$ was estimated from the graded exercise test.

2.2.3 Clinical assessments of cardiac rehabilitation

The aerobic exercise component of the cardiac rehabilitation (CR) program was performed according to current guidelines¹⁶ at an intensity of 40-70% of heart rate reserve (i.e., the difference between the age-predicted maximum and resting heart rates)¹⁷, or at a rate corresponding to an exertion score of 11-14 on the Borg scale¹⁸. Aerobic exercise was performed a minimum of 3 days per week at a duration of 20-to-30 minutes per session.

2.2.4 MRI data acquisition

Whole-brain MRI images were acquired on two Siemens 3T MAGNETOM[®] Verio systems (Siemens Medical Systems, Erlangen, Germany) equipped with 32-

channel head array coils. Sagittal T1-weighted images were acquired on each subject for gray matter volumetric analysis using a three-dimensional (3D) magnetization-prepared rapid gradient-echo imaging sequence (isotropic voxel resolution=1.0mm³; repetition time, echo time and inversion time = 2000, 2.98 and 900ms, respectively; acceleration factor = 3; and flip angle=9 degrees).

2.2.5 Voxel-based morphometry analysis

2.2.5.1 Effects of disease

T1-weighted images were segmented into gray matter (GM), white matter (WM) and cerebrospinal fluid (CSF) using the segmentation option in SPM8 (<http://www.fil.ion.ucl.ac.uk>). The tissue segments were then affine-registered to their respective Montreal Neurological Institute (MNI) tissue probability maps, averaged and smoothed with a 12-mm filter using DARTEL to create a study-specific template¹⁹. The individual GM images were spatially normalized to this template using a high-dimensional DARTEL registration and then multiplied by the Jacobian determinant (i.e., modulation) to correct for nonlinear differences in individual brain size. Finally, the GM images were smoothed with an 8-mm Gaussian filter. Local differences in GM volume (GMV) between groups were investigated with a gender-by-group two-factor analysis of variance, performed on the smoothed GMV images. An absolute threshold mask set at 0.1 was used to remove non-GM and extra-cranial effects. A significant positive effect of disease was identified at voxel levels that differed between groups at $p < 0.05$ after correction for multiple comparisons using the false discovery rate (FDR)²⁰.

2.2.5.2 Effects of Rehabilitation:

Pre and post CR T1-weighted images of the CAD patients were analyzed with the default options of the longitudinal module found in the VBM8 toolbox of SPM8. Briefly, each subject's data were analyzed in a series of steps that included; 1) intra-subject registration, 2) intra-subject bias correction, 3) segmentation, 4) non-linear DARTEL registration to study-specific template, 5) modulation of GM segments, and 6) spatial smoothing with an 8mm Gaussian filter. A repeated measures analysis of variance of the change in GM volume over time was performed on the smoothed GM image with a within-subject factor of time and between-subject factor of scanner. Gender-by-time analysis of variance was also explored. A positive significant change was identified at voxel levels that showed positive change in volume for $p < 0.05$ after correction for multiple comparisons using the more stringent family wise error (FWE). An absolute threshold mask was also set at 0.1.

To investigate evidence of GMV recovery with CR, binary masks of regions of interests (ROIs) were created using the MarsBaR ROI toolbox (<http://marsbar.sourceforge.net>) from clusters of voxels that showed statistically significant decline in GMV in the CAD group compared to controls (see table 2.2) with minimum voxel clusters of 50 contiguous voxels. Small volume correction was performed in SPM8 on contrast images from the repeated analysis of variance with the ROIs to restrict multiple comparisons to a smaller number of voxels, which reduced type II errors. Areas of GM recovery are reported as significant if clusters survive FWE correction at $p < 0.05$.

2.2.6 Statistical analysis

Statistical analyses were conducted with SPSS 20.0 statistical software (IBM Corp. Armonk, NY, and USA). Clinical assessments from the control group was compared to baseline data from the CAD patient group using a one-way multivariate analysis of variance to test for differences in cardiovascular health and cognitive function. Clinical parameters entered into the multivariate analysis for cardiovascular health include all variables listed in Table 2.1 except for age, gender, MoCA and VO₂max. Gender differences between groups was assessed by gender-by-group interaction and simple main effects of gender. Significant interaction and main effects are reported at $p < 0.05$. Spearman rank correlation analysis was performed between baseline total gray matter/ROI volumes and baseline MoCA scores, VO₂max and other clinical measures collected to investigate the association between overall cognition, fitness level, cardiovascular health, and brain atrophy. Total gray matter volume in mm³ for each subject was obtained from the VBM8 segmentation output, while mean values of regional gray matter volume were extracted from voxel clusters that showed significant difference between groups for each subject using MarsBaR, as described earlier.

A paired t-test was conducted on the clinical variables collected on the CAD patients pre and post CR to test for a difference between the means ($p < 0.05$). To test for association between fitness level and GMV post CR, a Spearman rank correlation analysis was performed between VO₂max and total gray matter/ROI volumes obtained from post CR data, and between change in GMV and change in VO₂max post CR.

2.3 Results

2.3.1 Cardiovascular disease effects

A total of 41 CAD patients and 21 controls participated in the study; their characteristics are provided in Table 2.1. Data from three controls and two CAD patients data were removed because of neurological incidental findings in the MRI data. Data from 36 patients and all controls were collected on one scanner, while data from the last 5 patients were acquired on a separate, but identical, scanner during the upgrade of the first one. All control subjects and 18 CAD patients completed the graded exercise testing with cardiorespiratory measures to maximum volitional exhaustion to establish maximal oxygen uptake ($VO_2\text{max}$).

The CAD group comprised of patients with clinical diagnosis at referral of angina (12.1%), myocardial infarct (12.1%) and coronary artery disease (69.7%). All patients were on a combination of drug therapy and 36.8% had percutaneous coronary intervention while 7.9% received coronary artery bypass grafting. Drug therapy included cholesterol lowering/statins (87.2%), beta-blockers (76.9%), ACE-inhibitors/Angiotensin II receptor blockers (56.4%) and anti-platelets including aspirin (84.6%). There were no significant interactions between gender and group for any of the clinical measures, including markers of fitness. No significant differences between patients and controls were found for measures of blood pressure, cardiac output, left ventricular ejection fraction, resting heart rate and blood glucose. However, compared to control, CAD patients had lower MOCA scores ($F = 4.3$ (1,53), $p < 0.05$), lower $VO_2\text{max}$ ($F = 17.04$ (1,53), $p < 0.001$), lower total cholesterol levels ($F = 16.22$ (1,56), $p < 0.001$), elevated body mass index, BMI ($F = 17.86$ (1,56), $p < 0.001$), and increased hs-CRP levels ($F =$

7.40 (1,55), $p < 0.01$). There was also significant difference in level of education ($p = 0.031$), as defined by the number of years of formal education, between patients (15.5 ± 2.7 years) and controls (18.3 ± 4.3 years).

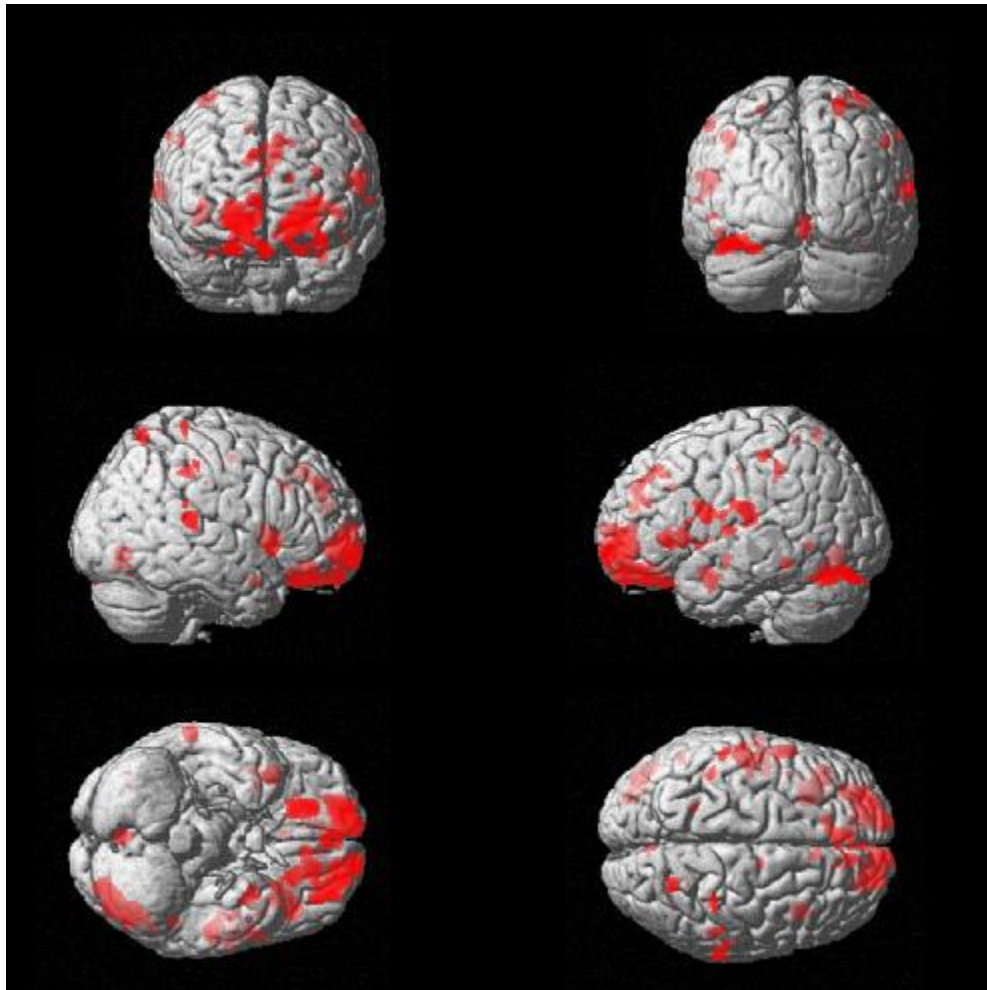
Table 2.1: Study participant characteristics. The mean and standard deviation are presented for clinical variables measured at baseline in CAD patients and controls.

Variable	Controls (n=21)	Pre-CR CAD patients (n=39)
Age	59 \pm 8	59 \pm 7
Gender (men/women)	11/10	28/11
BMI	24.8 \pm 3.3	29.8 \pm 4.7 ^a
Fasting blood glucose (mmol/L)	4.75 \pm 0.88	5.23 \pm 1.32
Total cholesterol (mmol/L)	4.17 \pm 0.94	3.16 \pm 0.79 ^a
hs-CRP (mg/l)	0.95 \pm 0.89	2.25 \pm 3.10 ^a
Rest supine systolic blood pressure (mmHg)	121 \pm 16	127 \pm 22
Rest supine diastolic blood pressure (mmHg)	69 \pm 8	71 \pm 12
Left ventricular ejection fraction (%)	68 \pm 9	64 \pm 8
Resting heart rate (beats per minute)	59 \pm 10	59 \pm 7
MoCA	28.16 \pm 1.7	26.86 \pm 2.1 ^a
VO ₂ max (mL/min/kg)	37 \pm 2	26 \pm 2 ^a

a = Statistical difference between groups at $p < 0.05$

VBM results of regional GMV differences between patients and controls are shown in Figure 2.1, and the corresponding MNI coordinates and Talairach anatomical labels are listed in Table 2.2. In general, the CAD patient group exhibited significantly lower GMV in the frontal lobe, parietal lobe, temporal lobe, and cerebellum. There was a significant difference in total GMV ($F = 5.5$ (1, 53), $p < 0.05$) between groups but no statistical difference in total intracranial volume. There were moderate positive associations between $VO_2\text{max}$ and total GMV ($\rho = 0.420$ (38), $p < 0.001$), and GMV in the left posterior cerebellum ($\rho = 0.616$ (38), $p < 0.001$) and right post central gyrus ($\rho = 0.403$ (38), $p < 0.01$). There was no significant gender-by-group interaction, nor was there any correlation between total/regional GMV and MoCA scores or any other clinical parameter measured. Repeating the VBM analysis after removing the data from the 5 patients acquired on the second system had no effect on these results, except to reduce the effect size of the observed regional changes by $5 \pm 13\%$.

Figure 2.1: Differences in GMV between CAD patients and age-matched controls measured at baseline.



t-statistics displayed on a rendered model of a single subject brain. The red blobs on coronal, sagittal and transverse planes indicate areas of decreased GMV in the CAD patient group.

Table 2.2: Local maxima of clusters of significant change in GM volume in the pre-CR CAD patient group compared to controls.

Cluster Number	Volume (mm)	Anatomical label	Brodmann Area	MNI Coordinate			t-value
				x	y	z	
1	2688	L superior frontal gyrus	10	-22	57	-10	5.03
		L superior frontal	10	-18	55	-23	3.00
		L medial frontal	11	-27	45	-6	4.66
2	1831	R superior frontal gyrus	10	18	58	-10	4.96
		L frontal lobe (rectal gyrus)	11	0	48	-23	4.76
		R superior frontal	10	14	54	-15	3.81
3	1515	L posterior cerebellum	NA	-40	-68	-12	4.90
4	510	R posterior cerebellum	NA	3	-73	-3	4.73
5	799	R medial frontal gyrus	9	9	47	29	4.64
		L medial frontal gyrus	8	-6	45	29	3.74
6	674	R inferior frontal gyrus	47	42	15	-3	4.52
7	977	L parietal lobe (post central gyrus)	40	-56	-20	19	4.42
		L Frontal (precentral gyrus)	4	-51	-13	42	3.74
8	202	L inferior frontal gyrus	44	-53	4	16	4.41
		L parietal (precentral)	4	52	-5	15	3.50
9	774	R orbitofrontal	11	22	38	-22	4.33
10	1601	L Inferior frontal gyrus	47	-42	28	-1	4.31
		L Insula		-33	17	0	4.01
11	134	L inferior parietal gyrus	40	-42	-36	41	4.13
12	518	R inferior parietal lobe	40	51	-33	40	4.07
13	83	L middle temporal gyrus	37	-51	-55	0	4.02
14	127	R superior parietal gyrus	7	24	-58	61	3.96
15	141	L temporal lobe (Fusiform)	37	-50	-42	-10	3.71
16	270	L superior temporal gyrus	38	-33	5	-17	3.63
17	50	R superior temporal gyrus	38	44	3	-19	3.50
18	69	R inferior temporal gyrus	20	39	-22	-31	3.45
19	74	R anterior cingulate gyrus (dorsolateral)	32	6	25	30	3.38

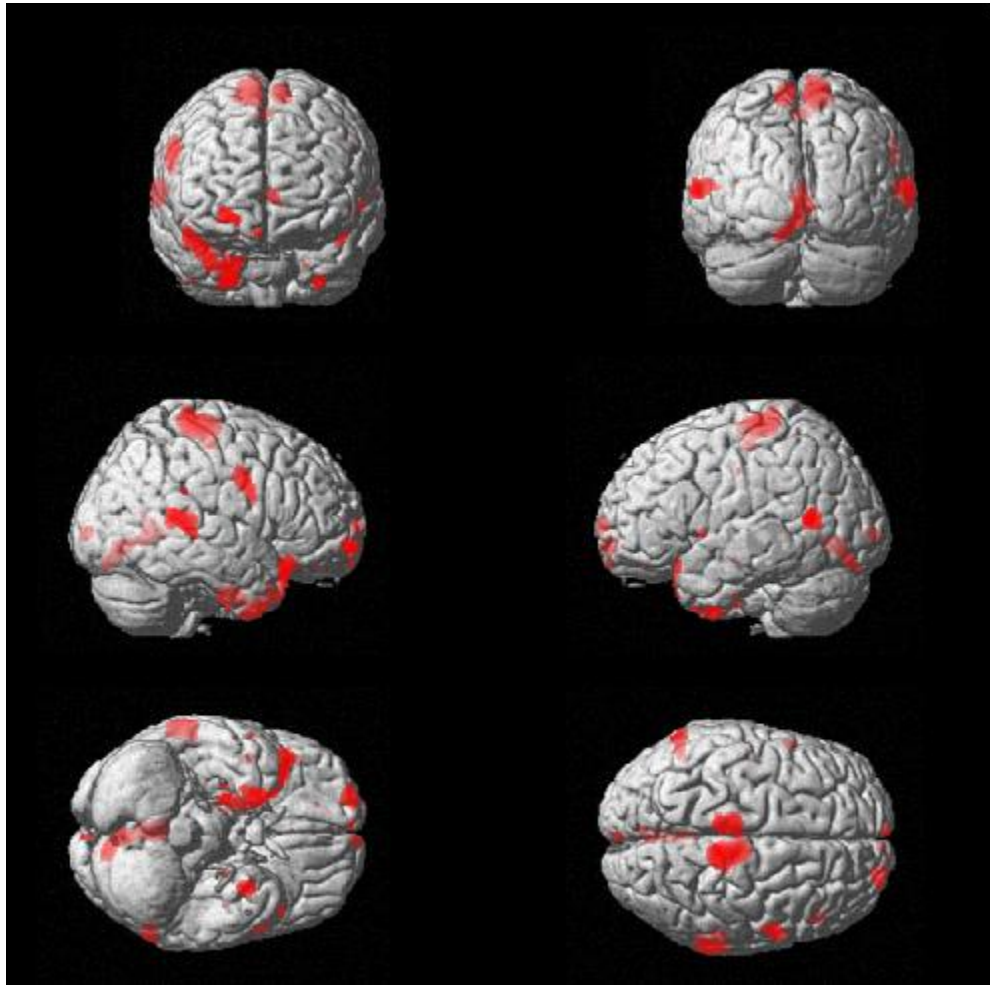
Coordinates are given in anatomical MNI space and maxima are shown at least 8.0 mm apart. The center of mass of each ROI is shown in bold. L = left; R = right.

2.3.2 Effects of cardiac rehabilitation

Twenty-four CAD patients (18 men and 6 women) completed the 6-month CR program and post-CR testing. The MRI data, pre and post rehabilitation, from the last five patients were acquired on the second scanner. Fifteen patients completed graded exercise testing to maximum volitional exhaustion on entry and exit from the CR program. No statistically significant differences were found in any of the clinical parameters between the pre and post CR tests. In addition, there was no change in MoCA scores ($p = 0.3$) after 6 months of CR. There was a trend (5%) towards increased $VO_2\text{max}$ ($p=0.06$) in the 15 patients tested after 6 months of CR.

Regions of positive change in GMV from VBM analysis of CAD patients, pre and post CR, are listed in Table 2.3 and displayed on Figure 2.2. The main increases in GMV after 6 months of CR were observed bilaterally in the frontal lobe, middle temporal gyrus and supplementary motor area (Table 2.3). Small clusters of increase in GMV were observed in some of the regions affected by CAD (see Table 2.4), signifying a recovery of volume following CR. There was no change in total GMV or total intracranial volume after CR. No significant correlation was found between $VO_2\text{max}$ post CR and regional GMV and between change in $VO_2\text{max}$ and regional increase in GMV. There was no significant scanner-by-time interaction or gender-by-time interaction ($p < 0.05$, FWE) and no difference in GMV or clinical measures between patients that successfully completed exercise testing and patients that were unable to.

Figure 2.2: GMV changes over time in CAD patient pre and post CR.



t-static displayed on a rendered model of a single subject brain. Red blobs on coronal, sagittal and transverse planes indicate areas of increased GMV in the CAD group after 6 months of CR.

Table 2.3: Local maxima of clusters of significant change in GM volume in the CAD post CR (Post >Pre).

Cluster Number	Volume (mm)	Anatomical label	Brodmann Area	MNI Coordinate			t-value
				x	y	z	
1	1095	Right frontal(paracentral) lobe	6	8	-33	66	13.67
2	304	Left middle temporal gyrus	21	-62	-60	9	11.63
3	504	Left frontal (paracentral) lobe	6	-8	-28	66	10.70
		Right anterior cerebellum	NA	3	-55	4	10.37
4	782	Left posterior cerebellum	NA	0	-73	-8	8.92
		Left cerebellum	NA	-8	-81	-15	8.44
5	191	Right superior frontal gyrus	10	22	63	-8	10.26
6	122	Left inferior temporal gyrus	20	-32	0	-47	8.88
7	1175	Right superior temporal	38	22	8	-45	8.88
		Right superior temporal	22	64	-42	10	8.12
8	427	Right middle temporal gyrus	22	66	-34	4	7.84
9	246	Right frontal (precentral) gyrus	6	56	0	31	7.79
10	28	Left superior temporal gyrus	22	-56	11	-2	7.33
11	54	Left medial frontal gyrus	10	-3	66	6	7.27
13	93	Right medial frontal gyrus	6	4	-19	54	7.13

Coordinates are given in anatomical MNI space, and maxima shown are at least 8.0 mm apart. The center of mass of each ROI is shown in bold. Corrected for multiple comparisons (FWE, $p < 0.05$).

Table 2.4: Cluster of GMV recovery after 6 months of CR (N=24). Small volume correction ($p < 0.05$, FWE).

Cluster Number	Volume (mm)	Anatomical label	Brodmann Area	MNI Coordinate			t-value
				x	y	z	
1	128	Right superior frontal gyrus	11	22	61	-10	10.26
2	23	Right middle temporal gyrus	22	67	-37	13	7.20
3	99	Left posterior cerebellum (declive of vermis)	NA	0	-72	-3	8.92

2.4 Discussion

The key findings of the current study were lower GMV in the prefrontal cortex, parietal and temporal lobes of CAD patients compared to age-matched controls (Figure 2.1 and Table 2.2) and increased GMV in the superior frontal gyrus, medial frontal gyrus and superior temporal gyrus after 6 months of cardiovascular rehabilitation (Figure 2.2 and Table 2.3). This study is the first to show evidence of regional cortical brain atrophy associated with cardiovascular disease and also the ability of cardiovascular rehabilitation to reverse disease-related cortical atrophy.

2.4.1 Cardiovascular disease effects

Our CAD group were patients diagnosed with either angina or myocardial infarction who were all receiving some form of treatment prior to the start of the study. Most patients were on a combination of drug therapy to lower lipid levels, maintain blood pressure, and to prevent reinfarction. The therapeutic impact of these treatments might

have contributed to the lack of any statistical differences in fasting blood glucose, resting supine blood pressure, cardiac output or heart rate between patients and controls. The CAD patients had lower lipid levels compared to controls, which can be attributed to the efficacy of statins in reducing serum levels of cholesterol²¹. However, mean hs-CRP, a marker of inflammation associated with increased risk of myocardial infarct or reinfarction, was higher for CAD patients than controls.

2.4.2 CAD-related effects: Brain atrophy

The findings of decreased GMV in the frontal, temporal and parietal lobes of CAD patients are similar to the patterns of brain atrophy previously observed in patients with either hypertension or diabetes, in which marked declines in GMV were found in the prefrontal cortex, superior temporal and middle temporal lobes, thalamus, and hippocampus³. The regions common to all of these studies are associated with varying cognitive functions – executive function, attention, and memory, visuospatial and psychomotor speed – and are believed to be susceptible to vascular disease²². A study of 400 men over the age of 40 found that cardiovascular disease was associated with poor performance in memory tests and a trend towards lower scores in mini-mental state examination²³. Similarly, Okonkwo et al.²⁴ reported an accelerated decline in the aforementioned cognitive domains in a large group of cardiovascular disease patients over a three year period that was not attributed to aging. In addition, numerous studies have linked markers of cardiovascular disease including impaired vascular hemodynamics (pulse wave variability, arterial stiffness, and ventricular function) to alterations in cognitive function^{25,26}. In general, the observation of decreased GMV in the

frontal, temporal and parietal lobes indicates that CAD accelerates age-related neocortical degeneration, possibility leading to declining cognitive function.

Our findings of bilateral atrophy in the posterior cerebellum and in the inferior parietal lobule of the brain in the CAD group is novel given that these regions are usually preserved with age and atrophy has only been reported in a few dementia studies^{27,28}. These studies linked poor performance on short-term memory and visuospatial tasks to GMV decline in either the cerebellum²⁷ or the inferior parietal lobule²⁸, highlighting the known importance of both regions in neurocognitive integration. Taken together, these observations suggest that in older adults, cardiovascular disease can precipitate changes in normally stable regions of the brain.

A significant difference in mean baseline MoCA scores between the CAD group and controls was found in the current study (Table 2.1). 24% of CAD patients had a score of 25 or less compared to 5% of controls. A MoCA score of less than 26 is typically considered to reflect mild cognitive impairment (MCI). However, there was no correlation between MoCA scores and regional brain atrophy. Considering the MoCA is a brief assessment tool of MCI²⁹, it may not be ideal for probing subtle cognitive decline in middle-aged adults since evidence of cognitive decline typically occurs after the age of 60³⁰. The apparent difference in MoCA scores between groups could possibly be a mere reflection of the difference in levels of education observed between groups. Education was associated with performance on MoCA ($r=0.518$, $p<0.01$), but not total or regional GMV. Similarly, Christensen et al³¹ found no link between level of education and global or regional brain atrophy in adults with no history of cognitive impairments. The use of tests more specific to the cognitive functions associated with the observed areas of brain

atrophy might reveal greater impairment. Nonetheless, the current data support the overall concern that CAD accelerates cortical atrophy with detrimental outcomes to cognitive ability.

The direct mechanism(s) that drive the greater brain atrophy associated with cardiovascular disease are unclear. One possible mechanism could involve cerebral hypoperfusion. Animal studies have shown that cerebral hypoperfusion from ischemic vessels can initiate pathophysiological changes in the brain structure and function of aging rats, resulting in decreased synaptic activity and impaired memory and visuospatial skills³². Human studies of diabetic and hypertensive patients have reported regional cerebral hypoperfusion in similar regions of the brain where atrophy has been reported^{33,34}. Investigating cerebral blood flow or cerebrovascular dynamics with morphometric imaging would help elucidate potential neurovascular changes in CAD patients.

A common cause underlying both CAD and brain atrophy could be physical inactivity. Physical inactivity is an important modifiable risk factor for heart disease given that inactive individuals are twice as likely to suffer a coronary event in their lifetime compared to physically active individuals³⁵. In this study, the CAD patients were 40% less fit than controls and the less fit individuals were more likely to have lower global and regional GMV. In general, physical inactivity is associated with regional brain atrophy³⁶ and cognitive decline³⁷ in healthy older adults.

2.4.3 Effect of rehabilitation: neuroplasticity

The propensity for age and CAD to adversely affect the function and morphology of certain regions of the brain, namely the prefrontal, superior parietal, inferior temporal and middle temporal, suggests that these regions are highly malleable and perhaps more adaptive to change. Recovery of volume within these brain regions with exercise in both healthy aging subjects and dementia patients signifies that these regions are highly plastic^{11,38,39}. These observations are in good agreement with our finding of increased GMV in the prefrontal, left middle temporal, left inferior temporal lobes in addition to the cerebellum, supplementary motor areas and right superior temporal gyrus of CAD patients after 6 months of CR.

The significance of aerobic fitness in improving cardiovascular and cerebral functions is well established and discussed in great detail in reviews by Erickson et al³⁹ and Lavie et al⁴⁰. Briefly, with CAD, aerobic fitness is associated with a significant decrease in relative risk of mortality, improved ventricular function, and improved vascular dynamics⁴¹. In older adults and dementia patients, exercise training was associated with increases in regional brain volume, improved cognitive function, and increased neuronal activity⁴⁰. Increases in regional GMV^{13,42} and cognitive function⁴³ have been reported after 6 months of moderate level of exercise training (40-70% of heart rate reserve). The prescribed 6 months of aerobic exercise, as part of the CR program, was sufficient to cause detectable changes in brain structures of CAD patients including changes in non-motor areas, despite the observed modest impact on aerobic fitness.

Findings of recovery of GMV in areas of the superior frontal lobe, superior temporal lobe and posterior cerebellum (Table 2.4) after a short period of exercise are

promising and indicate a unique positive outcome of CR. It could be postulated that recovery of brain volume in these regions could potentially be maintained over longer periods. Erickson et al.⁴³ found retention of regional brain volume in older adults that performed low intensity exercise nine years after cessation of the activity.

2.4.4 Study consideration

The impact of cardiac artery bypass grafting surgery (CABG) on neuroanatomy and cognitive function cannot be ignored. CABG is known to exert transient decrease in brain volume and cognitive function⁴⁴. The interaction between cardiovascular disease and CABG on regional GMV was not explored given that only 8% of CAD patients in this study underwent CABG and this occurred a few months prior to the start of the study.

It is possible that the GMV changes observed post CR in CAD patients might not reflect the full potential neurorehabilitatory benefits of CR giving the moderate improvement in GMV post exercise training. Considerable changes could be achieved with either high-intensity aerobic exercises or activities such as basket ball, hockey or squash that incorporate motor skills along with cognitive and perceptual skills (areas which showed significant GMV decline with CAD). The lack of association between VO₂max and GMV could be a result of the large number of patients who were unable to complete the graded exercise test for various reasons including the inability to reach maximal volitional exhaustion, which is common among CAD patients. Submaximal graded exercise tests or a 6 minute walk test could be used to evaluate cardiorespiratory capacity in CAD patients who cannot achieve maximal myocardial oxygen uptake.

However, submaximal VO_2 tests often lack diagnostic accuracy, particularly tests that exclude heart rate measures with electrocardiography.

The innate methodological limitations of VBM are also drawbacks to the interpretation of our findings. The registration, segmentation and normalization steps in VBM can introduce bias and distortion errors particularly in the border of small subcortical GM structures where some proximal voxels can be misclassified^{45,46}. This error is exaggerated in older brains prone to enlarged ventricles. We minimized these distortion errors with the use of a study-specific template and DARTEL registration method^{19,46}. However, this inherent segmentation and registration bias can pose a limitation to the investigation of CAD-related regional brain volume changes in vulnerable subcortical regions such as the hippocampus where decline in volume have been previous reported in CAD⁴⁷. For longitudinal studies, available intra-subject bias correction methods attempt to minimize the influence of baseline differences on images from subsequent time points. However, issues of registration asymmetry can be largely improved with symmetric diffeomorphic approaches proposed for future versions of SPM, particularly for non-quantitative T1-imaging data⁴⁸.

A potential limitation with this study was the use of two scanners in data acquisition. However, performing the analysis of the effects of CAD without the five patients imaged on the second scanner revealed no difference in the pattern of regional GMV differences reported in Table 2.2 and shown in Figure 2.1. Furthermore no significant effect was found by including scanner as a between-subject factor in the analysis of the rehabilitation data.

2.5 Conclusion

This study demonstrates that in stable CAD patients, cardiovascular disease is associated with brain atrophy in several brain regions, including those related to cognitive ability. This disease-related effect appears to be reversible as this study demonstrated that a modest aerobic program reversed some of the structural abnormalities.

2.6 References

1. IOM. in (Fuster, V. & Kelly, B.) (The National Academies Press, 2010). at <www.iom.edu>
2. World Health Organization. in (Mendis, S., Puska, P. & Norrving, B.) (2011).
3. De Toledo Ferraz Alves, T. C., Ferreira, L. K., Wajngarten, M. & Busatto, G. F. Cardiac disorders as risk factors for Alzheimer's disease. *J. Alzheimer's Dis.* **20**, 749–63 (2010).
4. Jefferson, A. L., Poppas, A., Paul, R. H. & Cohen, R. A. Systemic hypoperfusion is associated with executive dysfunction in geriatric cardiac patients. *Neurobiol. Aging* **28**, 477–483 (2007).
5. Jefferson, A. L. Cardiac output as a potential risk factor for abnormal brain aging. *J. Alzheimer's Dis.* **20**, 813–21 (2010).
6. Jefferson, A. L. *et al.* Lower Cardiac Output Is Associated with Greater White Matter Hyperintensities in Older Adults with Cardiovascular Disease. *J. Am. Geriatr. Soc.* **55**, 1044–1048 (2007).
7. Chilton, R. J. Pathophysiology of coronary heart disease: a brief review. *J. Am. Osteopath. Assoc.* **104**, S5–8 (2004).

8. Pflieger, M., Winslow, B. T., Mills, K. & Dauber, I. M. Medical management of stable coronary artery disease. *Am. Fam. Physician* **83**, 819–26 (2011).
9. Shephard, R. J. & Balady, G. J. Exercise as Cardiovascular Therapy. *Circulation* **99**, 963–972 (1999).
10. Smith, S. C. *et al.* AHA/ACCF Secondary Prevention and Risk Reduction Therapy for Patients With Coronary and Other Atherosclerotic Vascular Disease: 2011 Update: A Guideline From the American Heart Association and American College of Cardiology Foundation. *Circ.* **124**, 2458–2473 (2011).
11. Colcombe, S. J. *et al.* Cardiovascular fitness, cortical plasticity, and aging. *Proc. Natl. Acad. Sci. U. S. A.* **101**, 3316–21 (2004).
12. Larson, E. B. *et al.* Exercise Is Associated with Reduced Risk for Incident Dementia among Persons 65 Years of Age and Older. *Ann. Intern. Med.* **144**, 73–81 (2006).
13. Colcombe, S. J. *et al.* Aerobic Exercise Training Increases Brain Volume in Aging Humans. *J. Gerontology* **61**, 1166–1170 (2006).
14. American College of Sports Medicine. *ACSM guidelines for exercise testing and prescription.* (Williams & Wilkins, 1995).
15. Fletcher, G. F. *et al.* *Exercise Standards for Testing and Training: A Statement for Healthcare Professionals From the American Heart Association.* *Circulation* **104**, (2001).
16. Stone, J., Arthur, H. & Suskin, N. *Guidelines for Cardiac Rehabilitation and Cardiovascular Disease Prevention: Translating Knowledge into Action.* 3rd ed. (2009).
17. Karvonen, M., Kentala, K. & Mustala, O. The Effects of Training on Heart Rate: Longitudinal Study. *Ann. Med. Exp. Biol. Fenn.* **35**, (1957).

18. Borg, G. Psychophysical bases of perceived exertion. *Med. Sci. Sports Exerc.* **14**, 377–381 (1982).
19. Ashburner, J. A fast diffeomorphic image registration algorithm. *Neuroimage* **38**, 95–113 (2007).
20. Genovese, C. R., Lazar, N. a & Nichols, T. Thresholding of statistical maps in functional neuroimaging using the false discovery rate. *Neuroimage* **15**, 870–878 (2002).
21. Cholesterol Treatment Trialists' (CTT) Collaborators. The effects of lowering LDL cholesterol with statin therapy in people at low risk of vascular disease: meta-analysis of individual data from 27 randomised trials. *Lancet* **380**, 581–590 (2012).
22. Nordlund, A. *et al.* Cognitive Profiles of Mild Cognitive Impairment With and Without Vascular Disease. *Neuropsychology* **21**, 706–712 (2007).
23. Muller, M., Grobbee, D. E., Aleman, a, Bots, M. & van der Schouw, Y. T. Cardiovascular disease and cognitive performance in middle-aged and elderly men. *Atherosclerosis* **190**, 143–9 (2007).
24. Okonkwo, O. C. *et al.* Longitudinal trajectories of cognitive decline among older adults with cardiovascular disease. *Cerebrovasc. Dis.* **30**, 362–73 (2010).
25. Fujiwara, Y. *et al.* Arterial Pulse Wave Velocity as a Marker of Poor Cognitive Function in an Elderly Community-Dwelling Population. *Journals Gerontol. Ser. A Biol. Sci. Med. Sci.* **60** , 607–612 (2005).
26. Wendell, C. R., Zonderman, A. B., Metter, E. J., Najjar, S. S. & Waldstein, S. R. Carotid intimal medial thickness predicts cognitive decline among adults without clinical vascular disease. *Stroke* **40**, 3180–5 (2009).
27. Yoon, C. W. *et al.* Cerebellar atrophy in patients with subcortical-type vascular cognitive impairment. *Cerebellum* **12**, 35–42 (2013).

28. Greene, S. J., Killiany, R. J. & Initiative, A. D. N. Subregions of the inferior parietal lobule are affected in the progression to AD. *Neurobiol. Aging* **31**, 1304–1311 (2010).
29. Nasreddine, Z. *et al.* The Montreal Cognitive Assessment, MoCA: a brief screening tool for mild cognitive impairment. *J. Am. Geriatr. Soc.* **53**, 695–699 (2005).
30. Hedden, T. & Gabrieli, J. D. E. Insights into the ageing mind: a view from cognitive neuroscience. *Nat Rev Neurosci* **5**, 87–96 (2004).
31. Christensen, H. *et al.* Education, atrophy, and cognitive change in an epidemiological sample in early old age. *Am. J. Geriatr. Psychiatry* **17**, 218–26 (2009).
32. De la Torre, J. . Critically attained threshold of cerebral hypoperfusion: the CATCH hypothesis of Alzheimer’s pathogenesis. *Neurobiol. Aging* **21**, 331–342 (2000).
33. Last, D. *et al.* Global and Regional Effects of Type 2 Diabetes on Brain Tissue Volumes and Cerebral Vasoreactivity. *Diabetes Care* **30**, 1193–1199 (2007).
34. Dai, W. *et al.* Abnormal regional cerebral blood flow in cognitively normal elderly subjects with hypertension. *Stroke*. **39**, 349–54 (2008).
35. Powell, K. E., Thompson, P. D., Caspersen, C. J. & Kendrick, J. S. Physical activity and the incidence of coronary heart disease. *Annu. Rev. Public Health* **8**, 253–287 (1987).
36. Yuki, A. *et al.* Relationship between physical activity and brain atrophy progression. *Med. Sci. Sports Exerc.* **44**, 2362–2368 (2012).
37. Barnes, D. E., Yaffe, K., Satiriano, W. A. & Tager, I. B. A Longitudinal Study of Cardiorespiratory Fitness and Cognitive Function in Healthy Older Adults. *J. Am. Geriatr. Soc.* **51**, 459–465 (2003).

38. McAuley, E., Kramer, A. F. & Colcombe, S. J. Cardiovascular fitness and neurocognitive function in older Adults: a brief review. *Brain. Behav. Immun.* **18**, 214–220 (2004).
39. Erickson, K. I., Miller, D. L., Weinstein, A. M., Akl, S. L. & Banducci, S. Physical activity and brain plasticity in late adulthood: a conceptual and comprehensive review. *Ageing Res.* **4**, 34–47 (2012).
40. Lavie, C. J., Thomas, R. J., Squires, R. W., Allison, T. G. & Milani, R. V. Exercise training and cardiac rehabilitation in primary and secondary prevention of coronary heart disease. *Mayo Clin. Proc.* **84**, 373–83 (2009).
41. LD, B., LL, F., K, F.-S. & et al. Effects of aerobic exercise on mild cognitive impairment: A controlled trial. *Arch. Neurol.* **67**, 71–79 (2010).
42. Lautenschlager, N. T. *et al.* Effect of physical activity on cognitive function in older adults at risk for alzheimer disease: A randomized trial. *JAMA* **300**, 1027–1037 (2008).
43. Erickson, K. I. *et al.* Physical activity predicts gray matter volume in late adulthood: the Cardiovascular Health Study. *Neurology* **75**, 1415–22 (2010).
44. Selnes, O. a & McKhann, G. M. Neurocognitive complications after coronary artery bypass surgery. *Ann. Neurol.* **57**, 615–21 (2005).
45. Ashburner, J. & Friston, K. J. Voxel-based morphometry--the methods. *Neuroimage* **11**, 805–21 (2000).
46. Good, C. D. *et al.* A voxel-based morphometric study of ageing in 465 normal adult human brains. *Neuroimage* **14**, 21–36 (2001).
47. Koschack, J. & Irle, E. Small hippocampal size in cognitively normal subjects with coronary artery disease. *Neurobiol. Aging* **26**, 865–71 (2005).

48. Ashburner, J. & Ridgway, G. R. Symmetric diffeomorphic modeling of longitudinal structural MRI. *Front. Neurosci.* **6**, 197 (2013).

3 Chapter 3

Impaired Cerebrovascular Function in Coronary Artery Disease Patients, and Recovery Following Cardiac Rehabilitation.

3.1 Introduction:

Cardiovascular disease increases the rate of age-related cortical atrophy¹, the risk of dementia², and the risk of stroke. These relationships likely are due to progression of vascular disease into the cerebral circulation. Cerebrovascular disease and alterations to the structure and function of the brain are increasingly associated with cardiovascular disease risk factors such as hypertension, atherosclerosis and diabetes³. This comorbidity of cardiovascular disease and neurological impairments in older adults is a growing area of concern, since aberrant brain changes related to vascular disease appear to affect regions involved in cognitive function².

A number of studies have demonstrated that vascular disease processes accelerate brain decay and alter the natural age-related decline in cerebrovascular hemodynamics⁴. In asymptomatic older adults, decline in cardiac output is associated with global brain atrophy⁵, regional cerebral hypoperfusion⁶ and impairments in cognitive abilities⁷. Recently, we observed significant reductions in regional brain volume in the brains of coronary artery disease patients¹ that are consistent with observations of cerebral atrophy, hypoperfusion, and white matter disease in brains of older adults with increased risk for vascular disease³. Although these observations suggest a possible link between

cardiovascular disease and neurological dysfunction, the interaction of age, vascular disease and cortical degeneration is complex and not well understood^{4,6}. In addition, the effect of cardiovascular disease on cerebrovascular hemodynamics and function has not been fully characterized. Vascular diseases may accelerate cerebrovascular aging and in doing so, significantly alter normal cerebral blood flow distribution, inducing brain atrophy and cognitive decline⁶. However, no study to date has described regional cerebrovascular hemodynamics in individuals with ischemic vascular disease.

Building on our previous work, this study assessed cerebrovascular hemodynamics and relationships between hemodynamic changes and brain atrophy in the same cohort of coronary artery disease (CAD) patients and age matched controls. Furthermore the therapeutic effects of cardiac rehabilitation on cerebral blood flow (CBF) in CAD patients were assessed in a subsample. We explored regional changes in CBF and cerebrovascular reactivity to CO₂ (CVR) in cognitive areas of the brains of CAD patients, since increased vascular resistance, common in CAD can diminish CVR⁸. Measurements of CBF and CVR were performed using arterial spin labelling (ASL).

3.2 Materials and Methods:

3.2.1 Participants

Participants were part of a larger prospective study examining the effects of cardiovascular disease on brain health. The CAD patients were recruited from the London Health Sciences Center for Cardiac Rehabilitation and Secondary Prevention program, and controls matched in age, were recruited from the local community. The present sample are subjects from a previous study¹ and consists of 34 CAD patients (58 ±

7 years, 10 females) and 21 healthy controls (59 ± 8 years, 10 females) whom had MRI scans that included ASL acquisitions. Of the 34 patients, 17 (59 ± 6 years, 5 females) completed a 6-month CR program and participated in post-CR testing. CAD was defined by a history of one of the following: acute coronary syndrome (ST elevation or non-ST elevation myocardial infarct), angina, percutaneous coronary intervention, or coronary artery bypass surgery. Exclusion criteria included patients with congenital coronary abnormality, cardiomyopathy, severe congestive heart failure, second or third-degree atrioventricular block, more than two myocardial infarcts, sick sinus syndrome, major arrhythmias, uncontrolled hypertension or a history of diabetes for more than 5 years. Controls were excluded if they had clinical diagnosis of cardiovascular disease, hypertension and diabetes. All participants were free of neurological diseases, pharmaceutical or nutraceutical psychostimulants, nootropics and non-smokers. This study was approved by the Western University Health Sciences Research Ethics Board and written informed consent was obtained from all participants.

3.2.2 Experimental design

Experimental data were collected over three testing sessions: 1) a laboratory session for assessment of clinical markers of vascular health, 2) graded exercise testing and 3) brain MRI. Subjects refrained from caffeine, alcohol and physical activity at least 12 h before participating in each session. To capture global cognitive function, the Montreal Cognitive Assessment, (MoCA, <http://www.mocatest.org>) was administered during the laboratory testing. MoCA scores were corrected for level of education - defined by the total number of years of formal education, as described on

<http://www.mocatest.org>. The entire experimental protocol was repeated in the 17 CAD patients who performed 6 months of cardiac rehabilitation, which consisted of moderate-intensity aerobic and strength fitness training. The aerobic training protocol was performed as previously described¹ and as prescribed by the London Health Sciences Center Cardiac Rehabilitation and Secondary Prevention Program.

Cerebrovascular reactivity measurements were achieved by manipulations of arterial concentrations of CO₂. Subjects breathed room air for 5 min, followed by 5 min inhalation of 6% CO₂ mixed with 21% O₂ and balanced nitrogen, while end-tidal partial pressure of CO₂ (P_{ET}CO₂) was recorded continuously (Invivo 3150m, Invivo Corp., Orlando, Florida). Air and mixed CO₂ were delivered via a non-rebreathing facemask (Hans Rudolph Inc., Kansas City, Missouri) attached to a large non-diffusible gas reservoir bag. The breathing rate was paced at 15 breaths/minute guided by a metronome to minimize hyperventilation and maintain steady-state sampling of P_{ET}CO₂. The hypercapnia challenge was performed first in the laboratory in supine position to acclimatize participants prior to repeating the challenge during brain imaging. Participants unable to perform hypercapnia testing or who had a change in P_{ET}CO₂ (Δ P_{ET}CO₂) of 5mmHg or less in the laboratory examinations did not perform the challenge during the MRI session. Instead only resting CBF images were acquired.

3.2.3 Clinical measurements

To assess levels of plasma lipids, cholesterol, blood glucose, glycated hemoglobin (HbA1c) and high-sensitivity C-reactive protein (hs-CRP), blood samples were collected under fasting conditions and analyzed using standard assays and glucometer. Three-lead

electrocardiogram and finger blood pressure monitoring (Finometer; Finapres Medical Systems, Amsterdam, the Netherlands; calibrated to sphygmomanometric values) were performed concurrently over a 20 min period. Mean values for heart rate, systolic blood pressure, diastolic blood pressure and mean arterial pressure were reported from measures averaged over 5 min. Vascular hemodynamic measurements were performed on the right common carotid artery using Doppler ultrasound imaging (Vivid 7, GE Healthcare). Carotid vessel diameter, wall thickness and intima media thickness were measured from 2-dimensional (2D) B-mode images acquired in the long-axis plane by a single observer blinded to subject identity or group assignment. Arterial compliance and distensibility were calculated from measures of vessel diameter and pressure at end systole and end diastole⁹. A 2D transthoracic Doppler echocardiogram (Vingmed System FiVe, GE Healthcare, Chalfont St Giles, UK) was performed to assess left ventricular ejection fraction (EF) - a clinical index of cardiac function. Graded exercise testing was performed to volitional exhaustion to measure cardiorespiratory fitness level or capacity (maximal oxygen consumption, VO_2 max), in accordance with the American College of Sports Medicine guidelines for exercise testing.

3.2.4 MRI data acquisition

All MRI brain imaging was performed on a Siemens 3T Verio system (Siemens Medical Systems, Erlangen, Germany) using a 32-channel head coil. The head was immobilized with foam padding to minimize motion artefacts. Sagittal T1-weighted images were acquired using a three-dimensional magnetization-prepared rapid gradient-echo (MPRAGE) sequence (repetition time (TR), echo time (TE) and inversion time (TI)

= 2000, 2.98 and 900 ms, flip angle = 9° , field of view (FOV) = $256 \times 256 \text{ mm}^2$, 176 slices, isotropic voxel size = 1.0 mm^3 , acceleration factor = 3) to measure cortical thickness. ASL images were acquired during hypercapnia testing using a transverse 2D gradient-echo echo planar imaging (EPI) sequence (TR/TE = 3500/12 ms, FOV = $240 \times 240 \text{ mm}^2$, 12 contiguous slices, 6 mm thickness, voxel size = $3.8 \times 3.8 \times 6 \text{ mm}^3$, bandwidth = 2298 Hz/Px, acceleration factor of 2) and a pseudo-continuous label method¹⁰ applied 9 cm below the center of the imaging volume for a duration of 1.5 s. One-hundred and ten label and control pairs were acquired after a 1.0 s post-label delay. A non-selective inversion pulse was applied for background suppression during the post-label delay. To improve signal-to-noise (SNR) and sensitivity of ASL for CVR measurements, ASL imaging and hypercapnia testing were repeated after a 3 min recovery period. Additional imaging for CBF quantification included; a) proton density calibration scan (M_0) acquired with the ASL sequence using a TR of 7 s and no label or background suppression pulses, and b) axial single-shot inversion-recovery prepared balanced steady-state free precession imaging (IR-TrueFISP) acquired with 10 variable TI (175 to 8000 ms) on a single slice at the mid-sagittal section of the brain (TE = 1.21 ms, $1.7 \times 1.7 \times 4 \text{ mm}$, acceleration factor of 2). These images were used to measure the longitudinal relaxation time of blood (T_{1b}) in the sagittal sinus¹¹.

3.2.5 Perfusion-weighted analysis

Preprocessing and analysis of perfusion data were performed with SPM8 (<http://www.fil.ion.ucl.ac.uk>) and scripts written in MATLAB (2012a, The MathWorks, Natick, MA). All ASL and M_0 scans were aligned to the first time point of the first scan

to correct for head motion within sessions (two trials) and between sessions (pre and post-CR). Intra-subject alignment was performed on MPRAGE images using the VBM8 longitudinal toolbox (<http://dbm.neuro.uni-jena.de/vbm>) in SPM8 to minimize intra-subject registration errors. Using a rigid-body transformation, respective MPRAGE image volumes were aligned to corresponding ASL scans (i.e. baseline MPRAGE to baseline ASL and post-CR MPRAGE to post-CR ASL), and segmented into gray matter (GM), white matter (WM) and cerebrospinal fluid (CSF) probability images using the new segment tool in SPM8. The GM segments were transformed into binary masks thresholded for voxels with 80% or more GM content and applied to the ASL time series. This was done to minimize ASL signal contributions from WM and CSF. Forty label and control images were extracted from each 5 min block at steady-state, surround subtracted and time-averaged over the two trials to generate perfusion-weighted (ΔM) images. CBF was calculated using a standard single-compartment flow model¹⁰.

$$CBF(ml/100g/min) = \frac{6000 \cdot \lambda \cdot \Delta M \cdot e^{\left(\frac{\omega}{T1_b}\right)}}{2\alpha \cdot M_0 \cdot T1_b \cdot \left(1 - e^{\left(\frac{-(\tau + \omega)}{T1_b}\right)}\right)}$$

where λ = blood/tissue water partition coefficient, 0.9 g/mL; α = labelling efficiency assumed to be 85%¹¹ multiplied by 94% for background suppression; ω = post-labelling delay of 1.0 s incremental per slice; τ = label duration of 1.5 s and $T1_b$ = individual blood T1 value. The final individual normocapnia and hypercapnia CBF images were smoothed using a Gaussian filter with a FWHM of 6 mm and transformed to standard stereotactic space (MNI) using transformation parameters from segmentation of MPRAGE images. CVR was calculated pixel-by-pixel as the increase in CBF per mm Hg increase in

$P_{ET}CO_2$. All further reference to CBF refers to CBF measured at room air, unless otherwise stated.

To assess the sensitivity of the ASL sequence used in this study, the temporal signal-to-noise ratio (tSNR) of the perfusion-weighted time series was calculated for each subject. Temporal SNR was defined as the mean GM pixel signal relative to the mean GM pixel standard deviation. The reproducibility of repeated ASL measurements was determined from a subset of patients and controls (N=19) for baseline CBF and CVR using within-sessions coefficient of variation and intraclass correlation coefficient (ICC). ICC was calculated using SPSS and two-way random model with measures of consistency, where a value close to 1 represents a high reliability. For completeness, the test-retest reliability at baseline was also compared voxel-by-voxel using repeated measures analysis of variance. This was done to ensure that averaging the perfusion-weighted signal from the 2 trials did not bias group comparisons.

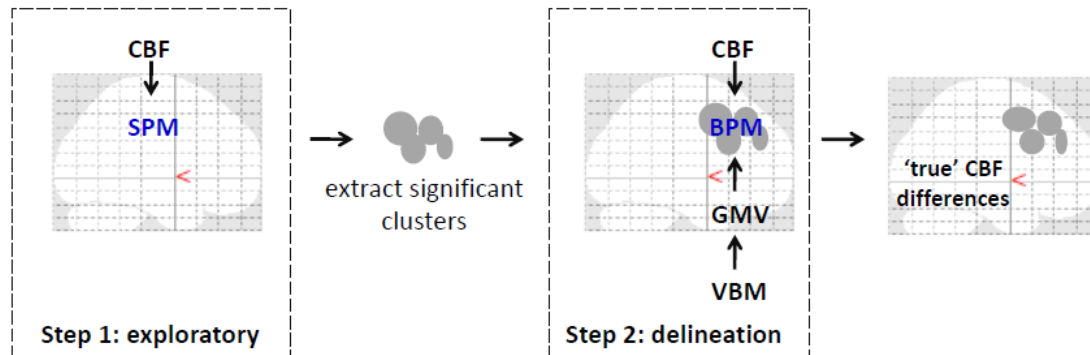
3.2.6 Assessment of structure-independent CBF effects

Our goal was to relate cerebral hemodynamic changes to underlying structural changes in brain volume¹ on a voxel-by-voxel basis to see if hemodynamic abnormalities (i.e. hypoperfusion or reduced CVR) and brain atrophy were mutually dependent. Thus, to delineate perfusion changes from underlying structural changes, a multimodal voxel-by-voxel multivariate analysis was performed as a two-step process as outlined in figure 3.1. First, an exploratory analysis was performed on the CBF images across all voxels with greater than or equal to 80% gray matter, to identify regions with significantly different gray matter CBF between CAD patients and controls. This was achieved using

two-tailed Student's t-test performed within SPM8. Next, these clusters were passed to the biological parametric mapping (BPM)¹² tool, where a voxel-by-voxel analysis of covariance (ANCOVA) was performed on CBF images with differences in regional gray matter volume (GMV) removed. The results reflected differences in regional gray matter perfusion independent of gray matter volume changes.

For the BPM analysis, individual GMV images were generated from MPRAGE volumes using voxel-based morphometry (VBM, <http://dbm.neuro.uni-jena.de/vbm/>) in SPM8 as described in a prior study¹. The GM segments were spatially normalized to a template averaged from all subjects, corrected for differences in brain size and smoothed with an 8-mm Gaussian filter. To describe changes in GMV within the clusters of interest, a voxel-by-voxel between-group comparison was performed on the GMV images and restricted to the clusters of interest using SPM8. An absolute threshold mask set at 0.1 was used to remove non-GM voxels. For all statistical analysis, type I errors from multiple comparison was minimized using False Discovery Rate (FDR) at $p < 0.05$ and cluster size greater than 10 voxels.

Figure 3.1: Illustration of the pipeline for multimodal voxel-wise ANCOVA performed to determine the singular effect of CAD on regional CBF.



Step 1 involved SPM voxel-wise between-group comparisons of CBF images across the brain. Significant clusters from this step were converted to binary masks and used in Step 2 to improve voxel-wise multimodal analysis and limit type II errors. In step 2, between-group differences in CBF were examined voxel-wise using BPM with GMV images from VBM analysis serving as covariates. Corrections for multiple comparisons using FDR ($p < 0.05$) was performed at each step. Clusters that remained signified regions where CBF changes drive the observed differences as in figure 3.2B and as listed in table 3.2. Illustration was overlaid on glass brains from SPM8 (<http://www.fil.ion.ucl.ac.uk/spm/>).

3.2.7 Statistical analysis

Statistical analyses were conducted with SPSS 20.0 statistical software (IBM Corp. Armonk, NY, and USA). Baseline clinical assessments and regional CVR measures from CAD patients were compared to data from the control group using two-tailed Student's t-test since age and gender were matched. Since, lower CVR was expected in the CAD⁸ group compared to controls, a one-tailed t-test was performed on regional mean CVR values extracted from each of the clusters from results of ANCOVA BPM analysis. Voxel-by-voxel comparisons were not performed on CVR images because of power constraints.

To test for effects of aerobic fitness, a paired t-test was performed on clinical data and regional CBF measures acquired on a subgroup of CAD patients before and 6 months

after cardiac rehabilitation. Regional CBF values were extracted from each of the clusters from the baseline ANCOVA BPM analysis. To demonstrate recovery of CBF with cardiac rehabilitation within regions, percent relative differences were computed for CAD patients at baseline and after CR. Baseline differences were relative to each regional mean CBF across all control subjects, while post-CR differences were relative to pre-CR regional CBF values. For completeness, relative differences were also computed for regional GMV. CVR analysis were not performed post CR due to a lack of statistical power.

3.3 Results

3.3.1 Study demographics

Perfusion data from one control subject and one CAD patient at baseline were excluded because of motion artefacts. Thirteen control subjects and 22 CAD patients participated in CVR measurements. The CVR data of one patient were excluded due to accelerated breathing (>25 breathes per minute) during hypercapnia, which can confound CVR results. The CAD group consisted of patients with clinical diagnosis at referral of angina (11.7%), myocardial infarct (17.6%) and coronary artery disease (67.6%). All patients were on a combination of drug therapy to lower lipid levels (statins = 83.3%), maintain blood pressure (beta-blockers = 72.2%; ACE-inhibitors/angiotensin II receptor blockers = 50%) and prevent reinfarction (anti-platelets/aspirin = 77.8%). Forty-one percent had percutaneous coronary intervention and 8.8% received coronary artery bypass grafting prior to participation in the study.

3.3.2 Baseline clinical measures

Results of clinical assessments compared between groups at baseline including global means of gray matter CBF and CVR are presented in Table 3.1. There were no significant differences between patients and controls in terms blood pressure, left ventricular function, resting heart rate and blood glucose. CAD patients had lower total cholesterol ($F = 15.34$ (1, 53), $p < 0.0001$) likely reflecting the therapeutic effect of the combined drug therapy received by patients. However, CAD patients had lower MoCA scores ($F = 4.63$ (1, 51), $p < 0.01$) after adjustment for level of education, lower VO_2 max ($F = 15.02$ (1, 37), $p < 0.0001$), elevated BMI ($F = 18.46$ (1, 53), $p < 0.0001$) and higher carotid artery intima media thickness ($F = 8.05$ (1, 43), $p < 0.001$). There was also a trend of reduced carotid compliance in the carotid ($p = 0.24$) and elevated hs-CRP ($p = 0.10$), a marker of inflammation and measure of myocardial infarction risk.

Table 3.1: Study demographics

Variables	Controls	Patients
Body mass Index (kg/m ²)	24.54 ± 3.11	29.84 ± 4.73*
Glucose (mmol/L)	4.72 ± 0.89	5.21 ± 1.38
Total cholesterol (mmol/L)	4.15 ± 0.96	3.09 ± 0.79*
hs-CRP (mg/L)	0.97 ± 0.91	2.10 ± 3.10
Systolic blood pressure (mm Hg)	120.28 ± 15.97	126.70 ± 21.20
Diastolic blood pressure (mm Hg)	68.18 ± 7.8	71.5 ± 12.41
Heart rate (beats per min)	58.34 ± 9.54	59.11 ± 6.85
Left ventricular ejection fraction (%)	67.41 ± 9.82	64.35 ± 7.24
Intima media thickness, carotid (mm)	0.53 ± 0.12	0.64 ± 0.12*
Compliance, carotid (mm/mm Hg)	0.0088 ± 0.003	0.0077 ± 0.003
MoCA	28.32 ± 1.67	26.82 ± 2.1*
VO ₂ max (mL/kg/min)	37.27 ± 9.94	26.9 ± 7.24*
Resting P _{ET} CO ₂ (mm Hg)	43 ± 4	40 ± 6
ΔP _{ET} CO ₂ (mm Hg)	11 ± 3	13 ± 4
Global mean CBF (mL/100g/min)	50.83 ± 11.68	46.49 ± 13.88
Global mean CVR (mL/100g/min/mm Hg)	2.57 ± 0.62	2.26 ± 0.63

Means and standard deviations of clinical assessments compared between CAD patients and controls. Statistical differences between groups at p<0.05 are indicated by *.

3.3.3 Baseline brain imaging: Cardiac disease effects

The mean $T1_b$ across all subjects was 1562.6 ± 69.8 ms. There was no difference between $T1_b$ for patients and controls. Mean GM tSNR for the ASL-EPI sequence was 4.0 ± 1.4 . Test-retest reliability of the CBF and CVR measurements performed voxel-wise, showed no differences between trials ($p < 0.001$, uncorrected). Because of the reproducibility of GM CBF and CVR, $CV = 6.4\%$ for CBF and 14.9% for CVR with corresponding ICC (2, 1) values of 0.93 and 0.82 for CBF and CVR respectively, ΔM signals were averaged over the 2 trials. No differences were found in global mean CBF or CVR between CAD patients and controls. Results from the multimodal voxel-wise multivariate analysis are listed in table 3.2 and are represented graphically on a single slice through the brain in figure 3.2. The results were as follows:

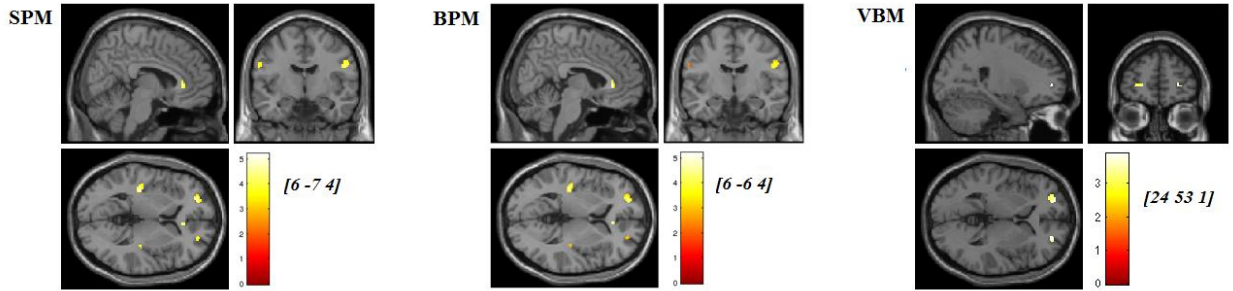
- 1) Eleven clusters were identified as having significantly lower CBF in the CAD patients from the SPM exploratory step. The corresponding anatomical labels are listed in table 3.2.
- 2) All eleven clusters remained significant after controlling for differences in GMV between the two groups. However, the magnitude of the effect of disease on CBF observed after atrophy correction was muted in nearly all regions, except in the right anterior cingulate cortex and bilateral middle temporal gyri (table 3.2).
- 3) The cluster size of nearly all regions was also preserved after BPM ANCOVA analysis except in the left precentral gyrus where the cluster size was reduced by 2 voxels.
- 4) Within the 11 regions, a significant decrease in GMV was observed in the CAD group in the right and left superior frontal and in the left precentral gyri. These 3

regions also had the greatest reductions in CBF changes following BPM analysis, as indicated by reduced t-value (table 3.2).

In general, the brains of CAD patients had significant reductions in regional GM CBF independent of GMV in the bilateral prefrontal, insula, middle temporal, superior temporal, postcentral gyri, and in the right anterior cingulate cortex. Concomitant decrease in GMV and atrophy-independent CBF were observed in the right and left superior frontal, and in the left precentral gyri.

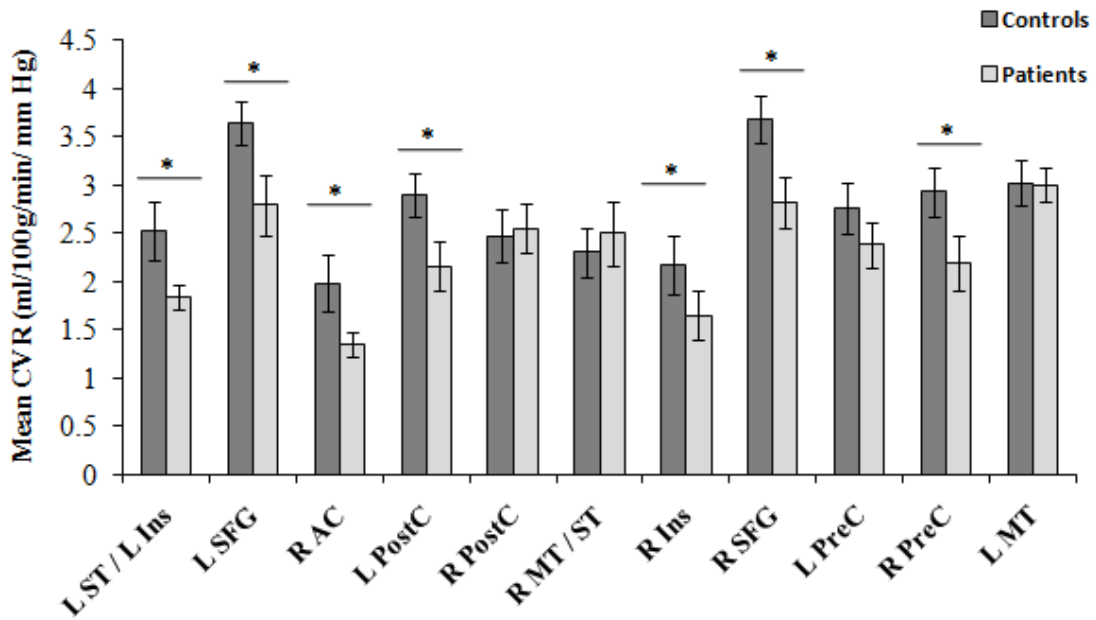
Between-group comparisons in regional CVR are shown in figure 3.3. Group means from each cluster and the standard error of the means are displayed. Significant decreases in CVR were observed in the CAD patients in the right anterior cingulate, bilateral superior frontal gyri, right insular, right precentral gyrus, left superior temporal/insula and left postcentral gyrus (all, $p < 0.05$).

Figure 3.2: Regions of interest analysis from voxelwise-comparisons.



Results of the region of interest analysis from voxel-wise comparisons between patients and controls; in gray matter CBF from SPM and from BPM analysis, and comparisons in gray matter volume derived from VBM. Clusters of significant difference between groups are depicted in yellow ($p < 0.05$, FDR, cluster threshold = 10 contiguous voxels) and overlaid on the axial, coronal and sagittal slices of a single subject. The corresponding anatomical coordinates $[x, y, z]$ are included.

Figure 3.3: Regions of differences in regional CVR compared between CAD patients and controls at baseline.



Statistical differences between groups at $p < 0.05$ are signified by * and error bars indicate standard errors of the mean. R = right; L = left; SFG = superior frontal gyrus; ST = superior temporal gyrus; Ins = insula; PostC = postcentral gyrus; MT = middle temporal gyrus; PreC = precentral gyrus; AC = anterior cingulate.

Table 3.2: Results of multimodal voxel-by-voxel multivariate analysis.

	Brain region (Brodmann Area)	Talariach coordinate (X Y Z)			# of voxels	SPM t	SPM p	BPM t	BPM p
<i>Regional gray matter CBF, controls > patients</i>									
1	L Superior temporal (41)	-34	-30	14	119	5.64	0.01	5.20	<0.001
	L Insula (13)	-38	-23	3		5.03	0.04	4.97	<0.001
2	L Superior frontal (10)	-22	50	-1	63	5.11	0.01	4.57	<0.001
3	R Anterior cingulate (24)	6	31	0	18	4.91	0.01	4.98	<0.001
4	L Postcentral gyrus (3)	-38	-20	42	36	4.79	0.01	3.55	<0.001
5	R Postcentral gyrus (6)	53	-6	28	35	4.71	0.01	3.95	<0.001
6	R Middle temporal (39)	46	-62	20	57	4.47	0.02	4.50	<0.001
	R Superior temporal (39)	55	-57	23		4.23	0.03	4.15	<0.001
7	R Insula (13)	36	-28	18	33	4.25	0.03	3.36	<0.001
8	R Superior frontal (10)	26	49	-1	21	4.21	0.03	3.23	0.002
9	†L Precentral gyrus (4)	-55	-8	28	14	4.18	0.03	2.49	0.008
10	R Precentral gyrus (6)	46	-10	28	10	4.11	0.03	3.01	0.003
11	L Middle temporal (39)	-46	-69	16	18	3.61	0.04	3.69	<0.001
<i>VBM: Regional GMV, controls > patients</i>									
1	L Superior frontal (10)	-22	56	2	40	3.90	0.009		
2	R Superior frontal (10)	26	54	2	21	3.88	0.009		
3	L Precentral gyrus (4)	-56	-10	34	14	3.00	0.014		

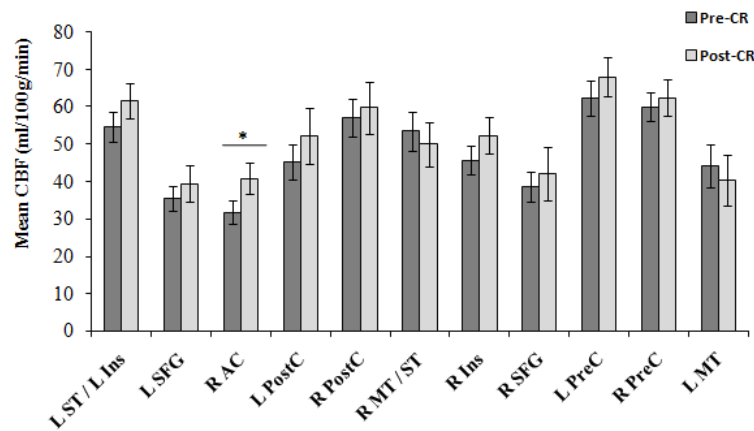
Results of regional voxel-by-voxel comparisons in regional CBF and in regional GMV between CAD patients at baseline. Effect magnitude is represented by t-static from SPM analysis and from BPM analysis, where changes in gray matter volume were accounted for. Results were corrected for multiple comparisons (FDR, $p < 0.05$). Coordinates of local maxima of clusters of significant difference are listed and given in anatomical Talariach space. R = right; L = left; † for the left precentral gyrus, the total number of voxels from BPM analysis was reduced to 12.

3.3.4 Cardiac rehabilitation effects

There were no differences within the CAD patient group in pre- and post-CR clinical tests. Mean VO_2 max at baseline and post-CR were 28.04 ± 10.47 mL/kg/min and 29.37 ± 8.74 mL/kg/min respectively. No difference in global mean gray matter perfusion was observed before (46.4 ± 11.4 mL/100g/min) and after (50.0 ± 18.5 mL/100g/min)

exercise training. Regional mean CBF at baseline and post-CR are shown in figure 3.4. A significant increase in CBF (~30%) was seen post exercise in the right anterior cingulate ($p = 0.02$), a region where a comparable decline in CBF compared to controls (~33%) was observed at baseline, and a region where no change in GMV was observed after exercise. An increase in GMV with exercise was found in the bilateral pre- and post-central gyri and in the right superior frontal gyrus, while a sustained decrease in GMV over time was seen in the left superior temporal and right insula regions.

Figure 3.4: Regions of differences in regional CBF compared in CAD patients before and after CR.



Statistical differences at $p < 0.05$ are signified by * and error bars indicate standard errors of the mean. See figure 3.3 for full name of regions.

3.4 Discussion

There is a growing interest in the potential role of vascular disease in advancing the age-related decline in cerebrovascular health and cognitive function. In a recent study, we described marked brain atrophy spanning the frontal, temporal and parietal lobes of CAD patients, and subsequent increase in brain volume with exercise¹. Here, in the same

cohort of CAD patients, accelerated cerebrovascular decline was observed in cognitive areas of the brain. Interestingly, these changes were greater than the corresponding declines in brain volume, suggesting that cerebral hypoperfusion associated with cardiovascular disease could mediate neuronal volume loss. In addition, recovery of perfusion in the right anterior cingulate was demonstrated after six months of exercise training. These findings indicate that cardiovascular disease is associated with regional cerebral hypoperfusion and diminished CVR, which indicate cerebrovascular dysfunction and that these changes may be reversible with exercise.

Vascular aging is associated with increased plaque burden, impaired vascular remodelling, arterial stiffness and endothelial dysfunction¹³, inducing perfusion deficits that in turn decrease the amount of oxygen available for optimal tissue function¹³. In the brain, for example by the age of 60, normal aging can reduce regional CBF by up to 15%¹⁴, offsetting the normal coupling of CBF to glucose metabolism^{14,15}. This age-related compromise in CBF is exacerbated by the presence of vascular disease, as demonstrated by our findings and supported by previous observations⁶. Compared to age-matched controls, we found decreased CBF in the brains of CAD patients in regions known to be affected by various forms of vascular disease (for review see de la Torre⁶ and Friedman et al³). For instance, hypertension is associated with accelerated decline in regional perfusion in the orbitofrontal, anterior cingulate and insular cortices¹⁶. In older adults with various forms of cardiovascular disease, reductions in frontal and temporal lobe CBF are associated with reduced regional cortical thickness and impairments in memory, attention and executive functions¹⁷. The combined effect of vascular ageing and high blood cholesterol leads to slow progression of atherosclerosis, where the narrowing

of coronary, systemic or cerebral vessels can impede blood flow to the corresponding tissue. With CAD, it is possible that subtle changes in blood supply to the brain could pose an additional risk to the aging brain⁵, particularly in individuals with suspected central arterial stenosis. We found significantly higher carotid intima media thickness, a marker of generalized atherosclerosis¹⁸, in CAD patients compared to controls as well as decreased carotid artery compliance. Increased carotid intima media thickness in older adults, even in the absence of clinical vascular disease, is associated with regional changes in CBF¹⁹, increased risk for AD¹⁸ and accelerated decline in performance on tests for memory, language (semantic association fluency) and executive function, over time²⁰. Arterial stiffness, even at the level of the aorta⁷, and other vascular remodelling responses to vascular disease impair CVR²¹, ultimately affecting higher-order cognitive processes.

CVR was significantly reduced in CAD patients in multiple regions including the anterior cingulate, superior frontal and postcentral gyrus. Typically, CBF reductions are likely either a result of reduced supply to tissue, signifying vascular dysfunction, or a result of reduced metabolic demand, signifying a decline in neuronal activity. The observed reduction in CVR in areas of reduced CBF in the CAD patients supports the former since it indicates that the brain's vascular response to a vasoactive stimulus was impaired, which suggests that the CBF response to increased functional activation may also be impaired²².

The decline in cognitive abilities in domains of executive function, attention, language, memory and visuospatial skills seen in vascular disease patients, independent of normal aging effects²³, is consistent with the regional pattern of decreased resting CBF

and CVR observed in these CAD patients. Interestingly, these patients also had lower MoCA scores compared to controls, after adjusting for level of education. Impaired CVR is associated with a decline in global cognitive function in dementia patients²⁴ and could reveal cognitive dysfunction sooner and with greater sensitivity than resting CBF. Lu et al²⁵ demonstrated that CVR in the prefrontal cortex showed an accelerated decline with age compared to CBF. These observations underscore the significance of CVR as a marker of cerebrovascular health and potentially of cognitive function in cardiovascular disease patients.

One of the main findings of the current study was the observation of differences in the spatial patterns of hypoperfusion and brain atrophy in the CAD patients. Of the 11 clusters identified as having lower basal CBF, only 3 clusters- all within the prefrontal cortex- showed a concurrent decrease in GMV following BPM analysis. A spatial mismatch between regional hypoperfusion and atrophy has also been observed in normal aging²⁶. These observations suggest that certain areas of the brain respond differently to hemodynamic and structural changes associated with aging and vascular disease. It is also possible that the CBF changes observed in CAD patients could precede structural changes. It is important to consider that the poor spatial resolution of ASL compared to structural imaging could lead to partial volume errors. To minimize this, differences in CBF between patients and controls were only conducted in voxels that were classified as being comprised of at least 80% gray matter, followed by BPM analysis to control for changes in GMV. An alternative approach would be to use linear regression methods such as outlined by Asllani et al²⁷ to extract a GM CBF image. However, this approach

can introduce substantial spatial blurring, which when applied to regions as small as those identified in the current study, could eliminate the observed effects.

Another notable finding of the current study was the recovery of CBF in the right anterior cingulate after mild-to-moderate aerobic fitness training. This finding agrees with a previous study that reported higher CBF in the anterior cingulate cortex in aerobically-trained older adults compared to sedentary controls²⁸. A positive correlation between CBF in the anterior cingulate and VO₂max has also been reported in CAD patients²⁹. Similar to Chapman et al²⁸, we observed no increase in global CBF after exercise training; however, the effects of exercise on global CBF are conflicting³⁰. Conversely, Colcombe et al associated the level of aerobic fitness with decreased activity in the anterior cingulate and increased activity in the middle frontal, superior frontal and parietal regions in older adults performing conflicting response tasks³¹. Though they attributed their observation to improved adaptations in the attentional network following exercise training³¹, it could also signify the effects of exercise in enhancing both cognitive and cardiovascular control³². Decreased activity in the anterior cingulate (subgenual) and medial prefrontal cortex along with increased activity in the insular cortex, are strongly associated with cardiovascular adjustments to acute stressors during physical, cognitive and emotional demands³². Although we did not find significant changes in CBF in the insular or prefrontal regions after exercise training, we previously reported increased brain volume in the medial prefrontal region in addition to other cognitive areas¹. Increased volume in the prefrontal, anterior cingulate and medial temporal lobes are consistently associated with improved higher cardiorespiratory fitness level³³. It is possible that one of the mechanisms by which aerobic fitness training

improves cardiovascular function is the augmentation of cortical control of cardiovascular homeostasis. We were unable to investigate regional CVR response to exercise training given the relatively small sample, a global increase in CVR has been reported in older adults following 12 weeks of mild-to-moderate aerobic exercise³⁴ and in stroke patients³⁵ after completing a 6-month exercise program. In general, our findings of recovery of regional CBF following cardiac rehabilitation continue to support the role of aerobic fitness in preservation of brain health following injury.

3.4.1 Study considerations

The findings presented in the current study although largely attributed to coronary artery disease, could also be associated with lifestyle factors³. Compared to controls, CAD patients had significantly lower fitness levels and were generally overweight. The effect of these lifestyle factors on cerebral perfusion and brain structure in the presence of vascular disease are yet to be determined. A large majority of the CAD patients were on antihypertensive and hypolipidemic drug. These agents are known to affect cerebrovascular hemodynamics and could mask vascular disease effects or attenuate exercise effects. Statins for instance are hypolipidemic agents associated with increased CBF and vascular reactivity³⁶, while antihypertensive drugs such as beta-blockers can limit submaximal exercise capacity³⁷. Furthermore, we did not explore potential ongoing cerebrovascular disease in the study population, specifically, white matter lesions, which could further contribute to cerebral hypoperfusion and atrophy. Our analysis, however, focused on vascular disease effects within gray matter. Areas associated with white matter hyperintensities are typically deep within white matter regions.

Other study considerations include the inherent limitations with the ASL imaging and the hypercapnic challenge. First, the 2D EPI readout used in this study for ASL imaging, limited data acquisition to slices superior to the anterior commissure - posterior commissure line. As such, regions near tissue-air/bone interfaces prone to increased susceptibility artefacts were excluded. Cerebral hypoperfusion may well exist in the inferior regions of the frontal and parietal lobes, since brain atrophy has been observed in these regions in the same cohort of CAD patients¹. Second, our choice of post-labelling delay was relatively short. It was selected to mediate the effects of short arterial transit time at high flow velocities during hypercapnia and increase SNR. This resulted in a tSNR comparable to newer ASL methods using three-dimensional gradient-spin echo³⁸ readouts, where whole brain coverage can be achieved at longer post-label delay and minimal susceptibility issues. A short post-labelling delay could result in an underestimation of CBF in patients with longer transit times, however no watershed artifacts, which are typical of transit time errors, were observed in the CBF images. Lastly, the CVR results were limited by a small sample size due to poor compliance with the hypercapnic manipulations, compounded by inter-subject variability in ventilation response during CO₂ inhalation. Reproducible changes in P_{ET}CO₂ were achieved by controlling the respiration rate using a metronome. However, commercial devices designed to control P_{ET}CO₂ breath by breath, such as the RespirAct (Thornhill Research, Toronto, Canada) would improve the sensitivity of CVR measurements.

3.4.2 Conclusion

This study represents a concerted attempt within a single cohort to investigate the association between cardiovascular disease and cerebral hemodynamics, as well as investigating the potential benefits of physical activity. The findings demonstrated a region-specific vulnerability to cardiovascular disease that appeared to accelerate the normal changes in CBF associated with aging. It is possible that reductions in regional CBF and CVR, related to vascular disease could drive cortical decline. However, the fundamental mechanisms underlining the association between vascular disease and cortical decline remain unclear and require further investigation. The ability of an aerobic fitness program designed for CAD patients to improve cerebral perfusion was demonstrated in a relatively small sample. This work sets the stage for future investigations in larger cohorts of vascular disease patients to understand how cardiopulmonary fitness training impacts cerebrovascular hemodynamics.

3.5 References

1. Anazodo, U. C., Shoemaker, J. K., Suskin, N. & St. Lawrence, K. S. An investigation of changes in regional gray matter volume in cardiovascular disease patients, pre and post cardiovascular rehabilitation. *NeuroImage Clin.* **3**, 388–395 (2013).
2. De la Torre, J. C. Cardiovascular risk factors promote brain hypoperfusion leading to cognitive decline and dementia. *Cardiovasc. Psychiatry Neurol.* **2012**, 367516 (2012).

3. Friedman, J. I. *et al.* Brain Imaging Changes Associated With Risk Factors for Cardiovascular and Cerebrovascular Disease in Asymptomatic Patients. *JACC Cardiovasc. Imaging* **7**, 1039–1053 (2014).
4. De Toledo Ferraz Alves, T. C., Ferreira, L. K. & Busatto, G. F. Vascular diseases and old age mental disorders: an update of neuroimaging findings. *Curr. Opin. Psychiatry* **23**, 491–7 (2010).
5. Jefferson, A. L. *et al.* Cardiac Index is Associated with Brain Aging: The Framingham Heart Study. *Circulation* **122**, 690–697 (2010).
6. De la Torre, J. . Critically attained threshold of cerebral hypoperfusion: the CATCH hypothesis of Alzheimer’s pathogenesis. *Neurobiol. Aging* **21**, 331–342 (2000).
7. Gauthier, C. J. *et al.* Hearts and minds: linking vascular rigidity and aerobic fitness with cognitive aging. *Neurobiol. Aging* **36**, 304–14 (2015).
8. Novack, B. P., Shenkin, H. A., Bortin, L., Goluboff, B. & Soffe, A. M. Effects of Carbon Dioxide Inhalation Upon The Cerebral Blood Flow And Cerebral Oxygen Consumption In Vascular Disease. *J. Clin. Invest.* **32**, 696–702 (1953).
9. Nielson, C. A. *et al.* Impact of a smoking cessation lifestyle intervention on vascular mechanics in young women. *Appl. Physiol. Nutr. Metab.* **580**, 572–580 (2014).
10. Wang, J. *et al.* Arterial transit time imaging with flow encoding arterial spin tagging (FEAST). *Magn. Reson. Med.* **50**, 599–607 (2003).
11. Xu, G. *et al.* Reliability and precision of pseudo-continuous arterial spin labeling perfusion MRI on 3.0 T and comparison with 15O-water PET in elderly subjects at risk for Alzheimer’s disease. *NMR Biomed.* **23**, 286–293 (2010).
12. Casanova, R. *et al.* Biological parametric mapping: A statistical toolbox for multimodality brain image analysis. *Neuroimage* **34**, 137–43 (2007).

13. Priebe, H.-J. The aged cardiovascular risk patient. *Br. J. Anaesth.* **85**, 763–778 (2000).
14. Bentourkia, M. *et al.* Comparison of regional cerebral blood flow and glucose metabolism in the normal brain: effect of aging. *J. Neurol. Sci.* **181**, 19–28 (2000).
15. Anazodo, U. C. *et al.* Feasibility of simultaneous whole-brain imaging on an integrated PET-MRI system using an enhanced 2-point Dixon attenuation correction method. *Front. Neurosci.* **8**, 1–11 (2015).
16. Beason-Held, L. L., Moghekar, A., Zonderman, A. B., Kraut, M. a & Resnick, S. M. Longitudinal changes in cerebral blood flow in the older hypertensive brain. *Stroke.* **38**, 1766–73 (2007).
17. Alosco, M. L. *et al.* The adverse effects of reduced cerebral perfusion on cognition and brain structure in older adults with cardiovascular disease. *Brain Behav.* **3**, 626–36 (2013).
18. Wendell, C. R. *et al.* Carotid atherosclerosis and prospective risk of dementia. *Stroke.* **43**, 3319–24 (2012).
19. Sojkova, J. *et al.* Intima-media thickness and regional cerebral blood flow in older adults. *Stroke.* **41**, 273–9 (2010).
20. Wendell, C. R., Zonderman, A. B., Metter, E. J., Najjar, S. S. & Waldstein, S. R. Carotid intimal medial thickness predicts cognitive decline among adults without clinical vascular disease. *Stroke.* **40**, 3180–5 (2009).
21. Lavi, S., Gaitini, D., Milloul, V. & Jacob, G. Impaired cerebral CO₂ vasoreactivity: association with endothelial dysfunction. *Am. J. Physiol. Heart Circ. Physiol.* **291**, H1856–61 (2006).
22. Stefanovic, B. *et al.* Functional reactivity of cerebral capillaries. *J. Cereb. Blood Flow Metab.* **28**, 961–72 (2008).

23. Okonkwo, O. C. *et al.* Longitudinal trajectories of cognitive decline among older adults with cardiovascular disease. *Cerebrovasc. Dis.* **30**, 362–73 (2010).
24. Cantin, S. *et al.* Impaired cerebral vasoreactivity to CO₂ in Alzheimer’s disease using BOLD fMRI. *Neuroimage* **58**, 579–87 (2011).
25. Lu, H. *et al.* Alterations in cerebral metabolic rate and blood supply across the adult lifespan. *Cereb. cortex* **21**, 1426–34 (2011).
26. Chen, J. J., Rosas, H. D. & Salat, D. H. Age-associated reductions in cerebral blood flow are independent from regional atrophy. *Neuroimage* **55**, 468–78 (2011).
27. Asllani, I., Borogovac, A. & Brown, T. R. Regression algorithm correcting for partial volume effects in arterial spin labeling MRI. *Magn. Reson. Med.* **60**, 1362–71 (2008).
28. Chapman, S. B. *et al.* Shorter term aerobic exercise improves brain, cognition, and cardiovascular fitness in aging. *Front. Aging Neurosci.* **5**, 75 (2013).
29. MacIntosh, B. J. *et al.* Cardiopulmonary fitness correlates with regional cerebral grey matter perfusion and density in men with coronary artery disease. *PLoS One* **9**, e91251 (2014).
30. Ogoh, S. & Ainslie, P. N. Cerebral blood flow during exercise: mechanisms of regulation. *J. Appl. Physiol.* **107**, 1370–80 (2009).
31. Colcombe, S. J. *et al.* Cardiovascular fitness, cortical plasticity, and aging. *Proc. Natl. Acad. Sci. U. S. A.* **101**, 3316–21 (2004).
32. Shoemaker, J. K., Wong, S. W. & Cechetto, D. F. Cortical circuitry associated with reflex cardiovascular control in humans: does the cortical autonomic network ‘speak’ or ‘listen’ during cardiovascular arousal. *Anat. Rec.* **295**, 1375–84 (2012).

33. Hayes, S. M., Hayes, J. P., Cadden, M. & Verfaellie, M. A review of cardiorespiratory fitness-related neuroplasticity in the aging brain. *Front. Aging Neurosci.* **5**, 31 (2013).
34. Murrell, C. J. *et al.* Cerebral blood flow and cerebrovascular reactivity at rest and during sub-maximal exercise: effect of age and 12-week exercise training. *Age (Omaha)*. **35**, 905–20 (2013).
35. Ivey, F. M., Ryan, A. S., Hafer-Macko, C. E. & Macko, R. F. Improved cerebral vasomotor reactivity after exercise training in hemiparetic stroke survivors. *Stroke*. **42**, 1994–2000 (2011).
36. Giannopoulos, S., Katsanos, A. H., Kosmidou, M. & Tsvigoulis, G. Statins and vascular dementia: a review. *J. Alzheimers. Dis.* **42 Suppl 3**, S315–20 (2014).
37. Van Baak, M. A., Böhm, R. O., Arends, B. G., van Hooff, M. E. & Rahn, K. H. Long-term antihypertensive therapy with beta-blockers: submaximal exercise capacity and metabolic effects during exercise. *Int. J. Sports Med.* **8**, 342–347 (1987).
38. Günther, M., Oshio, K. & Feinberg, D. a. Single-shot 3D imaging techniques improve arterial spin labeling perfusion measurements. *Magn. Reson. Med.* **54**, 491–8 (2005).

4 Chapter 4

Feasibility of Simultaneous Whole-brain Imaging of Cerebral Perfusion and Glucose Metabolism on a Whole-body Integrated PET-MRI Scanner.

The chapter is adapted from the paper entitled "*Feasibility of simultaneous whole-brain imaging on an integrated PET-MRI system using an enhanced 2-point Dixon attenuation correction method*", published in *Frontiers in Neuroscience*, 2015; (8) :434, by Udunna C Anazodo, Jonathan D Thiessen, Tracy Ssali, Jonathan Mandel, Matthias Günther, John Butler, William Pavlosky, Frank S Prato, R Terry Thompson, and Keith S St. Lawrence. It is reproduced here under a Creative Commons Attribution CC-BY license.

4.1 Introduction

Multimodal imaging approaches that simultaneously pull together structural, functional and molecular information have the potential to improve the characterization of normal and/or abnormal neurophysiology. The development of positron emission tomography (PET) and magnetic resonance imaging (MRI) hybrid systems provide the combined advantages of high molecular sensitivity of PET and high spatial resolution of MRI, among other benefits. The clinical potential of this hybrid approach extends beyond image fusion considering the ability of MRI to collect data associated with not only anatomy but also function, diffusion and metabolite concentrations¹, thereby maximizing

diagnostic accuracy² as image registration errors and total image acquisition times are minimized, and physiological and metabolic states are identical.

However, accurate correction of PET signal attenuation in PET-MRI hybrid systems using information derived from MRI is challenging. Inherent limitation(s) of various proposed attenuation correction methods can lead to PET quantification errors of up to 20%³⁻⁶, which limits adoption of PET-MRI in neuroimaging. Commercial PET-MRI hybrid systems rely on MRI-derived attenuation correction (MRAC) using a 2-point Dixon method⁷ based on segmentation of MR signals from water and fat into air, lung, fat and soft tissue⁸ but ignores bone, rendering this method less ideal for brain imaging. Various methods have been explored to produce optimal MRAC maps for neuroimaging that are as accurate as clinically accepted AC maps produced by computed tomography (CT). Ultra-short echo (UTE) MRI⁹ where bone is imaged and incorporated into AC maps, can suffer from low spatial resolution and inaccurate signal segmentation⁴. Methods that employ CT templates/atlas mapped to individual MRI^{10,11} or to guide MRI segmentation¹²⁻¹⁴, require complex algorithms that have limited reproducibility and at best still retain some level of inter-modality misregistration¹⁵, especially where large signal intensity differences exist between MRI and CT (e.g. cortical bone).

In this study we explored the feasibility of hybrid PET-MRI systems in simultaneous measurements of brain function with PET and MRI using an enhanced Dixon-based MRAC for PET signal attenuation correction in an integrated PET-MRI system. Simultaneous functional imaging was achieved by combining 3-dimensional (3D) pseudo-continuous arterial spin labelling (pCASL) with ¹⁸F-fluoro-deoxyglucose (FDG) PET since FDG is considered a suitable surrogate marker of brain function¹⁶ and

pCASL is a reliable MR perfusion method for assessment of brain function under resting and task-induced conditions in normal and disease states¹⁷. The goal was to investigate if regional correlations in relative cerebral blood flow (rCBF) to relative cerebral rate of glucose consumption (rCMRglc) measured with a hybrid PET-MRI scanner were comparable to previous studies using either PET alone¹⁸ or separate PET and MRI systems¹⁹. If successful, the obvious advantage is that future studies in neuropsychiatry or neurodegeneration, for instance, could correlate perfusion MRI to disease-specific PET tracers for better characterization of disease expression²⁰. The proposed enhanced Dixon MRAC combines bone segmentation from high-resolution 3D T1-weighted anatomical images, routinely acquired in brain imaging, with the standard Dixon MRAC method implemented by the manufacturer. Comparison between the Dixon and enhanced Dixon method was made across a number of brain regions to assess regional differences and performance.

4.2 Materials and Methods

4.2.1 Participants

This study was approved by the University Research Ethics Board, and written informed consent was obtained from all subjects. PET-MRI images were acquired from oncology patients recruited following the completion of a clinical PET-CT exam as part of their healthcare management. A total of 13 oncology patients were recruited (7 males and 6 females) (58 ± 8 years old). All subjects had no history of neurological disorder and no radiation therapy or chemotherapy prior to imaging and were referred for whole-body

PET-CT exam for staging of oncology. To minimize errors in MRI image quality from potential image artifacts produced by metal implants such as MR signal loss, only patients free of metallic implants and fixtures including dental implants were included in this study.

4.2.2 PET-MRI image acquisition

Whole-brain PET and MRI data were acquired simultaneously on a Siemens Biograph® mMR system. The PET subsystem consisted of 8 rings of 56 detector blocks, each housing 8 x 8 LSO crystals (size = 4 x 4 x 20 mm³) coupled to 3 x 3 array of APDs producing a transaxial field of view (FOV) of 59.4 cm and an axial FOV of 25.8 cm. The 3T MRI subsystem is similar to a Siemens 3T Verio with a maximum gradient strength of 45 mT/m and slew rate of 200 T/m/s, but a reduced bore size of 60 cm. For detailed description of the Biograph® mMR specifications cf. Delso et al. 2011²¹. All MR images were acquired using a PET-compatible 16-channel phased array head (12-channel) and neck (4-channel) radiofrequency (RF) coil.

PET-MRI data were acquired immediately following the completion of 20 minute whole-body PET-CT imaging and following a 60-minute uptake of a bolus FDG intravenous injection (5 MBq/Kg) administered in a dim lit room. All subjects fasted for a minimum of 6 hours and had blood glucose level between 4.8 to 5.8 mmol/L. Clinical whole-body PET-CT were acquired following standard oncology imaging protocol from the level of the eyes to the mid-thigh. A series of MR images were acquired during a 15

minute PET list-mode acquisition with subjects in supine position. The MRI data included:

- a) Coronal T1-weighted dual-echo 3D VIBE-Dixon for MRI Dixon-based attenuation correction of PET data (repetition time (TR) = 3.60ms, echo times (TE) = 1.23 and 2.46ms, flip angle = 10°, FOV = 500 x 328mm², 128 slices, voxel size = 4.1 x 2.6 x 3.1mm³, bandwidth = 965 Hz/Px, acceleration factor of 2, and total acquisition (TA) = 0.19s)²²;
- b) Sagittal T1-weighted 3D magnetization-prepared rapid gradient-echo (MPRAGE) sequence (TR/TE: 2000/2.98ms, inversion time (TI) = 900ms, flip angle = 9°, FOV = 256 x 256mm², 176 slices, isotropic voxel size = 1.0 mm³, bandwidth = 240 Hz/Px, an acceleration factor of 2 and TA = 4.48min);
- c) Transverse 3D single shot gradient-and-spin-echo (GRASE) pCASL sequence²³ (TR/TE = 3500/22.76ms, FOV = 240 x 240 mm², 24 slices, voxel size = 3.8 x 3.8 x 5mm³, bandwidth = 2298 Hz/Px, and acceleration factor of 2). The pCASL label consisted of 1.5s train of RF pulses applied 9cm below the center of the imaging volume with a mean gradient of 0.6 mT/m. Sixty-four label and control pairs were acquired after a post-label delay of 1.2 s for TA = 7 min. Two nonselective inversion pulses were applied for background suppression during the post-labeling delay. Proton density images (M₀) were acquired with the pCASL sequences for CBF quantification using a TR of 5 s, with no labeling or background suppression pulses.

4.2.3 MR attenuation map (μ -map) generation and PET image reconstruction.

Two MRAC segmentation methods were used for attenuation correction of the PET data: the standard 2-point Dixon method²² and 2-point Dixon method plus bone segmentation (Dixon+bone), which is described below. The Dixon MRAC μ maps were generated online from segmentation of fat and water signals in the in- and out-of-phase Dixon images into fat, soft tissue and air/background, as implemented by the manufacturer. Linear attenuation coefficients of 0 cm^{-1} , 0.086 cm^{-1} and 0.10 cm^{-1} were assigned to air, fat and soft tissue, respectively²². Attenuation correction factors for hardware including the RF coil and scanning bed were included in the Dixon μ -map. The Dixon+bone MRAC μ -maps were generated offline using SPM8 (<http://www.fil.ion.ucl.ac.uk>) and in-house MATLAB (2012a, The MathWorks, Natick, MA) scripts. This method overlays a bone mask created from bone segmentation of the MPRAGE image to a Dixon μ -map and applies a linear attenuation coefficient (μ_a) of 0.143 cm^{-1} ⁹, the μ_a value of bone at 511keV, to the bone mask.

The bone mask for each subject was created as follows. 1) The T1-weighted MPRAGE dataset was coregistered to the Dixon in-phase image in SPM8 using rigid-body transformation with a normalized mutual information cost function to place the MPRAGE in the same voxel space as the Dixon μ -map. 2) The coregistered MPRAGE image set was segmented into gray matter, white matter, cerebrospinal fluid, bone, soft tissue and air/background probability tissue maps in native space using the new segment function in SPM8 and ICBM Tissue Probabilistic Atlases (<http://www.loni.usc.edu/ICBM/>). The new segment toolbox employs the unified

segmentation method ²⁴ that combines affine registration to ICBM atlas, bias field correction and segmentation within one integrated model. 3) The bone probability map was down-sampled to the Dixon images matrix size, smoothed with a 4 mm Gaussian filter ²⁵ and thresholded for probabilities above 80% to minimize inclusion of non-bone signals. 4) The resulting binary image was eroded with morphological filtering and connected component analysis using a 3x3x3 voxel size of ones before assigning μ_a of 0.143cm^{-1} . Erosion was performed to minimize inclusion of non-bone voxels and the size of the structure elements were determined after empirical evaluation of bone voxels within a region known to have true bone content.

Each subject's PET list-mode data were reconstructed using the Siemens e7 tools to one image volume 344 x 344 x 127 matrix with an iterative algorithm (ordered-subsets expectation maximization: 3 iterations, 21 subsets; 3D Gaussian filter with a full width half maximum (FWHM) = 2.0 mm and 2.5 zoom factor) and corrected for decay, dead time, scatter and attenuation. The reconstruction was performed twice using either the Dixon (PET_{dx}) or the Dixon+bone ($\text{PET}_{\text{dxbone}}$) MRAC μ -map.

4.2.4 Image Analysis

To allow for group comparison between PET_{dx} and $\text{PET}_{\text{dxbone}}$, the PET images were spatially normalized to the Montreal Neurological Institute (MNI) PET template in SPM8 (<http://www.fil.ion.ucl.ac.uk>) using an affine transformation and non-linear warps, and smoothed with a 6-mm FWHM Gaussian filter. The gray matter (GM) probability map for each subject was spatially normalized to the T1 MNI template using the unified

segment approach in SPM, also smoothed with a 6-mm Gaussian filter, transformed to a binary mask at a threshold of 80% and applied to the PET_{dx} and PET_{dxbone} images.

The difference between the Dixon+bone and the Dixon MRAC method across the brain was computed as the percent relative difference (% RD) in mean activity concentration (Bq/ml) in thirteen a priori regions of interest (ROIs).

$$\%RD = \left[\frac{(PET_{dxbone} - PET_{dx})}{PET_{dx}} \right] \times 100.$$

ROI brain masks were created using the automated anatomical library²⁶ incorporated within WFU PickAtlas toolbox version 3.0²⁷. The ROIs were frontal lobe, cingulate gyrus, insula, parietal lobe, temporal lobe, hippocampus, amygdala, thalamus, caudate, globus pallidus, putamen, and cerebellum. The PET_{dx} and PET_{dxbone} images were scaled by their respective global gray matter mean value to allow for voxel-by-voxel comparison between glucose uptake and blood flow, and since absolute quantification of PET-FDG with tracer kinetic modeling was not feasible in this study and generally not feasible in clinical practice. Regional %RD in relative mean activity was also calculated in the scaled PET data (rPET). To investigate potential regional differences, the mean values extracted from individual ROIs were compared between the two PET data sets using paired t-tests with SPSS 20.0 statistical software (IBM Corp. Armonk, NY, USA). Statistical significant differences were set at threshold p-value <0.05.

pCASL preprocessing was performed with SPM8 and scripts written in MATLAB. The pCASL time series were motion corrected, pair-wise subtracted, and time-averaged. The mean signal was registered to the MPRAGE images using a rigid-body transformation and converted to CBF using a single-compartment flow model²⁸.

The CBF images were spatially normalized to the MNI template and smoothed using a Gaussian filter with a FWHM of 6 mm. A GM mask was applied to the CBF images that were normalized by the global mean. To determine the temporal signal-to-noise ratio (tSNR) of the perfusion-weighted time series when acquired with a PET-compatible head coil, tSNR was calculated for each subject as defined by the mean pixel signal in the whole brain relative to the mean pixel standard deviation.

Whole brain voxel-by-voxel independent samples t-tests restricted within a GM mask were performed on the individual relative images in SPM8 to investigate differences between rCBF and rPET images. Statistical significant differences were identified for clusters greater than 50 voxels at $p < 0.05$ after correcting for multiple comparisons using the False Discovery Rate (FDR). Voxel-by-voxel Pearson correlation was conducted on relative images averaged across subjects within the thirteen ROIs to correlate rCBF to rPET_{dx} and to rPET_{dxbone}.

4.3 Results

4.3.1 Study Participants

A full description of the study demographics is listed in Table 4.1, including age, gender and diagnosis. No neurological lesions or gross neuropathological abnormalities were observed on PET-MRI brain images. Images were reviewed by a Board Certified Radiologist and Nuclear Medicine physician. Mean and standard deviation of the time from FDG injection to PET-MR examinations were 103 ± 11.18 minutes.

Table 4.1: Study Demographics.

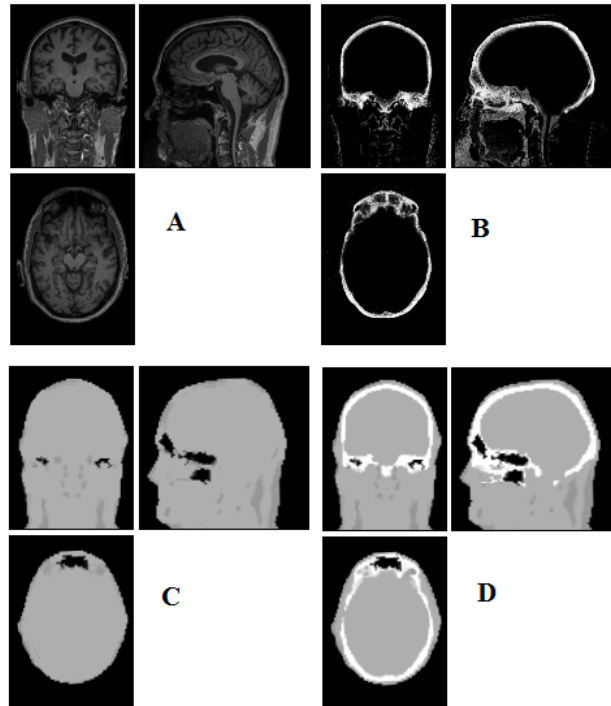
Number	Age (years)	Gender	Primary oncology disease	Net Injected Dose (MBq)
1	62	F	SPN	368
2	55	M	SPN	390
3	39	M	Germ Cell (Testicular)	500
4	64	M	SPN	422
5	62	F	SPN	288
6	62	F	SPN	229
7	54	M	SPN	437
8	51	F	SPN	200
9	56	M	SPN	418
10	65	F	Colorectal	337
11	61	F	NSCLC	411
12	71	M	SPN	388
13	53	M	NSCLC	396

SPN = Solitary Pulmonary Nodule, NSCLC = non-Small cell lung cancer, M= Male, F=Female.

4.3.2 Evaluation of MRAC methods.

An example of Dixon+bone μ -map created by adding bone to a Dixon μ -map from a representative subject is displayed in Figure 4.1. A gradual radial increase in relative difference between PET images reconstructed with Dixon+bone μ -map compared to Dixon μ -map were observed in all subjects. Figure 4.2a, illustrates the typical line profile (Figure 4.2b) through the center slice of the brain of one subject when the PET_{dx} and PET_{dxbone} images are compared. An increase of 5% in the center to nearly 20% in the areas around the cortex was seen.

Figure 4.1: Illustration of a Dixon+bone μ -map generated in a representative subject.

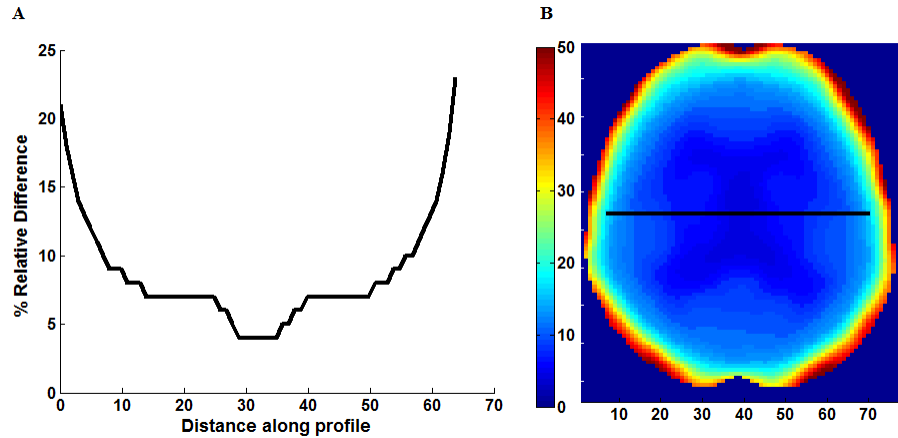


Images (A) T1-weighted MPRAGE, (B) bone probability map, (C) Dixon μ -map and (D) Dixon+bone μ -map are shown in axial, coronal and sagittal views of a single slice.

Group mean values and standard deviation of absolute and relative activity in PET_{dx} and PET_{dxbone} for whole brain and regions of interest are listed in Table 4.2. Paired student t-test showed that the absolute mean activity in PET data reconstructed with Dixon+bone μ -map was statistically higher than PET reconstruction with Dixon μ -map in all thirteen ROIs. Conversely, lower relative activity was found in $rPET_{dxbone}$ when compared to $rPET_{dx}$ in all ROIs except, occipital and cerebellum. These regional differences are depicted in Figure 4.3a as the percent relative difference in mean activity

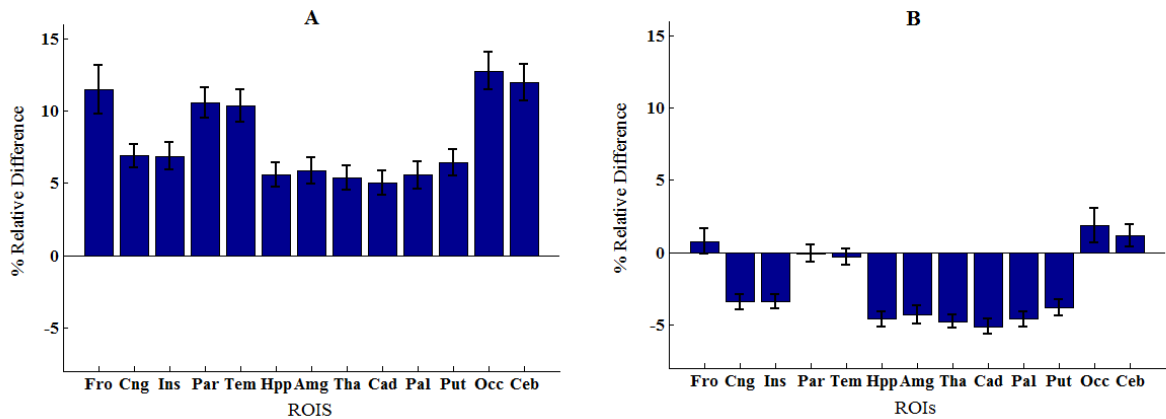
between PET_{dx} and PET_{dxbone} , and in Figure 4.3b as the percent relative difference in $rPET_{dx}$ and $rPET_{dxbone}$ for all thirteen ROIs.

Figure 4.2: Line profile



Line profile (A) across the center slice of a map (B) of relative difference (% RD) between PET images reconstructed with Dixon and Dixon+bone μ -maps. Images are presented from a representative subject.

Figure 4.3: Regions of interest group means percent relative difference (% RD).



%RD in (A) mean activity concentration and (B) mean relative activity between PET signals reconstructed with Dixon and Dixon+bone μ -maps. Errors bars represent standard deviation on the means. Regions abbreviations: Fro = Frontal, Cng = Cingulate, Ins = Insula, Par = Parietal, Tem = Temporal, Hpp = Hippocampus, Amg = Amygdala, Cad = Caudate, Pal = Globus Pallidus, Put = Putamen, Occ = Occipital and Ceb = Cerebellum.

Table 4.2: Group mean and standard deviation (std) of absolute and relative PETdx and PETdxbone activity concentration (kBq/ml) in regions of interest across the brain.

Region	Absolute mean activity				T	Relative mean activity				t
	PET _{dx}		PET _{dxbone}			PET _{dx}		PET _{dxbone}		
	Mean	std	mean	std		mean	std	mean	Std	
Frontal	12.70	2.60	14.12	2.86	15.21	0.96	0.04	0.97	0.03	2.95*
Cingulate	13.90	2.88	14.88	3.04	17.74	1.06	0.05	1.02	0.05	-22.66
Insula	13.47	2.35	14.39	2.50	17.08	1.03	0.04	0.99	0.04	-24.74
Parietal	13.49	2.71	14.91	2.97	16.99	1.03	0.03	1.02	0.03	-0.74*
Temporal	11.63	2.26	12.84	2.51	15.11	0.88	0.02	0.88	0.02	-2.01*
Hippocampus	10.35	1.85	10.93	1.97	14.21	0.79	0.05	0.75	0.05	-32.13
Amygdala	10.42	1.87	11.03	2.01	13.53	0.80	0.07	0.76	0.07	-26.43
Thalamus	14.11	2.77	14.87	2.92	13.91	1.07	0.06	1.02	0.06	-34.88
Caduate	11.33	3.10	11.90	3.24	12.47	0.85	0.09	0.81	0.09	-29.34
Pallidum	14.23	2.66	15.02	2.83	12.93	1.08	0.07	1.03	0.07	-36.10
Putamen	16.83	3.21	17.91	3.43	14.21	1.28	0.08	1.23	0.08	-31.08
Occipital	13.18	2.63	14.87	2.95	16.90	1.00	0.06	1.02	0.07	5.74
Cerebellum	10.68	1.78	11.97	2.03	16.46	0.82	0.08	0.83	0.08	5.36
Whole brain	13.16	2.56	14.56	2.81	17.82	1.04	0.10	1.07	0.10	3.05*

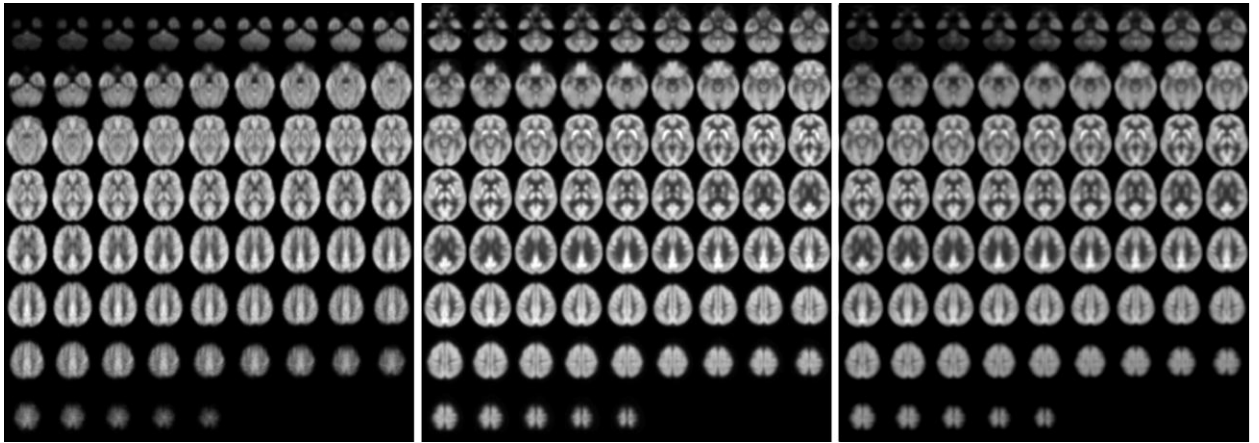
Results of paired differences between PET_{dx} and PET_{dxbone} are presented as value of the t-statistic (t), where all regional differences met the statistical threshold of p<0.05 except for * where p value >0.05.

4.3.3 Correlations of perfusion to glucose uptake

Images of relative CBF, PET_{dx} and PET_{dxbone} averaged across all subjects are displayed in Figure 4.4. In general, these group-wise images are similar in appearance. On visual inspection, the group-averaged PET data reconstructed with Dixon+bone μ -map had an apparent higher intensity compared to PET data reconstructed with Dixon μ -map, particularly around the cortex. An additional difference between the data sets was the aliasing artifact observed in the CBF images, which are most visible in distal images.

The mean group gray matter CBF was 43.82 ± 4.46 ml/100g/min. The mean tSNR of whole brain pCASL signal in gray matter across all subjects was 2.83 ± 1.18 .

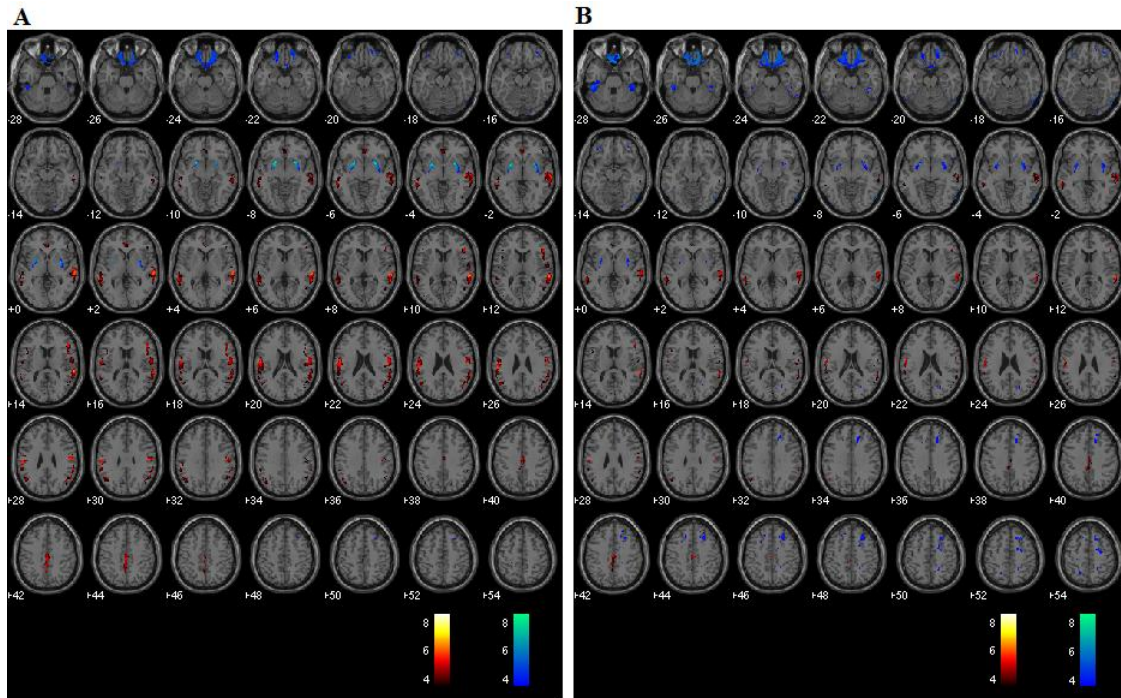
Figure 4.4: Whole-brain group maps of relative perfusion and relative glucose uptake.



Whole-brain group maps from; left to right: pCASL-CBF, FDG-PET reconstructed with Dixon+bone MRAC and FDG-PET reconstructed with Dixon MRAC. Spatial blurring seen in the bottom row images of the perfusion maps could be minimized with segmented multi-shot 3D GRASE acquisitions.

The average voxel-by-voxel correlation coefficient across whole-brain grey matter was $r= 0.63$ ($p<0.001$) between rCBF and rPET_{dx}, and $r= 0.53$ ($p<0.001$) between rCBF and rPET_{dxbone}. The correlation coefficient for each ROI, derived from voxel-wise comparison between rCBF and rPET_{dx} and between rCBF and rPET_{dxbone}, are presented in Table 4.3 along with corresponding total number of voxels. For the comparison between rCBF and rPET_{dx}, moderate-to-high correlations were observed in all ROIs with the highest in the caudate and the lowest in the deep-lying structures of the limbic system such as the hippocampus and amygdala.

Figure 4.5: Whole brain voxel-by-voxel comparison between rCBF and rCMRglc



Comparison between relative cerebral blood flow and relative FDG-PET activity reconstructed with Dixon (A) and Dixon+bone (B) μ -maps. Areas with greater relative perfusion are shown in red while areas with greater relative glucose uptake are shown in blue. Statistical differences are set at threshold for cluster > 50 voxels, $p < 0.05$ corrected for multiple comparisons with FDR.

Similar trends were observed between rCBF and $rPET_{dx+bone}$. Results of voxel-by-voxel independent samples t-test listed on Table 4.4, showed areas of significant increase or decrease in relative perfusion compared to relative FDG-PET signals reconstructed with Dixon and with Dixon+bone μ -maps for clusters that met the set statistical threshold. Maps of statistical differences between rCBF and either $rPET_{dx}$ or $PET_{dx+bone}$ overlaid on axial slices of a single subject T1-weighted image are displayed in Figure 4.5. Regions with higher relative perfusion are marked in red while regions with higher relative glucose uptake are marked in blue.

Table 4.3: Results of voxel-by-voxel Pearson correlation within thirteen regions of interest.

ROI	k_e	rCBF vs. rPET _{dx}	rCBF vs. rPET _{dxbone}	rCBF vs. PET-CT (Cha et al., 2013)
Frontal	70169	0.61	0.52	0.41
Cingulate	7598	0.77	0.76	0.61
Insula	3541	0.54	0.53	0.63
Parietal	26845	0.63	0.58	0.5
Temporal	32962	0.72	0.63	0.67
Hippocampus	1797	0.43	0.41	-0.26
Amygdala	414	0.42	0.40	0.087
Thalamus	2149	0.68	0.68	0.45
Caudate	1895	0.85	0.85	0.78
Pallidum	573	0.41	0.41	Not measured
Putamen	2009	0.48	0.46	0.81
Occipital	21333	0.82	0.73	0.12
Cerebellum	21838	0.54	0.46	0.33

Correlation coefficients (r , $p < 0.001$) are listed for comparisons between relative ASL-CBF and relative PET-FDG measurements corrected with Dixon and Dixon+bone μ -maps, and comparisons from a previous study using 2D-pCASL sequence and PET-CT. Total number of voxels (k_e) within each ROI for the MRAC comparisons are included.

Table 4.4: Results of independent samples t-test in gray matter comparing rCBF to rPET.

Cluster number	Cluster size	X	y	z	t-value	Anatomical label
rPET_{dx} > rCBF						
1	431	-22	12	-8	8.67	Left putamen
2	435	28	8	-6	7.84	Right putamen
3	1591	16	34	-28	5.38	Right orbital frontal
4	457	66	-52	-18	4.88	Right inferior temporal
5	569	26	-14	68	4.26	Right precentral
6	685	-20	-54	68	4.25	Left postcentral
7	126	-44	-24	-32	4.23	Left inferior temporal
8	61	22	-90	-16	4.16	Right occipital
9	126	20	-54	70	3.71	Right postcentral
rPET_{dx} < rCBF						
1	1773	0	-22	42	6.91	Left paracentral
2	7935	62	-34	10	6.90	Right superior temporal
3	6368	-56	-28	24	6.24	Left inferior parietal
4	947	-4	42	-4	5.73	Left anterior cingulate
5	268	4	-74	0	4.92	Right lingual
6	59	-2	-86	14	4.55	Left cuneus
7	77	14	-28	6	3.59	Right thalamus
rPET_{dxbone} > rCBF						
1	650	26	8	-6	7.9	Right putamen
		-24	6	-6	7.8	Left putamen
2	1591	16	34	-28	6.10	Right orbital frontal
3	1332	66	-52	-18	5.71	Right inferior temporal
		66	-58	6	5.63	Right middle temporal
4	4373	26	-14	68	5.25	Right precentral
5	2848	-20	-36	58	5.05	Left postcentral
6	65	-18	-38	38	4.21	Left cingulate
7	79	26	-16	-32	4.09	Right parahippocampal
8	83	4	-34	-12	3.77	Right anterior cingulate
9	70	20	-6	20	3.61	Right caudate
10	76	-20	-72	16	3.58	Left precuneus
rPET_{dxbone} < rCBF						
1	1318	62	-34	12	6.14	Right superior temporal
		62	-28	2	5.52	Right middle temporal
2	630	0	-22	44	5.91	Left paracentral
3	668	-62	-38	48	5.16	Left middle temporal
4	238	48	10	18	4.88	Right inferior frontal
5	210	-48	-60	34	4.79	Left angular
6	72	4	-72	18	4.57	Right cuneus
7	73	-46	30	4	4.25	Left inferior frontal
8	82	-44	10	18	4.15	Left insula
9	186	6	42	-8	3.87	Right medial frontal

Results of independent samples t-test in gray matter comparing rCBF to rPET_{dx} and comparing rCBF to rPET_{dxbone} for clusters > 50 voxels (p<0.05, FDR). MNI coordinates (x, y and z) and corresponding anatomical location are included.

4.4 Discussion

The feasibility of an integrated whole-body PET-MRI system in simultaneous acquisition of perfusion MRI and metabolic PET neuroimaging with an enhanced attenuation correction method was investigated in this study. Following efforts by other groups to minimize errors in PET signal attenuation corrected with MRI^{9,13,14,29}, and given the lack of consensus on acceptable MRAC methods for bone attenuation³⁰, we explored a practical workaround for MRAC. Regional correlates of relative cerebral glucose consumption acquired with FDG-PET, to relative cerebral perfusion acquired with pCASL were also explored. In general, a good correlation between perfusion and glucose consumption was observed over the entire brain, but regional variability in coupling was observed, with the highest correlation in the occipital, and the lowest in the striatum structures.

Direct segmentation of high resolution T1-weighted MR data into various tissue classes for MR attenuation correction of PET have been proposed by Zaidi et al³¹ and Wagenknecht et al³². Segmentation of voxel intensities were performed with sophisticated algorithms that use fuzzy clustering or *a priori* knowledge of tissue location and shape to derive MRAC μ -maps with ~6% maximum absolute relative difference compared to ground truth^{25,31}. However, these methods are time consuming, require post-processing algorithms that are not readily available, and in Zaidi et al's method³¹; require user intervention to improve bone segmentation. In addition, these proposed approaches are sensitive to MR intensity inhomogeneity errors which, when left unaccounted for can exacerbate inherent MR signal issues such as partial volume effects and motion artifacts, potentially inflating bias in MRAC μ -maps. In this study, bone segmentation of T1-

weighted data was easily derived with SPM, an automated pipeline routinely used for brain segmentation in neuroimaging. For each voxel, the unified segmentation method in SPM determines intensity distributions of tissue types using a mixed model cluster analysis and spatial priors from a T1-weighted atlas derived from large number of subjects²⁴. Unlike aforementioned direct segmentation methods, the unified method accounts for non-uniformities in intensity distributions, improving segmentation accuracy³³.

In general, a ~10% increase in whole brain mean FDG activity corrected with Dixon+bone compared to standard Dixon MRAC was observed. A gradual increase in mean FDG activity from ~5% in the center to ~20% in the cortex was observed in PET data corrected with Dixon+bone compared to the same PET data corrected with just Dixon alone, as illustrated in Figure 4.2 for one individual. This finding was consistent with a recent study comparing PET images corrected with the standard Dixon method to images corrected with Dixon plus bone information derived from individual CT³. In this study, Andersen et al³ reported a 15% difference in mean activity from the center to the edge of the brain in PET signal reconstructed with Dixon compared to Dixon plus CT bone. Errors caused by not including bone information are more pronounced at the edge than the center of the brain as photons from the edge of the brain travel longer average path lengths through skull than photons from the center³.

Regional variability in mean activity between PET_{dx} and PET_{dxbone} was also observed in the ROI analysis. Cortical structures such as frontal and temporal lobe had significantly higher relative differences than central brain regions such as basal ganglia and limbic systems (Figure 4.3a). All thirteen brain regions investigated had statistically

significant lower mean activity when reconstructed with the standard Dixon compared to the reconstruction with the Dixon plus bone (Table 4.2). Similar regional variability in PET-corrected with standard Dixon MRAC compared to CT attenuation maps have recently been observed by other groups^{4,5}. Scaling the PET images by their global mean removed the overall underestimation but resulted in regional over- and under-estimations (Figure 4.3b). These regional trends matched results from a previous study⁴ and indicate that irrespective of the chosen reference region, cerebellum⁴ or global mean as used in the current study, relative PET measurements reconstructed with Dixon still possess MRAC-related bias, albeit slightly reduced. Although signal normalization to a reference value can reduce systemic errors in PET reconstruction, it can inflate regional values particularly in cases where group differences actually exist between the reference values³⁴. This might explain the apparent increase in relative PET activity with standard Dixon compared to Dixon+bone (table 4.2) or UTE⁴ in nearly all regions of the brain. Altogether, the results are in line with previous studies showing that the addition of bone information, either from MRI (UTE/MPRAGE) or CT, to the MRAC maps removes the radial bias³ and reduces differences in PET signals from ~20 % to 10% when compared to the gold standard, CTAC^{4,9,11,14}.

The clinical significance of incorporating bone attenuation in PET reconstruction was highlighted by correlating relative cerebral glucose uptake acquired with FDG-PET to relative cerebral perfusion acquired with pCASL across regions in the brain. Recent evidence suggest that a pattern of regional distribution of perfusion to glucose metabolism exist in healthy brains^{19,35,36} and disruptions to regional blood flow-glucose metabolism coupling are potential markers of brain dysfunction³⁷. In general, a good

correlation between perfusion and glucose uptake was observed in this study over the entire brain. Regional variability in relative correlations was found, with the highest correlations in the occipital and caudate, and the lowest in the limbic structures regardless of the MRAC method used (Table 4.3). However, associations between perfusion and PET signals reconstructed with Dixon+bone closely resemble patterns of regional relative perfusion to glucose metabolism reported elsewhere, with FDG-PET and PET perfusion tracers^{18,20,38}, and with FDG-PET and ASL using standalone PET and MRI scanners^{19,39,35}.

When compared to Cha et al¹⁹, where similar regions were explored with a similar pCASL labeling scheme, higher regional correlations of rCBF to rPET_{dxbone} were observed in the current study, except in the insula and putamen (Table 4.3). This apparent increase (~30%) in regional coupling of perfusion to glucose metabolism is likely a result of the improved registration accuracy provided by simultaneous imaging and the improved tSNR provided by using a 3D pCASL method^{23,40}. The temporal SNR of 3D-GRASE pCASL was not compromised by the use of a PET-compatible head coil, and the mean tSNR reported here was in line with values reported elsewhere^{23,40}.

Results from voxel-by-voxel t-tests between rCBF and rPET demonstrated regions of hyper- or hypo-perfusion not matched to glucose metabolism (Figure 4.5 and Table 4.4). These findings, specifically from PET data corrected with Dixon+bone MRAC, are in line with previous findings of increased resting perfusion to resting metabolism in areas of the brain associated with the default mode network^{18,19}, suggesting that these brain regions require increased blood flow due to the sustained state of arousal³⁶. Apparent bias in bone attenuation from standard Dixon MRAC was evident

in the comparison between relative perfusion and glucose uptake as demonstrated in Figure 4.5 and in comparison to previous studies^{19,35,39}. In particular, unexpected increases in rCBF were observed in the left paracentral, left inferior parietal and right superior temporal gyrus when compared to PET_{dx}. The spatial pattern of these differences, notably their occurrence closer to the edge of brain, is suggestive of attenuation errors. Indeed, these regions of elevated rCBF were either removed or significantly reduced when compared to PET_{dxbone}.

It is possible that segmentation errors such as voxel misclassifications in Dixon+bone μ -maps could account for some differences in correlations between the current study and observations reported elsewhere. Differences in μ_a for bone assigned to MR or CT derived μ -maps, and differences in PET scanner geometry and reconstruction parameters including number of iterations, subsets and smoothing kernels could also influence final observations. In addition, limitations inherent to pCASL and to PET-FDG imaging such as partial voluming, differences in cellular localization of blood water and FDG tracers, and optimal selection of post-labelling delay in ASL with minimal compromise to SNR could affect accuracy of regional comparisons (cf. Cha et al¹⁹). The evaluation of Dixon+bone μ -maps would have benefited from comparison to ground truth using CT data, which was not feasible in this study. The PET-CT whole body survey acquired on all subjects prior to PET-MRI imaging, permitted coverage solely from the level of the eyes to the thighs as per clinical protocol, limiting whole brain comparisons. As such, absolute and regional performance of the enhanced Dixon μ -maps was not evaluated. Over estimation of bone information was observed in the inferior regions of the brain and can be seen in the Dixon+bone μ -maps (Figure 4.1) and in the comparisons

of PET_{dxbone} to pCASL CBF (Figure 4.5). Regions close to the base of the skull where bone anatomy is thin can yield low MR bone signals with MPRAGE²⁵ or UTE⁴ sequences, and these regions are prone to signal misclassification errors in soft tissue/bone/air interfaces in areas around the sinuses- an issue that affects most atlas-based MR-derived attenuation correction methods. Efforts were made to minimize bone misclassification by morphological filtering of non-bone voxels. A recent study demonstrated that SPM8-based method for generating MRAC is robust with a reported accuracy of under 4% when compared to CTAC²⁹. The results presented here were in good agreement with previous studies, suggesting that these issues had little or no effect on the study outcome. This suggests that ASL-CBF imaging could be used to in future studies to investigate the relationships between altered brain function and disease-specific PET tracers. The regional correlation of pCASL CBF to FDG-PET demonstrated here for the first time with simultaneous imaging can be further improved with imaging of concurrent uptake of the pCASL and FDG tracer.

In general, the agreement between this study and previous studies using CT attenuation maps indicate that Dixon attenuation maps enhanced with bone information from high resolution T1-weighted images can provide a feasible method for correction of PET signal attenuation in PET-MRI neuroimaging. Errors in MRI-derived attenuation correction maps including tissue misclassification can be further minimized by methods that employ tissue classifiers from CT atlas to better guide segmentation of UTE or MPRAGE data¹³.

4.5 References

1. Pichler, B. J., Kolb, A., Nägele, T. & Schlemmer, H.-P. PET/MRI: paving the way for the next generation of clinical multimodality imaging applications. *J. Nucl. Med.* **51**, 333–6 (2010).
2. Dukart, J. *et al.* Combined evaluation of FDG-PET and MRI improves detection and differentiation of dementia. *PLoS One* **6**, e18111 (2011).
3. Andersen, F. L. *et al.* Combined PET/MR imaging in neurology: MR-based attenuation correction implies a strong spatial bias when ignoring bone. *Neuroimage* **84**, 206–16 (2014).
4. Dickson, J. C., O’Meara, C. & Barnes, A. A comparison of CT- and MR-based attenuation correction in neurological PET. *Eur. J. Nucl. Med. Mol. Imaging* **41**, 1176–1189 (2014).
5. Hitz, S. *et al.* Systematic Comparison of the Performance of Integrated Whole-Body PET/MR Imaging to Conventional PET/CT for 18F-FDG Brain Imaging in Patients Examined for Suspected Dementia. *J. Nucl. Med.* **55**, 923–931 (2014).
6. Keereman, V., Mollet, P., Berker, Y., Schulz, V. & Vandenberghe, S. Challenges and current methods for attenuation correction in PET/MR. *MAGMA* **26**, 81–98 (2013).
7. Dixon, W. T. Simple proton spectroscopic imaging. *Radiology* **153**, 189–194 (1984).
8. Coombs, B. D., Szumowski, J. & Coshov, W. Two-Point Dixon Technique for Water-Fat Signal Decomposition with B0 Inhomogeneity Correction. *Magn. Reson. Med.* **38**, 884–889 (1997).
9. Catana, C. *et al.* Toward implementing an MRI-based PET attenuation-correction method for neurologic studies on the MR-PET brain prototype. *J. Nucl. Med.* **51**, 1431–8 (2010).

10. Beyer, T. *et al.* MR-based attenuation correction for torso-PET/MR imaging: pitfalls in mapping MR to CT data. *Eur. J. Nucl. Med. Mol. Imaging* **35**, 1142–6 (2008).
11. Marshall, H. R. *et al.* Description and assessment of a registration-based approach to include bones for attenuation correction of whole-body PET/MRI. *Med. Phys.* **40**, 082509 (2013).
12. Hofmann, M. *et al.* MRI-based attenuation correction for PET/MRI: a novel approach combining pattern recognition and atlas registration. *J. Nucl. Med.* **49**, 1875–83 (2008).
13. Poynton, C. B. *et al.* Probabilistic atlas-based segmentation of combined T1-weighted and DUTE MRI for calculation of head attenuation maps in integrated PET/MRI scanners. *Am. J. Nucl. Med. Mol. Imaging* **4**, 160–71 (2014).
14. Kops, E. R., Wagenknecht, G., Scheins, J., Tellmann, L. & Herzog, H. Attenuation correction in MR-PET scanners with segmented T1-weighted MR images. *2009 IEEE Nucl. Sci. Symp. Conf. Rec.* 2530–2533 (2009).
doi:10.1109/NSSMIC.2009.5402034
15. Pappas, I. P. I., Styner, M., Malik, P., Remonda, L. & Caversaccio, M. Automatic method to assess local CT-MR imaging registration accuracy on images of the head. *AJNR. Am. J. Neuroradiol.* **26**, 137–44 (2005).
16. Greenberg, J. H. *et al.* Metabolic Mapping of Functional Activity in Human Subjects with the [18F]Fluorodeoxyglucose Technique. *Science (80-.)*. **212**, 678–680 (1981).
17. Brown, G. G., Perthen, J. E., Liu, T. T. & Buxton, R. B. A primer on functional magnetic resonance imaging. *Neuropsychol. Rev.* **17**, 107–25 (2007).
18. Gur, R. C. *et al.* Regional differences in the coupling between resting cerebral blood flow and metabolism may indicate action preparedness as a default state. *Cereb. Cortex* **19**, 375–82 (2009).

19. Cha, Y.-H. K. *et al.* Regional correlation between resting state FDG PET and pCASL perfusion MRI. *J. Cereb. Blood Flow Metab.* **33**, 1909–1914 (2013).
20. Musiek, E. S. *et al.* Direct comparison of fluorodeoxyglucose positron emission tomography and arterial spin labeling magnetic resonance imaging in Alzheimer's disease. *Alzheimers. Dement.* **8**, 51–9 (2012).
21. Delso, G. *et al.* Performance measurements of the Siemens mMR integrated whole-body PET/MR scanner. *J. Nucl. Med.* **52**, 1914–22 (2011).
22. Martinez-Möller, A. *et al.* Tissue classification as a potential approach for attenuation correction in whole-body PET/MRI: evaluation with PET/CT data. *J. Nucl. Med.* **50**, 520–6 (2009).
23. Günther, M., Oshio, K. & Feinberg, D. a. Single-shot 3D imaging techniques improve arterial spin labeling perfusion measurements. *Magn. Reson. Med.* **54**, 491–8 (2005).
24. Ashburner, J. & Friston, K. J. Unified segmentation. *Neuroimage* **26**, 839–51 (2005).
25. Wagenknecht, G. *et al.* Attenuation Correction in MR-BrainPET with Segmented T1-weighted MR images of the Patient ' s Head - A Comparative Study with CT. *IEEE Nucl. Sci. Symp. Conf. Rec. (1997)*. 2261–2266 (2011).
26. Tzourio-Mazoyer, N. *et al.* Automated anatomical labeling of activations in SPM using a macroscopic anatomical parcellation of the MNI MRI single-subject brain. *Neuroimage* **15**, 273–89 (2002).
27. Maldjian, J. a., Laurienti, P. J., Kraft, R. a. & Burdette, J. H. An automated method for neuroanatomic and cytoarchitectonic atlas-based interrogation of fMRI data sets. *Neuroimage* **19**, 1233–1239 (2003).
28. Wang, J. *et al.* Arterial transit time imaging with flow encoding arterial spin tagging (FEAST). *Magn. Reson. Med.* **50**, 599–607 (2003).

29. Izquierdo-Garcia, D. *et al.* An SPM8-Based Approach for Attenuation Correction Combining Segmentation and Nonrigid Template Formation: Application to Simultaneous PET/MR Brain Imaging. *J. Nucl. Med.* **55**, 1825–1830 (2014).
30. Bailey, D. L. *et al.* Summary report of the First International Workshop on PET/MR imaging, March 19-23, 2012, Tübingen, Germany. *Mol. Imaging Biol.* **15**, 361–71 (2013).
31. Zaidi, H., Montandon, M.-L. & Slosman, D. O. Magnetic resonance imaging-guided attenuation and scatter corrections in three-dimensional brain positron emission tomography. *Med. Phys.* **30**, 937 (2003).
32. Wagenknecht, G., Kops, E. R., Tellmann, L. & Herzog, H. Knowledge-based Segmentation of Attenuation- relevant Regions of the Head in T1-weighted MR Images for Attenuation Correction in MR / PET Systems. *IEEE Nucl. Sci. Symp. Conf. Rec. (1997)*. 3338–3343 (2009).
33. Tsang, O. *et al.* Comparison of tissue segmentation algorithms in neuroimage analysis software tools. *Conf. Proc. IEEE Eng. Med. Biol. Soc.* **2008**, 3924–8 (2008).
34. Borghammer, P. *et al.* Normalization in PET group comparison studies--the importance of a valid reference region. *Neuroimage* **40**, 529–40 (2008).
35. Newberg, A. B. *et al.* Concurrent CBF and CMRGlc changes during human brain activation by combined fMRI-PET scanning. *Neuroimage* **28**, 500–6 (2005).
36. Vaishnavi, S. N. *et al.* Regional aerobic glycolysis in the human brain. *Proc. Natl. Acad. Sci. U. S. A.* **107**, 17757–62 (2010).
37. Vlassenko, A. G. *et al.* Spatial correlation between brain aerobic glycolysis and amyloid- β (A β) deposition. *Proc. Natl. Acad. Sci. U. S. A.* **107**, 17763–7 (2010).
38. Bentourkia, M. *et al.* Comparison of regional cerebral blood flow and glucose metabolism in the normal brain: effect of aging. *J. Neurol. Sci.* **181**, 19–28 (2000).

39. Chen, Y. *et al.* Voxel-level comparison of arterial spin-labeled perfusion MRI and FDG-PET in Alzheimer disease. *Neurology* **77**, 1977–85 (2011).
40. Vidorreta, M. *et al.* Comparison of 2D and 3D single-shot ASL perfusion fMRI sequences. *Neuroimage* **66**, 662–671 (2013).

5 Chapter 5

Conclusions and Future Work

5.1 Summary of Findings

This thesis explored the role of cardiovascular disease in advancing pathological brain aging using novel neuroimaging techniques. As well as investigated the potential neuroprotective benefit of aerobic exercise training performed as part of a cardiovascular rehabilitation (CR) program. Magnetic resonance imaging (MRI) methods were used to measure gray matter volume (GMV) changes and changes in cerebrovascular hemodynamics, specifically CBF and CVR, in a group of coronary artery disease patients (CAD). In this final chapter, major findings of the studies performed in this thesis are summarized. The clinical relevance of the findings is discussed and areas of possible future directions are outlined.

5.1.1 Changes in Brain Structure Associated with Cardiovascular Disease

Although prior evidence demonstrated decreased brain volume in older adults with increased risks for cardiovascular disease¹, changes in regional brain volume have not been previously investigated in individuals diagnosed with cardiovascular disease. Chapter 2 describes an exploratory study where regional GMV was compared between CAD patients and age-matched controls using voxel-based morphometry, to examine the impact of cardiovascular disease on brain structure. CAD patients exhibited decreased GMV in the frontal, temporal and parietal lobes, and in the posterior cerebellum. These

findings are in line with patterns of brain atrophy previously reported in hypertensive and diabetic patients¹, and support evidence of accelerated cognitive decline in cardiovascular disease patients². In general, the results suggest that cardiovascular disease accelerates brain aging, affecting regions that are typically stable during normal aging.

5.1.2 Impact of Cardiovascular Disease on Brain Hemodynamics

Since CAD is a by-product of atherosclerosis and impaired cerebrovascular hemodynamics are associated with markers of atherosclerosis, such as arterial stiffness³, it follows that brains of CAD patients showing signs of structural decline (chapter 2) would also have disruptions in hemodynamics. In chapter 3, cerebrovascular hemodynamics (i.e., CBF and CVR) and relationships between hemodynamic changes and brain atrophy was studied in the same cohort of CAD patients and controls. Continuous measurements of cerebrovascular hemodynamics were performed during acquisition of ASL images while subjects breathed room air (baseline) or hypercapnic air (6% CO₂, 21% O₂ and balanced air) for 5 min each. Reduced resting CBF was observed in CAD patients in the superior frontal, anterior cingulate, pre-and post-central gyri, and superior temporal regions, along with decreased CVR in the anterior cingulate, post central and superior temporal regions. These changes were independent of changes in brain volume, suggesting that cerebrovascular dysfunction precedes brain atrophy.

5.1.3 Potential Neuroprotective Benefits of Cardiac Rehabilitation

Since established exercise-based preventative programs are readily available to cardiac patients and a myriad of evidence demonstrates positive effects of exercise⁴, the

potential neuroprotective benefits of physical activity on the brains of CAD patients were explored. Chapters 2 and 3 describe pre- and post-intervention results from CAD patients for whom declines in regional brain volume, CBF and CVR were observed pre-intervention. The exercise intervention consisted of a moderate intensity aerobic fitness training lasting 6 months. Findings of increased brain volume in several regions of the brain associated with cognitive control, as well as regions linked to motor coordination, showed for the first time, the significance of exercise-based CR programs on brains of CAD patients. Equally notable was the discovery of recovery in CBF in the anterior cingulate and brain volumes in the superior frontal, superior temporal and posterior cerebellum. These findings were in brain regions where a measurable decrease was observed before rehabilitation. For instance, a ~33% decrease in CBF was observed at baseline in the right anterior cingulate in CAD patients compared to control, while a ~30% increase in CBF was seen post exercise.

5.1.4 Can CBF Measured with ASL Serve as a Suitable Marker of Brain Function

Current studies suggest that CBF measured with ASL correlates with cerebral glucose consumption (CMR_{glc}) measured with PET-FDG⁵⁻⁷, a well established measure of brain function, and could serve as suitable alternative to PET-FDG⁸. However these studies were performed using separate MRI and PET scanners and, therefore, voxel-wise comparison of CBF and CMR_{glc} could be confounded by image registration errors and differences in brain physiological state between imaging sessions. Chapter 4 describes efforts to correlate ASL-CBF to PET-CMR_{glc} acquired simultaneously on an integrated PET and MRI system. Marked regional variations in CBF to CMR_{glc} were observed with

the highest associations in the caudate and cingulate and the lowest in the limbic structures. All findings were well matched to observations from previous studies, suggesting that perfusion and glucose metabolism are well matched, but variable distribution of perfusion to glucose metabolism coupling exist in healthy brains.

5.2 Relevance of Findings

In this thesis, neuroimaging in cardiovascular disease showed a pattern of brain decline that is more severe than changes observed in normal brain aging, but reversible with moderate aerobic exercise training. The findings from studies described in this thesis bear some clinical relevance. First, the findings challenge the monodisciplinary approach currently applied to management of cardiovascular disease in older adults. It is clear that the brain is affected from cardiovascular disease, specifically diseases of atherosclerotic origin. Individuals with a history of cardiovascular disease or at an increased risk for vascular disease are more likely to have stroke and related cerebrovascular disease⁹. If the expected increase in population of older adults includes an equal increase in cardiovascular disease survivors, a better understanding of the complex interaction between cardiovascular dysfunction and brain health is imperative, and will require a multidisciplinary approach. The studies in this thesis provide a framework for further multidisciplinary investigations, as will be discussed below. Second and more importantly, the work presented here emphasizes the clinical significance of exercise-based CR programs in terms of benefit to both cardio- and cerebrovascular health. In Canada, although exercise-based CR programs have been established for over 40 years, only 1 in 3 eligible patients participate in CR¹⁰. A major source for underutilization is the

lack of physician referral to CR¹¹. The work laid out in thesis demonstrates the need for further research in current CR delivery models to see if inclusion of cerebrovascular health assessment and monitoring can improve overall efficacy of rehabilitation programs.

5.3 Future work

5.3.1 Longitudinal and Epidemiology studies

Although the results presented in chapters 2 and 3 provide strong evidence of cardiovascular disease effects on cerebrovascular structure and function, the cross-sectional nature of study design, provides a snapshot at best of cardiac disease effects. Longitudinal studies of disease progression may reveal further information of cardiac disease contributions to brain dysfunction. For instance, in the Baltimore Longitudinal Study of Aging, regional CBF was measured in healthy older adults and treated hypertensive patients over a period of 6 years¹². The study found an accelerated decrease in regional CBF in the frontal, anterior cingulate and occipital regions over time, but the duration of hypertension only contributed to decreased CBF in the frontal and anterior cingulate regions¹². Another longitudinal study of older adults with cardiovascular disease measured diverse domains of cognitive performance using a battery of neuropsychological tests, at study entry, 1 year and 3 years later². The study reported worsening of cognitive performance across all measured domain, but varied trajectory of decline with faster decay for visuospatial skills and smaller relative rate of decline for executive function and psychomotor speed². Both studies demonstrate that certain brain regions have a greater vulnerability to vascular disease over time. It would be interesting

to observe changes in brains of CAD patients over time and examine the disease effects as the brain ages.

5.3.2 Exercise

The neurovascular benefits of low-moderate intensity exercise programs performed over a short period time (few weeks to 6 months) in healthy older adults are still being explored. Current knowledge of long-term effects is limited and has only been explored in one study, which found that walking at least 72 city blocks a week was associated with preserved GM volume 9 years later, but walking more than 72 blocks did not incur any added benefit¹³. Lingering questions on exercise threshold effects, that is the minimum exercise duration and intensity required to detect structural and functional brain changes, are yet to be clearly addressed. For individuals with cardiovascular disease, exercise can be both beneficial or detrimental to cardiovascular health and overall well being¹⁴, particularly when performed in unsupervised environments. In addition, standard pharmacological therapies for management of cardiovascular disease such as statins, beta-blockers and aspirin, are known to attenuate exercise effects¹⁵ and modulate CBF¹⁶. An immediate question to address would be: does a single duration of exercise training, for instance a 6-month aerobic exercise regimen such as in CR, confer long-term neuronal protection for cardiovascular disease patients?

5.3.3 Characterizing white matter structure in coronary artery disease patients.

White matter (WM) lesions are prevalent in individuals with increased risk for vascular disease¹⁷. Cerebral hypoperfusion is thought to significantly impair WM connectivity affecting the speed of cognitive processing¹⁸. In healthy older adults, higher cardiorespiratory fitness is associated with preservation of age-related declined in WM microstructure¹⁹. Associations of vascular disease to disruptions in WM structural integrity and subsequent effects on cognitive function are unclear. It is quite possible that reports of accelerated cognitive decline in cardiovascular disease patients² could be linked to disruptions in WM integrity that are related to vascular disease²⁰. In the same token, improvements in cognitive performance ascribed to exercise training²¹ could be mediated by exercise-induced plasticity of WM structure²². Therefore, it would be interesting to elucidate WM regions vulnerable to cardiovascular disease, investigate relationships of WM abnormalities to cognitive impairments, and explore the role of CR in mediating disease effects on WM microstructure.

5.4 References

- 1 Friedman JI, Tang CY, de Haas HJ, Changchien L, Goliash G, Dabas P *et al.* Brain Imaging Changes Associated With Risk Factors for Cardiovascular and Cerebrovascular Disease in Asymptomatic Patients. *JACC Cardiovasc Imaging* 2014; **7**: 1039–1053.
- 2 Okonkwo OC, Cohen R a, Gunstad J, Tremont G, Alosco ML, Poppas A. Longitudinal trajectories of cognitive decline among older adults with cardiovascular disease. *Cerebrovasc Dis* 2010; **30**: 362–73.

- 3 Desjardins M. Vascular correlates of aging in the brain : Evidence from imaging data. *IRBM* 2015; **1**: 1–8.
- 4 Erickson KI, Miller DL, Weinstein AM, Akl SL, Banducci S. Physical activity and brain plasticity in late adulthood: a conceptual and comprehensive review. *Ageing Res* 2012; **4**: 34–47.
- 5 Cha Y-HK, Jog M a, Kim Y-C, Chakrapani S, Kraman SM, Wang DJ. Regional correlation between resting state FDG PET and pCASL perfusion MRI. *J Cereb Blood Flow Metab* 2013; **33**: 1909–1914.
- 6 Chen Y, Wolk D a, Reddin JS, Korczykowski M, Martinez PM, Musiek ES *et al.* Voxel-level comparison of arterial spin-labeled perfusion MRI and FDG-PET in Alzheimer disease. *Neurology* 2011; **77**: 1977–85.
- 7 Newberg AB, Wang J, Rao H, Swanson RL, Wintering N, Karp JS *et al.* Concurrent CBF and CMRGlc changes during human brain activation by combined fMRI-PET scanning. *Neuroimage* 2005; **28**: 500–6.
- 8 Musiek ES, Chen Y, Korczykowski M, Saboury B, Martinez PM, Reddin JS *et al.* Direct comparison of fluorodeoxyglucose positron emission tomography and arterial spin labeling magnetic resonance imaging in Alzheimer’s disease. *Alzheimers Dement* 2012; **8**: 51–9.
- 9 Pearson T a., Blair SN, Daniels SR, Eckel RH, Fair JM, Fortmann SP *et al.* AHA Guidelines for Primary Prevention of Cardiovascular Disease and Stroke: 2002 Update: Consensus panel guide to comprehensive risk reduction for adult patients without coronary or other atherosclerotic vascular diseases. *Circulation* 2002; **106**: 388–391.
- 10 Grace SL, Bennett S, Ardern CI, Clark AM. Cardiac rehabilitation series: Canada. *Prog Cardiovasc Dis* 2014; **56**: 530–5.
- 11 Mampuya WM. Cardiac rehabilitation past, present and future: an overview. *Cardiovasc Diagn Ther* 2012; **2**: 38–49.

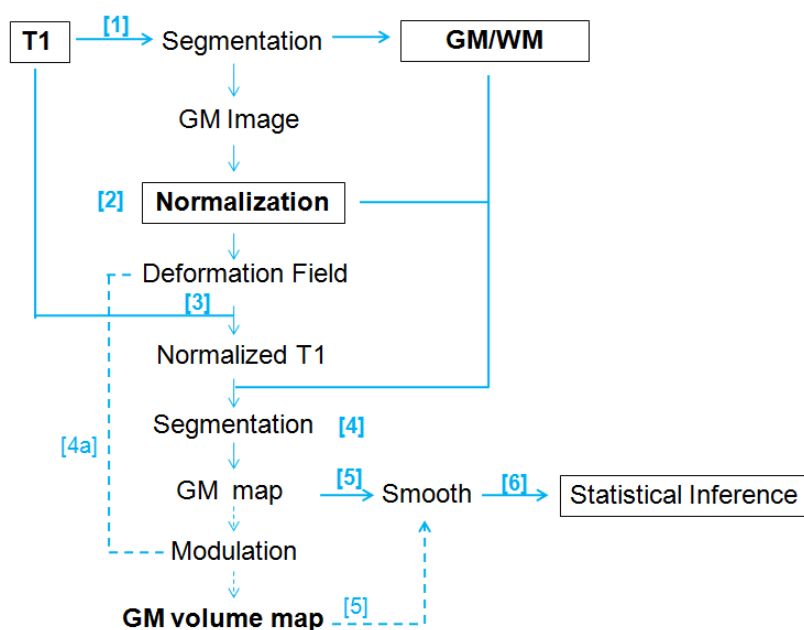
- 12 Beason-Held LL, Moghekar A, Zonderman AB, Kraut M a, Resnick SM. Longitudinal changes in cerebral blood flow in the older hypertensive brain. *Stroke* 2007; **38**: 1766–73.
- 13 Erickson KI, Raji C a, Lopez OL, Becker JT, Rosano C, Newman a B *et al.* Physical activity predicts gray matter volume in late adulthood: the Cardiovascular Health Study. *Neurology* 2010; **75**: 1415–22.
- 14 Thompson PD. Exercise prescription and proscription for patients with coronary artery disease. *Circulation* 2005; **112**: 2354–2363.
- 15 Van Baak MA, Böhm RO, Arends BG, van Hooff ME, Rahn KH. Long-term antihypertensive therapy with beta-blockers: submaximal exercise capacity and metabolic effects during exercise. *Int J Sports Med* 1987; **8**: 342–347.
- 16 Giannopoulos S, Katsanos AH, Kosmidou M, Tsivgoulis G. Statins and vascular dementia: a review. *J Alzheimers Dis* 2014; **42 Suppl 3**: S315–20.
- 17 Breteler MMB, van Swieten JC, Bots ML, Grobbee DE, Claus JJ, van den Hout JHW *et al.* Cerebral white matter lesions, vascular risk factors, and cognitive function in a population- based study: The Rotterdam Study . *Neurol* 1994; **44** : 1246.
- 18 Madden DJ, Bennett IJ, Song AW. Cerebral white matter integrity and cognitive aging: contributions from diffusion tensor imaging. *Neuropsychol Rev* 2009; **19**: 415–35.
- 19 Johnson NF, Kim C, Clasey JL, Bailey A, Gold BT. Cardiorespiratory fitness is positively correlated with cerebral white matter integrity in healthy seniors. *Neuroimage* 2012; **59**: 1514–1523.
- 20 Jacobs HIL, Leritz EC, Williams VJ, Van Boxtel MPJ, Elst W Van Der, Jolles J *et al.* Association between white matter microstructure, executive functions, and processing speed in older adults: The impact of vascular health. *Hum Brain Mapp* 2013; **34**: 77–95.

- 21 Colcombe S, Kramer AF. Fitness effects on the cognitive function of older adults: a meta-analytic study. *Psychol Sci* 2003; **14**: 125–30.
- 22 Gons R a, Tuladhar a M, de Laat KF, van Norden a G, van Dijk EJ, Norris DG *et al*. Physical activity is related to the structural integrity of cerebral white matter. *Neurology* 2013; **81**: 971–976.

Appendices

Appendix A: An Overview of the Optimized VBM approach as implemented in SPM8

Figure A1 : Flow chart of optimized VBM as implemented in SPM8.



In optimized VBM¹ [1], the original T1 image volume in native space is segmented into GM and WM images, followed by the removal of unconnected non-brain voxels in skin, skull and dura from the segmented images using fully automated morphological operations (erosion and conditional dilation). [2] The resulting GM and WM images are spatially normalized to GM/WM templates further eliminating contributions of non-brain voxels and improving spatial normalization of GM/WM images. [3] The normalization parameters are then applied to the original T1 image

volume placing the images in stereotactic standard space. [4] Subsequent segmentation of the normalized T1 images into GM, WM and CSF partitions is performed to generate a GM concentration map. [5] Spatial smoothing is applied to the GM map by convolving the images with an isotropic Gaussian kernel. This renders the data more normally distributed and compensates for the inexact nature of the spatial normalization. [6] Finally, a generalized linear model fit is applied to the smoothed GM images for group comparisons or correlations with covariates of interest.

Alternatively, segmented GM images in spatial correspondence to the template can be [4a] multiplied ("modulated") by the Jacobian determinant derived from the spatial normalization step [2]. This compensates for the non-linear effect of spatial normalization and preserves the total amount of GM in the normalized data¹. Individual variations in brain sizes can be accounted for by either including the total intracranial volume, which is the sum of GM, WM, and CSF, as covariates of no interest during the statistical model fit (i.e. global normalization), or by modulating only the non-linear components of the Jacobian determinant, which is recommended (dbm.neuro.uni-jena.de/vbm/). Hence, unmodulated smoothed normalized GM images represent relative concentration of GM while modulated smoothed normalized GM images can represent absolute volume of GM or relative volume corrected for differences in brain sizes. In chapter 2 and 3, absolute GM volumes corrected for differences in brain sizes were used to investigate regional differences in brain structure.

To improve signal-to-noise ratio and the sensitivity of detecting local changes in gray matter, the T1 images are bias corrected for image intensity non-uniformity prior to segmentation and the resultant GM volume or concentration maps are smoothed by

convolving the images with an isotropic Gaussian kernel. Bias correction accounts for the smooth intensity variations due to spatially-dependent response of the head receiver coils. While spatial smoothing renders the data more normally distributed and compensates for the inexact nature of the spatial normalization. However, since spatial smoothing can blur an image minimizing the ability to detect local changes, the size of the Gaussian kernel should match the size of the expected effect.

References

1. Good, C. D. *et al.* A voxel-based morphometric study of ageing in 465 normal adult human brains. *Neuroimage* **14**, 21–36 (2001).

Appendix B : Copyright Agreement information



Title: An investigation of changes in regional gray matter volume in cardiovascular disease patients, pre and post cardiovascular rehabilitation

Author: U.C. Anazodo, J.K. Shoemaker, N. Suskin, K.S. St. Lawrence

Publication: NeuroImage: Clinical

Publisher: Elsevier

Date: 2013

Copyright © 2013 The Authors. Published by Elsevier Inc.

LOGIN

If you're a **copyright.com user**, you can login to RightsLink using your copyright.com credentials. Already a **RightsLink user** or want to [learn more?](#)

Creative Commons Attribution-NonCommercial-No Derivatives License (CC BY NC ND)

This article is published under the terms of the [Creative Commons Attribution-NonCommercial-No Derivatives License \(CC BY NC ND\)](#).

For non-commercial purposes you may distribute and copy the article and include it in a collective work (such as an anthology), provided you do not alter or modify the article, without permission from Elsevier. The original work must always be appropriately credited.

Permission is not required for this non-commercial use. For commercial use please continue to request permission via RightsLink.

Dear Udunna Anazodo,
The article is published under a CC-BY license and the authors retain the copyright. You can reproduce the article provided its original citation is clearly indicated.

Best regards,

[Redacted signature]

Editorial Office Manager, Frontiers

www.frontiersin.org | [Redacted]

[Redacted]

[Redacted]

On Wed, Jul 8, 2015 at 11:33 PM, Udunna Anazodo <[Redacted]> wrote:
Hello,

Title: Feasibility of simultaneous whole-brain imaging on an integrated PET-MRI system using an enhanced 2-point Dixon attenuation correction method.

Authors: Anazodo UC, Thiessen JD, Ssali T, Mandel J, Günther M, Butler J, Pavlosky W, Prato FS, Thompson RT, St Lawrence KS.

Citation: Front Neurosci. 2015 Jan 5;8:434. doi: 10.3389/fnins.2014.00434. eCollection 2014.

I am kindly requesting permission to reproduce the above article for inclusion in a forthcoming doctoral thesis publication called "An investigation of cardiovascular disease contributions to". This thesis will be published by the University of Western Ontario tentatively in September 2010 as both a book and as a handout. I have provided my email below for transmission of a signed copy of the permission request. Thank you

Appendix C: Ethics Approval



Use of Human Participants - Ethics Approval Notice

Research Ethics

Principal Investigator: Dr. Kevin Shoemaker
File Number: 100115
Review Level: Delegated
Approved Local Adult Participants: 200
Approved Local Minor Participants: 0
Protocol Title: Architecture of Cortical Somatosensory and Autonomic Neural Networks Supporting Muscular Movement: Impacts of Vascular Disease and Exercise Interventions. (REB #17810)
Department & Institution: Health Sciences\Kinesiology, Western University
Sponsor: Canadian Institutes of Health Research

Ethics Approval Date: November 08, 2012 **Expiry Date:** December 31, 2016
Documents Reviewed & Approved & Documents Received for Information:

Document Name	Comments	Version Date
Change in Study Personnel	Carly Barron has been added to the study team. M. Frances and T. Hartley have been removed.	
Revised Letter of Information & Consent		

This is to notify you that The University of Western Ontario Research Ethics Board for Health Sciences Research Involving Human Subjects (HSREB) which is organized and operates according to the Tri-Council Policy Statement: Ethical Conduct of Research Involving Humans and the Health Canada/ICH Good Clinical Practice Practices: Consolidated Guidelines; and the applicable laws and regulations of Ontario has reviewed and granted approval to the above referenced revision(s) or amendment(s) on the approval date noted above. The membership of this REB also complies with the membership requirements for REB's as defined in Division 5 of the Food and Drug Regulations.

The ethics approval for this study shall remain valid until the expiry date noted above assuming timely and acceptable responses to the HSREB's periodic requests for surveillance and monitoring information. If you require an updated approval notice prior to that time you must request it using the University of Western Ontario Updated Approval Request Form.

Members of the HSREB who are named as investigators in research studies, or declare a conflict of interest, do not participate in discussion related to, nor vote on, such studies when they are presented to the HSREB.

The Chair of the HSREB is Dr. Joseph Gilbert. The HSREB is registered with the U.S. Department of Health & Human Services under the JRB registration number IRB 00000940.

Principal Investigator: Dr. William Pavlosky
File Number: 102895
Review Level: Delegated
Approved Local Adult Participants: 30
Approved Local Minor Participants: 0
Protocol Title: A pilot study comparing PET/MRI scans to PET/CT scans of the same oncology patients.
Department & Institution: Schulich School of Medicine and Dentistry/Nuclear Medicine, St. Joseph's Health Care London
Sponsor:
Ethics Approval Date: June 05, 2013 **Expiry Date:** July 31, 2015
Documents Reviewed & Approved & Documents Received for Information:

Document Name	Comments	Version Date
Addition of Co-investigator	Dr. Anil Shastry has been added as a co-investigator.	
Revised Western University Protocol	Dr. William Pavlosky has replaced Dr. Jonathan Mandel as the Principal investigator.	
Revised Letter of Information & Consent		2013/04/09

This is to notify you that The University of Western Ontario Research Ethics Board for Health Sciences Research Involving Human Subjects (HSREB) which is organized and operates according to the Tri-Council Policy Statement: Ethical Conduct of Research Involving Humans and the Health Canada/ICH Good Clinical Practice Practices: Consolidated Guidelines; and the applicable laws and regulations of Ontario has reviewed and granted approval to the above referenced revision(s) or amendment(s) on the approval date noted above. The membership of this REB also complies with the membership requirements for REB's as defined in Division 5 of the Food and Drug Regulations.

The ethics approval for this study shall remain valid until the expiry date noted above assuming timely and acceptable responses to the HSREB's periodic requests for surveillance and monitoring information. If you require an updated approval notice prior to that time you must request it using the University of Western Ontario Updated Approval Request Form.

Members of the HSREB who are named as investigators in research studies, or declare a conflict of interest, do not participate in discussion related to, nor vote on, such studies when they are presented to the HSREB.

The Chair of the HSREB is Dr. Joseph Gilbert. The HSREB is registered with the U.S. Department of Health & Human Services under the IRB registration number IRB 00000940.

Curriculum Vitae

UDUNNA C ANAZODO, BSc, MRT(N)

EDUCATION

Western University, Schulich Medicine & Dentistry, London, Ontario, Canada
Doctor of Philosophy, Medical Biophysics; Focus: Brain Imaging, September 2015

University of Toronto, Department of Radiation Oncology, Toronto, Ontario, Canada
Bachelor of Science, Medical Radiation Sciences, May 2008.
Advanced Diploma, Nuclear Medicine Technology, May 2008.

York University, Toronto, Ontario, Canada
Bachelor of Science (Honors), Psychology with Minor in Biology, August 2002.

HONORS and AWARDS

Canadian Institute of Health Research (CIHR), IA Age+Prize award.	2014
CIHR Strategic Training Program in Vascular Research	2011 – 2013
CIHR Institute of Aging Age Travel award.	2011
Schulich Graduate Scholarship, University of Western Ontario	2009 – 2014

PUBLICATIONS

Udunna C Anazodo., Jonathan D Thiessen., Tracy Ssali., Jonathan Mandel., Matthias Günther, John Butler., William Pavlosky., Frank S Prato., R Terry Thompson., Keith St Lawrence. Feasibility of simultaneous whole-brain imaging on an integrated PET-MRI system using an enhanced 2-point Dixon attenuation correction method. *Frontiers in Neuroscience* (2015). DOI: 10.3389/fnins.2014.00434

Gelman, N., Silavi A., **Anazodo U.** A Hybrid Strategy for Correcting Geometric Distortion of Echo-Planar Images. *Magnetic Resonance Imaging* (2014), vol. 32(5), pp. 590-593.

Anazodo U.C., Shoemaker, J.K., Suskin, J., St Lawrence, K. An investigation of changes in regional gray matter volume in cardiovascular disease patients, pre and post cardiovascular rehabilitation. *NeuroImage Clinical* 3C (2013), pp. 388-395.

Conference Proceedings

2015

U Anazodo, J.K. Shoemaker, N. Suskin, Danny JJ Wang, K. S. St Lawrence. (June 2015). Evidence of neuroplasticity in coronary artery disease patients after cardiac rehabilitation. Proceedings for the 27th International Symposium on Cerebral Blood flow and Metabolism 2015, Vancouver, Canada.

Udunna Anazodo, Kevin Shoemaker, Neville Suskin, Danny JJ Wang, Keith St Lawrence. (June 2015) Correlation of brain atrophy to decreased CBF and CVR in coronary artery disease patients. Proceedings of the 21st International society of Magnetic Resonance in Medicine, Salt Lake City, Utah. (*Talk*)

Tracy Ssali, **Udunna Anazodo**, Yves Bureau, John Butler, Matthais Günther and Keith St Lawrence (June 2015). Feasibility of Arterial Spin Labeling for Detection of Low Frequency Activation. Proceedings for the 27th International Symposium on Cerebral Blood flow and Metabolism 2015, Vancouver, Canada. (*Talk*)

Tracy Ssali, **Udunna C Anazodo**, Mahsa Shokouhi, Bradley J MacIntosh, and Keith St Lawrence (June 2015). Intra and Inter-subject Reproducibility of Arterial Transit Time. Proceedings of the 21st International society of Magnetic Resonance in Medicine, Salt Lake City, Utah. (*Talk*)

Jing Zhang, Elizabeth Finger, **Udunna C Anazodo**, Julia MacKingley, John Butler, Frank S Prato and Keith St Lawrence. (June 2015) Simultaneous ASL/FDG-PET Imaging of Frontotemporal Dementia. Proceedings of the 21st International society of Magnetic Resonance in Medicine, Salt Lake City, Utah.

Udunna C Anazodo, Matthew Kewin, Elizabeth Finger, Jonathan D Thiessen, Jennifer Hadway, John Butler, William Pavlosky, Frank S Prato, R Terry Thompson, and Keith S St. Lawrence (May 2015). Preliminary evaluation of MRI-derived input function for quantitative measurement of glucose metabolism in an integrated PET-MRI scanner. *European Journal of Nuclear Medicine and Molecular Imaging Physics* 2015, 2 (Suppl 1): A80.

2014

Udunna Anazodo, Kevin Shoemaker, Neville Suskin, Keith St Lawrence. (June 2014) Investigation of regional changes in CBF and vascular reactivity in cardiac disease patients. Proceedings of the 20th Organization of Human Brain Mapping, Hamburg, Germany.

Udunna Anazodo, Tracy Ssali, Jonathan Mandel, John Butler, Matthias Günther, Frank Prato, Thompson Terry, Keith St Lawrence. (June 2014) Simultaneous investigation of regional CBF and glucose metabolism with 3D-pCASL and 18[F]-FDG. Proceedings of the 20th Organization of Human Brain Mapping, Hamburg, Germany.

Tracy Ssali, Mahsa Shokouhi, **Udunna Anazodo**, John Butler, Keith St. Lawrence. (June 2014). Detection of Inter-session Functional Activation by Arterial Spin Labeling. Proceedings of the 20th Organization of Human Brain Mapping, Hamburg, Germany.

2011-2013

Anazodo U.C., Shoemaker, J.K., Suskin, J., St Lawrence, K. (June 2013). The impact of cardiovascular disease on cortical structure of an aging brain. Proceedings of The 19th Organization for Human Brain Mapping, Seattle, Washington.

Anazodo U.C., Stodika R., Butler J., Mandel J., Thompson T., Prato F. S., Wang D.J.J., St Lawrence K.S. (April 2013). Simultaneous imaging of cerebral perfusion and glucose metabolism in PET/MRI. Proceedings of the 21st International society of Magnetic Resonance in Medicine, Salt Lake City, Utah.

Anazodo U.C., Suskin, J., Wang, K., Shoemaker, J.K., St Lawrence, K. (June 2011). Grey and white matter cerebrovascular reactivity mapping in cardiovascular disease patients. Proceedings of The 16th Organization for Human Brain Mapping, Quebec, City, QC, Canada

Anazodo U.C., Suskin, J., Wang, K., Shoemaker, J.K., St Lawrence, K. (May 2011). The precision of ASL in measuring cerebrovascular reactivity in cardiovascular disease. Proceedings of the 19th International society of Magnetic Resonance in Medicine.

Anazodo U.C., Suskin, J., Wang, K., Shoemaker, J.K., St Lawrence, K. (January 2011). Measuring cerebrovascular reactivity in cardiovascular disease patients. 2011 Imaging Network of Ontario. (*Talk*)

Invited Talks

Udunna Anazodo. Feasibility of enhanced 2-point Dixon attenuation correction method for whole-brain imaging on an integrated PET-MRI system. October 6th -7th 2014. Siemens Experts' mMR brain attenuation correction workshop, Copenhagen, Denmark.

Udunna Anazodo. Impact of cardiovascular disease on brain health. December 4th 2013. Canadian Institutes of Health Research (CIHR) - Strategic Training in Vascular Research Program, London, Ontario, Canada.

Udunna Anazodo. Comparing FDG-PET to Perfusion with ASL. September 28th 2013. Siemens Biograph mMR User Group Meeting, Lawson Health Research Institute, London, Ontario, Canada.

Udunna Anazodo. Cardio-cortical Interaction: Brain atrophy and plasticity. August 20 2013. Toronto Western Research Neuroimaging Rounds, Toronto Western Hospital, Toronto, Canada.

RELATED WORK EXPERIENCE

Research Assistant

Department of Biology, York University 2000 - 2001

Registered Nuclear Medicine Technologist

St Joseph's Healthcare, London, Ontario 2010 – 2015

Woodstock General Hospital, Woodstock , Ontario 2010 – 2015

Brampton Nuclear Services, Brampton, Ontario 2008 – 2009